NOVEMBER 1969 DAC 62146

THE EFFECTS OF A HYDROGEN ENVIRONMENT ON THE MECHANICAL PROPERTIES OF FORGED Ti-6Al-4V ELI WELDMENTS

FINAL REPORT

THE EFFECTS OF A HYDROGEN ENVIRONMENT ON THE MECHANICAL PROPERTIES OF FORGED Ti-6Al-4V ELI WELDMENTS

FINAL REPORT
27 June 1969 to 1 November 1969

NOVEMBER 1969 **DAC 62146**

Prepared for National Aeronautics
and Space Administration
George C. Marshall Space Flight Center
Marshall Space Flight Center, Alabama

Contract No. NAS 8–21470

Prepared by: G.F.PITTINATO
Materials & Methods Research
and Development Department

Catalog No. PDL 92706–5

MCDONNELL DOUGLAS ASTRONAUTICS COMPANY
WESTERN DIVISION

5301 Bolsa Avenue, Huntington Beach, CA 92647 (714) 897-0311

MCDONNELL DOUGLAS CORPORATION

ABSTRACT

A summary is given of the work performed in a 16-month program to study the effects of hydrogen on forged (STA) Ti-6Al-4V ELI material containing a fillerless weld. The program was divided into the following three tasks. Task I - Literature Survey, Task II - Tensile Tests of Welded Ti-6Al-4V ELI, Task III - Fatigue Tests of Welded Ti-6Al-4V ELI.

The tensile data showed that there was no gross change in the tensile properties of oxide free samples of Ti-6Al-4V ELI as a result of testing in hydrogen gas. There was, however, a slight decrease (approximately 1 to 3%) in the tensile properties for those samples tested in hydrogen environments regardless of the additional testing parameters.

A hydrogen environment was found to increase the fatigue crack growth rate in Ti-6Al-4V ELI (STA) and weld material in the temperature range of ambient to -100°F. At -200°F, there was no significant difference between the crack growth rates obtained in helium and hydrogen gas. The degree of hydrogen enhanced crack growth was found to be dependent on the stress intensity range, temperature, and microstructure of the material. The hydrogen enhanced crack growth was explained by using a model involving hydrogen diffusion.

TABLE OF CONTENTS

LIST OF ILLUSTRATIONS

LIST OF TABLES

INTRODUCTION

The increasing use of titanium alloys in hydrogen environments has resulted in considerable interest in their mutual compatibility. It is well known that hydrogen in solution or precipitated as a hydride can seriously embrittle titanium alloys. Material evaluation studies conducted on hydrogenated titanium alloys clearly demonstrate the serious degradation of mechanical properties associated with the presence of large quantities of absorbed hydrogen.[1,2,3]

The parameters which control the rate and quantity of hydrogen that titanium alloys will absorb when exposed to a hydrogen environment are not well defined. At relatively high temperatures, titanium alloys rapidly absorb hydrogen with the rate and quantity of absorption being dependent primarily on the temperature.[4] However, at ambient and cryogenic temperatures, absorption depends on a number of additional parameters including the condition of the material's surfaces, the amount of stress in the material, and the purity of the hydrogen gas.[5,6,7,8] Since many applications of titanium alloys in space vehicles involve ambient to cryogenic temperatures in hydrogen environments, it is important to understand the conditions that promote absorption and subsequent embrittlement at these temperatures.

The object of this investigation was to determine the effects of a hydrogen environment on the tensile properties and crack growth rate of forged and welded Ti-6Al-4V ELI material in the solution treated and aged (STA) condition. To accomplish this objective, the program was divided into three basic tasks as follows:

Task I -- A survey of the technical literature on the absorption of external hydrogen by titanium was made.

Task II -- Tensile tests were conducted on forged material at ambient temperature using chemically clean Ti-6Al-4V ELI specimens with transverse welds. The effect of hydrogen pressure, stress, strain, abrasion with iron, and microstructure on the hydrogen absorption and subsequent tensile properties of the unprotected material was determined.

Task III -- Fatigue tests were conducted on forged material using precracked Ti-6Al-4V ELI specimens with transverse welds. The effect of hydrogen on the crack growth rate of the material as a function of temperature (ambient, 0°, -100°, -200°F) and microstructure (weld and STA parent material) was determined.

TASK I -- LITERATURE SURVEY

General Discussion of Metal-Gas Reactions

It was recognized by Smithells that three main processes occur when a metal surface is exposed to a gaseous atmosphere.[9] The first reaction that will occur is the adsorption of gas onto the metal surface. The gas will then be absorbed into the surface followed by diffusion into the interior of the metal. In the particular case of titanium and hydrogen gas, a fourth reaction can be present. That reaction is the formation of titanium hydrides.[7] The rate of permeation of the gas through the metal may be controlled by any one or all of the above mentioned variables.

In the following summary, a detailed discussion is given on the reactions occurring between metal surfaces and gaseous atmospheres as applied to the titanium-hydrogen system. The effects of these reactions on the mechanical properties of the material are also examined.

Adsorption

Adsorption is the first process that occurs when a gas is placed in contact with a metal surface. The gas impinging on the surface condenses and is held in place by the force field produced by the surface atoms of the metal. Langmuir has suggested that the range of the surface forces responsible for absorption are on the order of 10^{-8} cm.[10] Since the range of the forces is less than the diameter of most gas molecules, the adsorbed layer of gas would be expected to be only a few molecules thick. According to Langmuir, as the surface becomes covered with a layer of adsorbed gas, molecular dissociation occurs whereby the gas molecules lose their identity in the adsorbed layer.

The amount of gas adsorbed by a unit surface area of a metal is dependent on the gas pressure and the temperature of the metal surface.[11] Langmuir has shown that the total amount of gas adsorbed onto a unit area of a surface is a hyperbolic function of the gas pressure.[10] In the case of a diatomic gas, such as hydrogen, the equation was modified to involve the square-root of the

gas pressure. In particular at low pressures, where the adsorbed layer is incomplete, the total amount of gas adsorbed is proportional to the square-root of the gas pressure.

The temperature dependency of the adsorption reaction, in many cases, cannot be represented by a specific function. Benton and White have determined the amount of hydrogen that will adsorb onto nickel powder at three different pressures as a function of temperature.[12] Their studies show that with increasing temperatures, the quantity of gas adsorbed falls to a minimum value and then increases. After achieving a maximum value, the amount of gas adsorbed again decreases with increasing temperatures. Smithells states that this type of adsorption, referred to as chem-sorption, is associated with gas-metal systems that can form a definite chemical compound.[9] This type of adsorption would be expected to occur in the titanium-hydrogen system since titanium hydrides can readily be formed. The temperature dependency of hydrogen adsorption on titanium is not known. However, it has been shown that hydrogen will adsorb onto a clean surface of pure titanium at 14°K in a vacuum of 10^{-6} torr.[13]

The effect of an adsorbed gas on the mechanical properties of a metal were discussed by Petch.[14] He proposed that the fracture stress for iron can be lowered by the surface adsorption of hydrogen gas. The stress required to enlarge a surface crack in a solid is given as a direct function of the material's surface energy. Calculations made by Petch show that the surface energy for iron is lowered by an adsorbed layer of hydrogen thus resulting in a corresponding decrease in the material's fracture stress.

Absorption of Hydrogen by Titanium

The rate and quantity of hydrogen absorbed by titanium is a function of a number of variables. These variables include temperature, environmental conditions, surface cleanliness, microstructure, alloy content, applied stress, and gas pressure.

Temperature

The absorption of hydrogen by titanium is strongly temperature dependent. Bomberger and Knapek showed that Ti-6Al-4V did not absorb hydrogen during an exposure of 30 days at 392°F.[5] However, the hydrogen content of the material increased from 4 ppm to 645 ppm after 30 days at 752°F. Using commercially pure titanium and a hydrogen gas pressure of 2 cm, Gulbransen and Andrew examined the rate of hydrogen absorption as a function of time and temperature.[15] Absorption was found to start at about 554°F with the rate of the reaction increasing rapidly with increasing temperature. In several tests conducted at ambient temperature, evidence was found of hydrogen absorption by pure and alloyed titanium.[6,7,8,16] A few studies were performed at very low temperatures; in these studies no evidence of adsorption was found below -100°F.[6,17]

Environmental Conditions

The absorption of hydrogen by titanium at low temperatures is dependant on the purity of the hydrogen atmosphere. Contamination of the hydrogen gas by small quantities of oxygen or water significantly reduce the tendency for absorption.[6,16] Quantitative results were presented by Bomberger and Knapek who showed that 0.1 to 1.0% of oxygen or water strongly inhibited hydrogen absorption by titanium alloys.[5]

Surface Cleanliness

In all low temperature studies of hydrogen absorption by titanium, the need for an oxide-free surface was evident.[6,7,8,16,18] Unless the oxide was removed or broken in some way, no reaction occurred. Sustained load tests conducted at ambient temperature in hydrogen gas give direct evidence of this requirement.[19] Crack growth occurred only after the crack was extended in hydrogen gas thus exposing a clean oxide free surface to the hydrogen.

Microstructure and Alloy Content

Hydrogen absorbed by commercially pure titanium or predominantly alpha alloys is concentrated primarily at the material's surface in the form of titanium hydrides.[16,20] Therefore, the quantity of hydrogen absorbed is dependent

on the diffusi ate of hydrogen through the hydride layer. However, it was found that the depth of the hydride layer was also affected by the material's microstructure. An acicular structure showed a greater depth of hydride penetration than an equiaxed structure.[21]

Titanium alloys containing small amounts of the beta phase were found to absorb more hydrogen than pure titanium or all alpha alloys.[20,21,22] This was particularly noticeable when the material was heat treated to produce an acicular structure. In a Ti-Fe alloy containing 2% retained beta, the equiaxed structure absorbed twice as much hydrogen as pure titanium, while the acicular structure absorbed three times as much hydrogen.[20] This data clearly indicates that in alpha-beta alloys, the total amount of hydrogen absorbed is directly related to the amount and distribution of the beta phase.

Stress

The effect of stress on the amount of hydrogen absorbed by four different titanium alloys was determined at 752°F.[5] It was found that the amount of hydrogen absorbed tended to be greater in the stressed material as compared to the unstressed material. In the four alloys tested, the application of stress approximately doubled the amount of hydrogen absorbed.

Hydrogen Gas Pressure

In a study of the reactions of titanium with hydrogen, pure titanium at ambient temperature was exposed to hydrogen gas at pressures ranging from 2 psig to 1000 psig.[16] A definite correlation was found between the thickness of the hydride surface layer and the hydrogen pressure. It was shown that the thickness of the hydride layer increased with increasing hydrogen pressure.

The embrittlement of alloyed titanium by high pressure hydrogen was examined by exposing notched Ti-6Al-4V (STA) specimens to 10,000 psi hydrogen for 24 hours prior to testing.[23] The test results showed a reduction of approximately 35 percent in the notch strength as compared to that found in 10,000 psi helium. Visual examination of the fracture surface showed the appearance of a dark band part way around the fracture. The size of this dark band appeared to be directly proportional to the degree of embrittlement.

Diffusion of Hydrogen in Titanium Alloys

The absorption rate of hydrogen by titanium alloys is dependent on the rate of hydrogen diffusion into the material. Wasilewski and Kehl measured the diffusivity of hydrogen in hcp and bcc Ti-H alloys in the temperature range of 650° to 1000°C.[24] Their results yielded the following equations for the diffusion coefficients of hydrogen in α and β titanium:

$$D_\alpha = 1.8 \times 10^{-2} \exp\left[\frac{-12{,}380 \pm 680}{RT}\right]$$

$$D_\beta = 1.95 \times 10^{-3} \exp\left[\frac{-6{,}640 \pm 500}{RT}\right]$$

where D is in sq. cm. per sec., T in °K, and R the gas constant in cal. per g-atom -K°.

A similar study was made by Papazoglou and Hepworth who determine the diffusion coefficient for hydrogen in hcp and bcc titanium in the temperature range of 610° to 900°C.[4] Their data showed the diffusion coefficient for hydrogen in hcp titanium to be as follows:

$$D_\alpha = 3.0 \times 10^{-2} \exp\left[\frac{-14{,}700 \pm 650}{RT}\right]$$

Only three measurements of diffusivity in bcc titanium were made at 900°C, the diffusivity in β was found to be 1.8×10^{-4} sq. cm. per sec.

The diffusivity data for hcp solutions of Wasilewski and Kehl appear to be larger than those determined by Papzoglou and Hepworth. Because of the direct experimental approach taken by Papzoglou and Hepworth, their data is considered to be more reliable.

Location of Hydrogen in Titanium

When hydrogen is absorbed by titanium, it can either form a solid solution or precipitate out as a hydride. The probability of hydride precipitation depends heavily on the alloy content.[25] Aluminum, in particular, increases

the solubility limit for hydrogen thereby decreasing the tendency for hydride precipitation.[26] When the hydrogen content exceeds the solubility limit of the material, hydride precipitation occurs.[27,28,29]

In an alpha-beta alloy, the absorbed hydrogen is concentrated primarily in the beta phase.[30,31] Since the solubility of hydrogen in the beta phase is considerably higher than in the alpha phase,[4,30] the alpha-beta alloys can absorb more hydrogen without hydride precipitation than the all alpha alloys.

Hydrogen Embrittlement of Titanium Alloys

High concentrations of hydrogen in pure or alloyed titanium can seriously embrittle the material. This embrittlement is commonly separated into two distinct types based upon rate of load application.[32,33] They are impact embrittlement and low-strain-rate embrittlement. Both are believed to result from a decrease in solubility of hydrogen in titanium with the behavior differences attributed to differences in kinetics of hydride precipitation. If massive hydrides are already present, impact embrittlement is observed. If no hydrides are present, the alloy will be supersaturated with respect to hydrogen and the application of stress will result in hydride precipitation.[34] Low-strain-rate embrittlement is then observed.

Impact embrittlement is usually associated with hydrogen contaminated alpha alloys, the low temperature close-packed-hexagonal form of titanium.[3,26,35,36] The embrittlement becomes more severe with increasing hydrogen content, increasing strain rate, decreasing temperature, and the presence of notches. A high hydrogen content can also result in impact embrittlement in beta alloys, the body-centered-cubic form of titanium, as well as alpha-beta alloys.[37,39] The hydrogen content requirement for impact embrittlement for the latter alloy is in excess of that required for low-strain-rate embrittlement.

Low-strain-rate embrittlement is usually observed in hydrogen contaminated alpha-beta alloys, but has also been reported in both all alpha and all beta alloys.[40-44] The severity of this type of embrittlement increases with increasing hydrogen content, decreasing strain rate, and decreasing temperature. Further temperature decrease results in a recovery of ductility which has been attributed to the decreased rate of hydrogen diffusion.[45]

TASK II -- TENSILE TESTS

Experimental Procedure

Material

The material used in this study consisted of three Ti-6Al-4V ELI grade forgings each measuring 40 inches long, 6 inches wide, and 0.75 inches thick. Each forging was solution treated and aged per specification MIL-H-81200. The vendor report showed that the material conformed to the requirements of MIL-T-9047D, Type III, Composition B, Table 1. The microstructure of the forgings was found to be typical of forged Ti-6Al-4V in the (STA) condition, Figure 1.

C	Fe	Al	V	N	H	O_2
.025	.05	6.0	3.9	.012	.005	.11

Yield .2% Off. KSI	Ultimate KSI	% Elong.	% Red. of Area
141.4	158.2	11	31.7

Table 1

VENDOR TEST RESULTS.

Sample Preparation

Milling the 0.75 inch thick forgings to the required sample thickness of 0.033 inches involved two separate processes. The forgings were first chemically milled to a thickness of approximately 0.050 inches. The chemical milling solution, consisting of 79.06% H_2O, 11.92% HNO_3, 5.09% HF, 3.77% Butyl Cellosolve and 0.16% Propaste No. 6708, was maintained at 85 $\pm$ 5°F. To minimize hydrogen absorption, the temperature and chemical composition of the chemical milling solution was carefully controlled. An average hydrogen content of 80 ppm was found in the chemically milled forgings as compared to 50 ppm in the as received material.

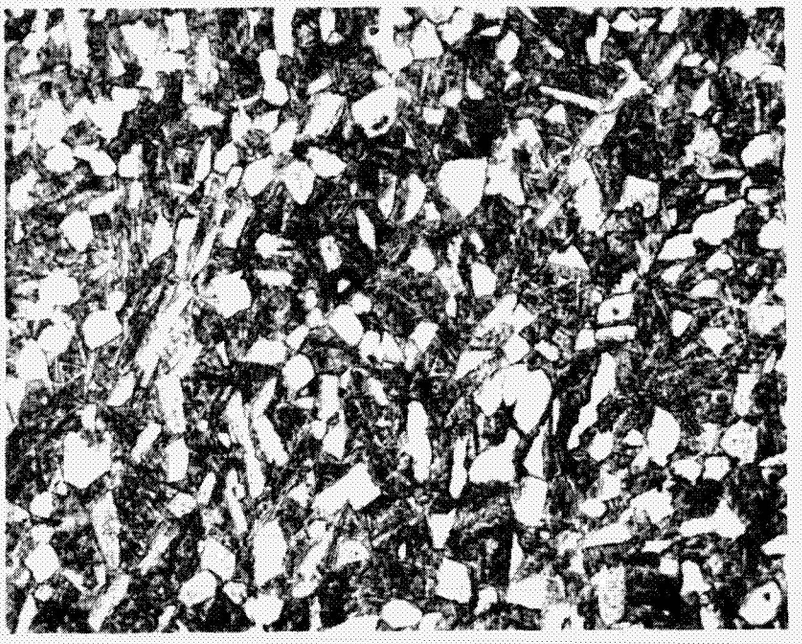

MAGN: 400X M 2420

FICURE 1. MICROSTRUCTURE OF Ti-6Al-4V ELI FORGING IN THE (STA) CONDITION.

The chemical milling resulted in the forgings being relatively flat in the longitudinal direction but concave in the transverse direction. To obtain parallel surfaces, further reduction of the forgings was accomplished by surface grinding. A method was devised for holding the material during surface grinding by using an epoxy resin. Each forging was grit blasted and bonded to a 0.500 inch thick plate of 6061 aluminum. The epoxy resin selected was Epon 934 since this particular resin is susceptible to thermal shock. 6061 aluminum was used for the backing plate material because its coefficient of expansion is approximately two and one half times that for Ti-6Al-4V. These characteristics of the bonding materials were essential for easy removal of the forgings from the backing plates following surface grinding.

A uniform distribution of epoxy resin was obtained between the forgings and the backing plates by bonding the materials between two aluminum pressure plates. Several sheets of silicone rubber were placed between the forgings and the pressure plates to produce an even distribution of force. The materials were then bonded under slight pressure at 160°F for 2 hours. The bonded structure was sufficiently rigid to permit surface grinding to a tolerance of $\pm$ 0.001 inches. Following surface grinding, the bonded structures were submerged in liquid nitrogen. The thermal shock combined with the stress due to differential thermal expansion resulted in releasing the forgings from the aluminum backing plates. It was found that because of the irregular plane surfaces of the forgings, it was necessary to grind on alternate surfaces several times to obtain parallelism. Using this technique, all of the forgings were surface ground to a thickness of 0.033 $\pm$ 0.002 inches.

The Ti-6Al-4V forgings were sheared lengthwise in preparation for welding. Edge irregularities were removed by machining. The forgings were then welded back together using the Gas-Tungsten-Arc (GTA) process in accordance with Douglas Process Standard 14121. The welds were of the straight butt type with no filler. Each weld was radiographed and dye penetrant inspected. Minor porosity was found in the start and stop areas, but only four isolated pores were found in the remainder of the welds. All welds were crack free.

The welded forgings were sheared into sample blanks measuring 4-1/2 inches by 1-1/2 inches. Areas in the weldments which contained porosity as indicated by radiography were avoided in the shearing of the blanks. The sample blanks were stress-relieved and aged by heat treating at 1000°F for 2 hours in an argon atmosphere. Flat specimens were obtained by clamping the sample blanks between 1/4 inch thick stainless steel plates during the heat treatment. The sample blanks were then machined to the final sample configuration shown in Figure 2.

Visual examination of the welds in the tensile samples showed that a slight amount of undercut was present in the area adjacent to the heat affected zone. Although this undercut was estimated to be only 0.001 to 0.002 inches deep, complete oxide removal in this area during subsequent sample preparation would be difficult. Therefore, the surfaces of the tensile samples were ground flat using the following procedure. The machined tensile samples were mounted on a flat plate using double back tape and hand ground using successively 80, 240, and 320 grit wet emery paper. This treatment reduced the thickness of the samples by approximately 0.003 inches thus making the over-all thickness approximately 0.030 inches. Following surface grinding, the reduced sections of the samples were coated with red layout dye.

Equipment

The tensile samples were prepared for testing in an Eringard Dry Box, Figure 3. The purification system connected to the dry box was capable of maintaining the oxygen and moisture levels in the dry box below 1 ppm. A moisture monitor and an oxygen analyzer were connected to the system to provide a record of the moisture and oxygen levels of the argon gas during sample preparation.

The tensile sample test chamber is shown in Figure 4. The test chamber utilizes a stainless steel shell, high vacuum flanges and a stainless steel bellows. Copper gaskets were used with the ultra high vacuum flanges to provide a leak tight system.

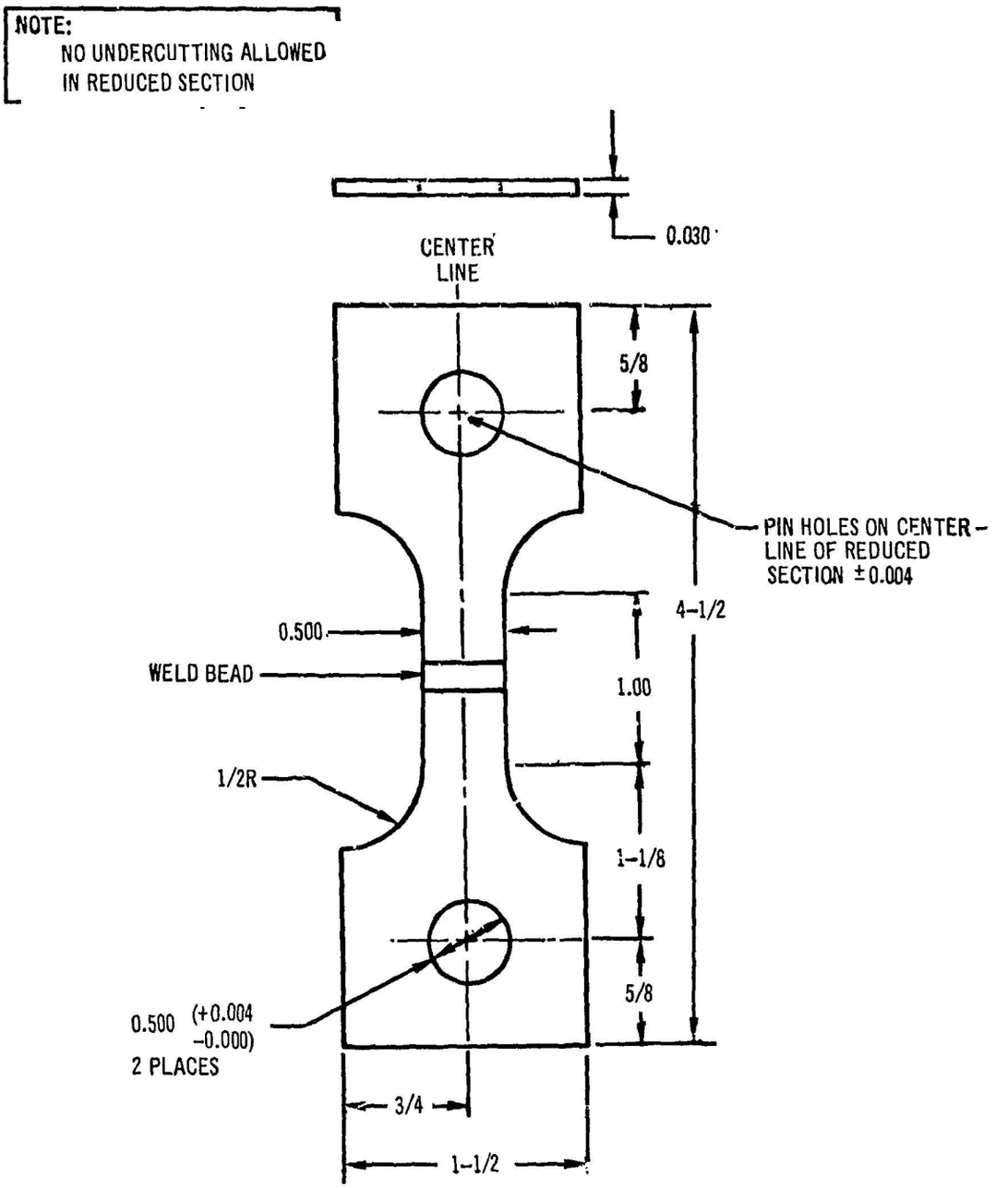

FIGURE 2. TENSILE SPECIMEN.

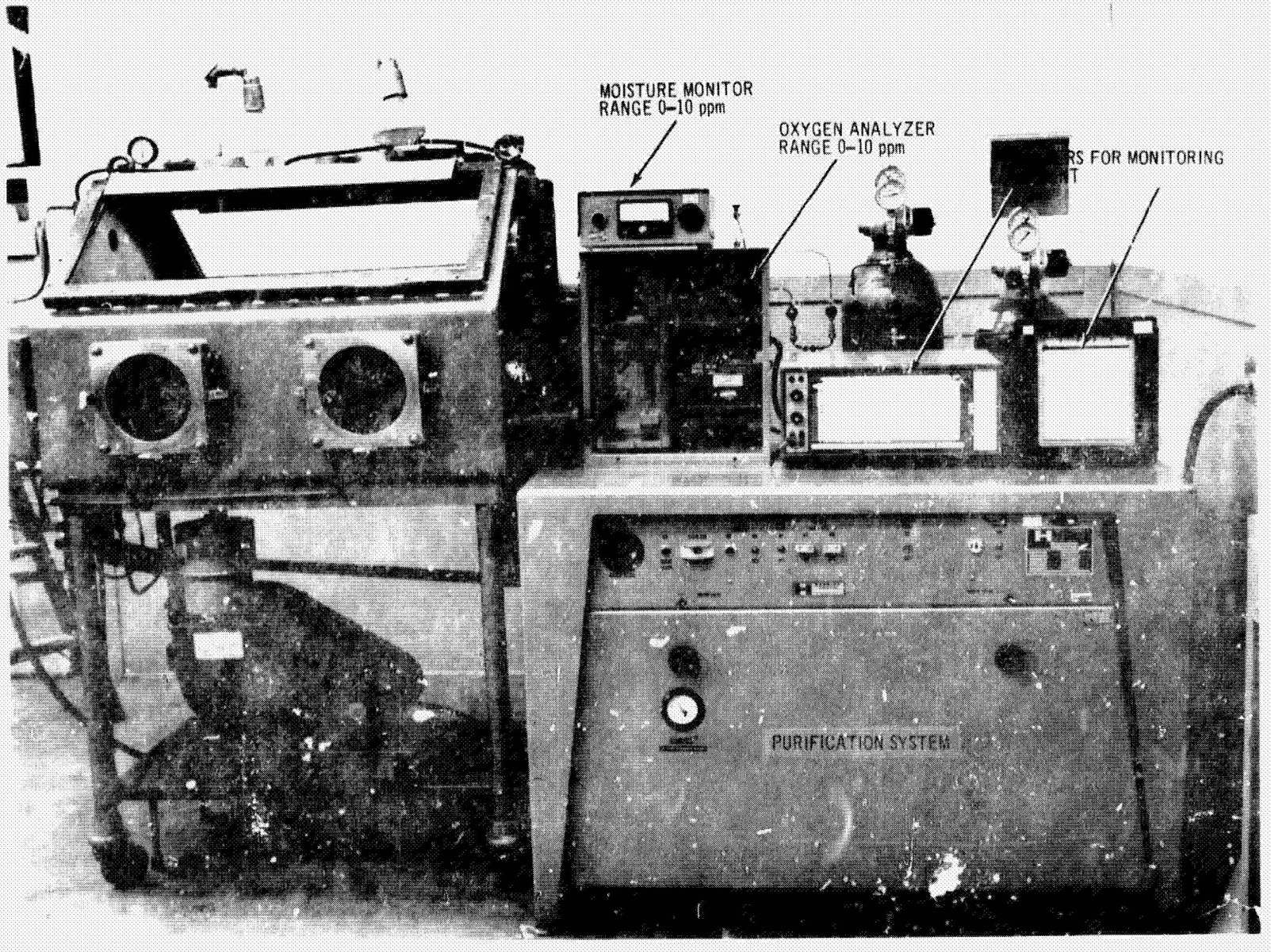
MOISTURE MONITOR
RANGE 0–10 ppm
OXYGEN ANALYZER
RANGE 0–10 ppm
PURIFICATION SYSTEM

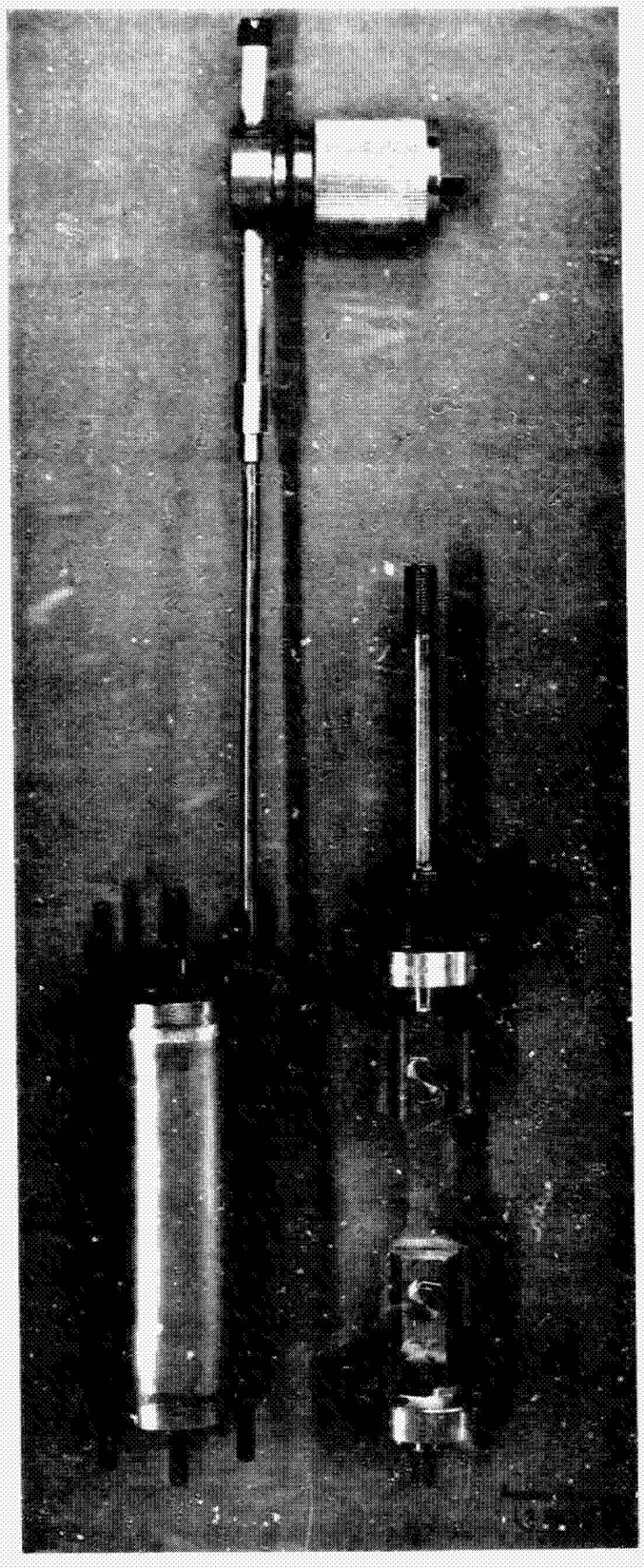

FIGURE 4. TENSILE SAMPLE TEST CHAMBER.

Test Procedure

The test samples, test chambers, and 320 grit emery paper were placed in the Eringard Dry Box in preparation for the oxide removal treatment. The equipment and samples were permitted to out-gas until the monitoring equipment showed that the dry box atmosphere contained less than 2 ppm of oxygen and less than 1 ppm of moisture. Since the out-gassing for most of the samples was permitted to occur overnight, oxygen levels of approximately 1 ppm and moisture contents of approximately 0.6 ppm were obtained for most of the test specimens.

The oxide removal treatment consisted of abrading the reduced section of the tensile samples until the red layout dye was completely removed. Immediately after abrading, one inch gage marks were scribed into the surface of the reduced section of each sample. The samples were then inserted into the hydrogen test chambers which were sealed and removed from the Eringard Dry Box.

The sealed test chamber with the sample in the argon atmosphere was installed on the tensile machine and connected to the purge-and-fill system. The connecting lines between the hydrogen tank and the sample chamber were purged three times by evacuating the system to 10^{-1} torr and back filling with ultra high purity hydrogen gas that contained less than 1 ppm of oxygen and moisture. After the third back fill with hydrogen gas, the valve to the sample chamber was opened and the chamber was purged three times using the same procedure. For the control samples, helium gas was substituted for hydrogen gas.

The samples were tested in an Instron tensile machine at a constant deflection rate of 0.002 in./min. Strain measurements were made by using the cross-head travel, a standard mode of operation for the Instron. The samples that required exposure to hydrogen gas under stress were tensile loaded after the chamber was filled with hydrogen to 75% of the yield strength and held for 24 hours. Before testing to failure, the samples were unloaded so that a full load-deflection curve could be obtained. All of the samples tested in hydrogen were placed in liquid nitrogen for storage. This cold storage minimized possible hydrogen diffusion and resulting changes in the microstructure near the surfaces of the samples.

Post-test Examination

Metallographic specimens were prepared through the fracture surfaces of samples that were tested in helium and in hydrogen gas.

The fracture surfaces of one sample representing each test condition were examined by using electron fractography. Conventional two stage plastic-carbon replication techniques were used.

Hydrogen gas analyses were made on samples representing each test condition by using vacuum-hot-extraction methods.

Results and Discussion

Tensile Tests

The tensile properties of welded Ti-6Al-4V ELI forged material tested at ambient temperature in helium and hydrogen gas are presented in Table 2. The data shows that the tensile properties of the material were not significantly affected by hydrogen environments of 14.7 and 50 psi absolute pressure. Similar results were found for the samples that were exposed to hydrogen gas for 24 hours under a sustained load prior to tensile testing. There was, however, a slight decrease (approximately 2%) in the average ultimate strength for those samples tested in hydrogen gas.

The results of the tensile tests evaluating the effects of pre-strain and iron abrasion on hydrogen absorption and subsequent tensile properties are given in Table 3. A comparison can be made between the tensile properties of the sample abraded with iron, sample 3-8, and the samples tested in helium gas. The data indicates that abrading the material with iron results in a lowering of the tensile properties (approximately 3%) when tested in hydrogen gas. A similar decrease in tensile properties was found for sample 3-9 which was exposed to hydrogen gas for 332 hours. Prestraining the material prior to hydrogen exposure, sample 3-7, also appears to lower the mechanical properties of the material.

Sample Number	Dry Box Atmosphere O_2 ppm	Dry Box Atmosphere H_2O ppm	Test Conditions: Gas	Test Conditions: Absolute Pressure PSI	Test Conditions: Exposure Time Hours	0.2% Yield Strength KSI	Ultimate Strength KSI	Elongation 1 inch Gage Length
5- 1	-	-	He	14.7	0	131.4	155.1	8.3*
5- 2	-	-	He	14.7	0	130.4	154.9	6.1
5- 3	-	-	He	14.7	0	132.1	154.7	7.4
Avg.			He	14.7	0	131.3	154.9	7.3
5- 6	1.4	0.5	H_2	14.7	0	129.9	152.9	7.1
5- 8	1.0	0.8	H_2	14.7	0	130.6	151.6	6.1
5- 9	1.0	0.8	H_2	14.7	0	133.3	154.2	7.8
Avg.			H_2	14.7	0	131.3	152.9	7.0
5- 4	1.3	0.5	H_2	50	0	129.2	152.9	7.0
5-11	1.2	0.7	H_2	50	0	130.8	151.0	7.4
5-12	1.2	0.7	H_2	50	0	129.3	152.0	5.1***
Avg.			H_2	50	0	129.8	152.0	7.2
5-13	0.9	0.5	H_2	14.7	24**	130.3	150.6	7.4
3- 4	1.2	0.2	H_2	14.7	24**	131.5	154.2	7.4
3- 6	0.9	0.2	H_2	14.7	24**	128.7	155.6	6.4
Avg.			H_2	14.7	24**	130.2	153.5	7.1
5-10	0.6	0.6	H_2	50	24**	129.5	148.7	6.3
3- 5	1.2	0.2	H_2	50	24**	128.3	152.5	6.7
3- 2	0.9	0.5	H_2	50	24**	130.4	155.2	6.1
Avg.			H_2	50	24**	129.4	152.1	6.4

*Measured over a 1/2 inch gage length
**Sustained load, 75% of yield strength
***Failed in weld area

Table 2

TENSILE PROPERTIES OF WELDED Ti-6Al-4V ELI FORGED PLATE TESTED AT AMBIENT TEMPERATURE.

Sample Number	Sample Preparation	Dry Box Atmosphere O_2 ppm	Dry Box Atmosphere H_2O ppm	Test Conditions: Gas	Test Conditions: Absolute Pressure PSI	Test Conditions: Exposure Time Hours	0.2% Yield Strength KSI	Ultimate Strength KSI	Elongation 1 Inch Gage Length
5-1	-	-	-	He	14.7	0	131.4	155.1	8.3*
5-2	-	-	-	He	14.7	0	130.4	154.9	6.1
5-3	-	-	-	He	14.7	0	132.1	154.7	7.4
Avg.				He	14.7	0	131.3	154.9	7.3
3-8	1. Remove oxide in dry box. 2. Abrade surfaces with pure iron in dry box.	1.0	0.1	H_2	50	24**	126.0	149.7	9.0
3-1	1. Abrade surfaces in air. 2. Strain 3% in air.	-	-	Air	14.7	24**	129.7***	153.5***	6.6
3-7	1. Remove oxide in dry box. 2. Strain 3% in H_2.	1.1	0.1	H_2	50	24**	126.8***	149.4***	7.5
3-9	1. Remove oxide in dry box.	0.9	0.2	H_2	50	332**	125.0	149.0	7.4

*Measured over a 1/2 inch gage length.
**Sustained load, 75% of yield strength.
***Yield measured after 3% pre-strain; ultimate measured after sustained load.

Table 3

TENSILE PROPERTIES OF WELDED Ti-6Al-4V ELI FORGED PLATE TESTED AT AMBIENT TEMPERATURE.

Metallography

The tensile samples were found to consistently fail in the base material away from the welds, Figure 5. Although the base material exhibited considerable plastic deformation, the weld areas showed evidence of only a small amount of plastic strain.

The fractured tensile samples shown in Figure 5 were examined for evidence of a hydrogen-titanium reaction by using both optical and electron microscopy methods. Microscopic examination of the plane surfaces of the samples tested in hydrogen and helium gas showed indications of surface cracks in the base material and not in the welds, Figure 6. However, by using electron microscopy, it was found that the surface markings in Figure 6 were localized areas of high plastic strain and not surface cracks, Figure 7.

Metallographic specimens were prepared through the fracture surfaces of selected samples tested in hydrogen gas. Examination of these specimens revealed no indications of a hydrogen-titanium reaction adjacent to the surface that was abraded and exposed to hydrogen gas, Figure 8.

Fractography

Electron fractographs were made on the broken tensile samples to establish the fracture mode. One specimen representing each test condition in Table 2 was examined. The fracture surfaces were examined in an area directly adjacent to the sample's surface since that would be the most likely area to show embrittlement. All of the samples showed that failure occurred by dimple rupture thus indicating a ductile failure, Figure 9.

Gas Analysis

Hydrogen gas analysis were made on samples representing each test condition shown in Table 2 by using hot extraction techniques. Since absorbed hydrogen would be concentrated at the tensile sample's surface, it was concluded that gas analysis of the bulk tensile samples would not yield definitive results. Therefore, filings were removed from both the base material and the weld area

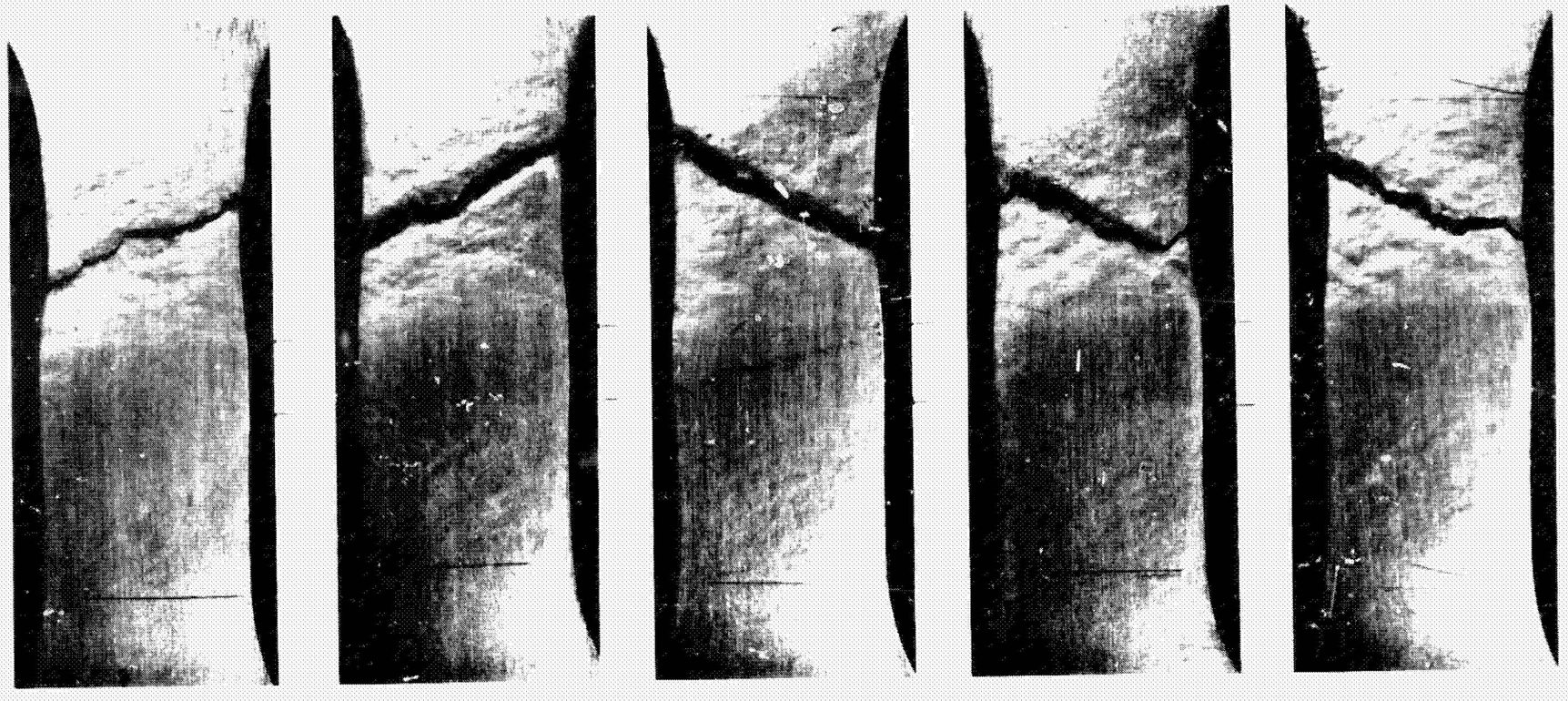

SAMPLE 5-3	SAMPLE 5-6	SAMPLE 5-4	SAMPLE 5-13	SAMPLE 5-10
He gas at 14.7 psi	H_2 gas at 14.7 psi	H_2 gas at 50 psi	H_2 gas at 14.7 psi Exposed to H_2 gas for 24 hours at a sustained load of 75% of the yield prior to testing.	H_2 gas at 50 psi Exposed to H_2 gas for 24 hours at a sustained load of 75% of the yield prior to testing.

FIGURE 5. FRACTURED TENSILE SAMPLES OF WELDED Ti-6Al-4V ELI FORGED PLATE TESTED AT AMBIENT TEMPERATURE UNDER THE INDICATED TEST CONDITIONS. MAGN: 2.5X

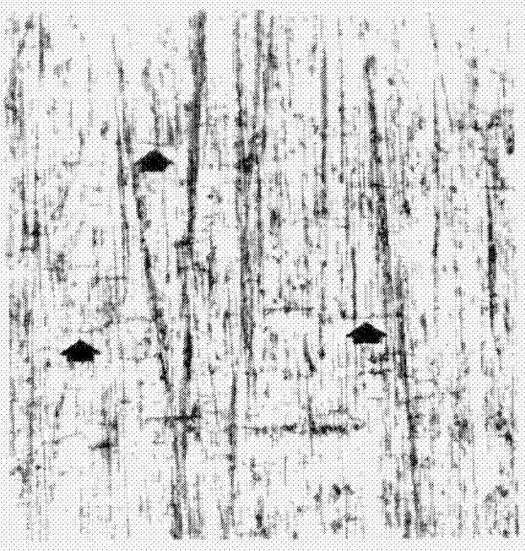

Base Material

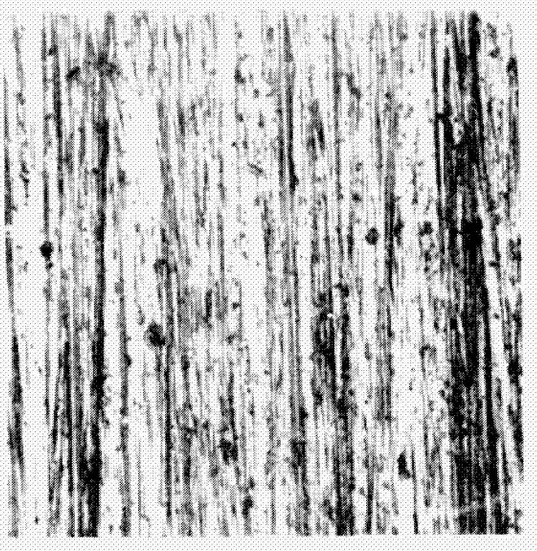

Weld Material

SAMPLE 5-1 Tested in He gas at 14.7 psi pressure

Base Material

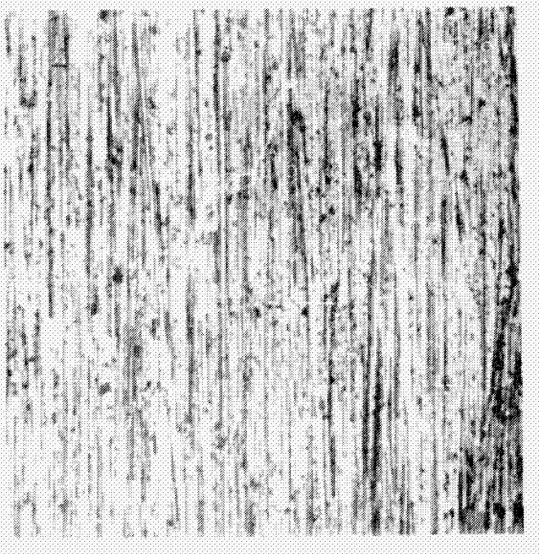

Weld Material

SAMPLE 3-2 Tested in H_2 gas at 50 psi pressure

Exposed to H_2 gas for 24 hours at a sustained load of 75% of the yield prior to testing.

FIGURE 6. PHOTOMICROGRAPHS OF THE PLANE SURFACES OF Ti-6Al-4V TENSILE SAMPLES SHOWING INDICATIONS OF SURFACE CRACKING IN THE BASE MATERIAL. MAGN: 200X

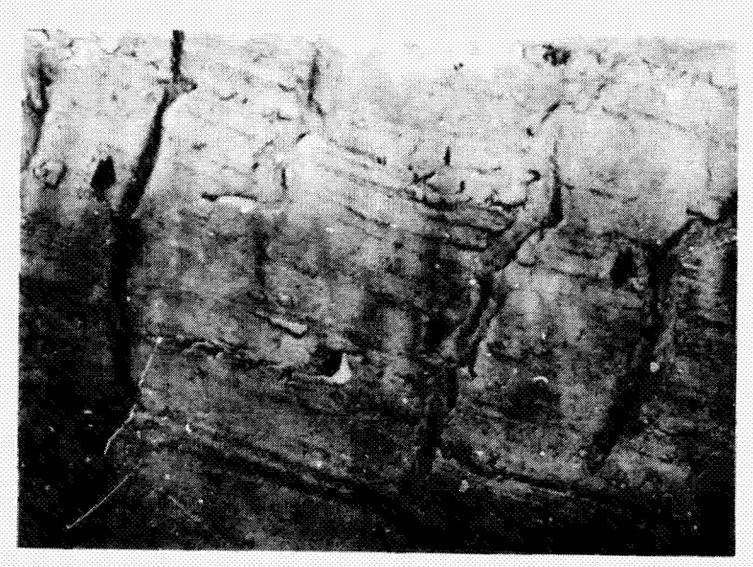

SAMPLE 5-1 Tested in He gas at 14.7 psi pressure

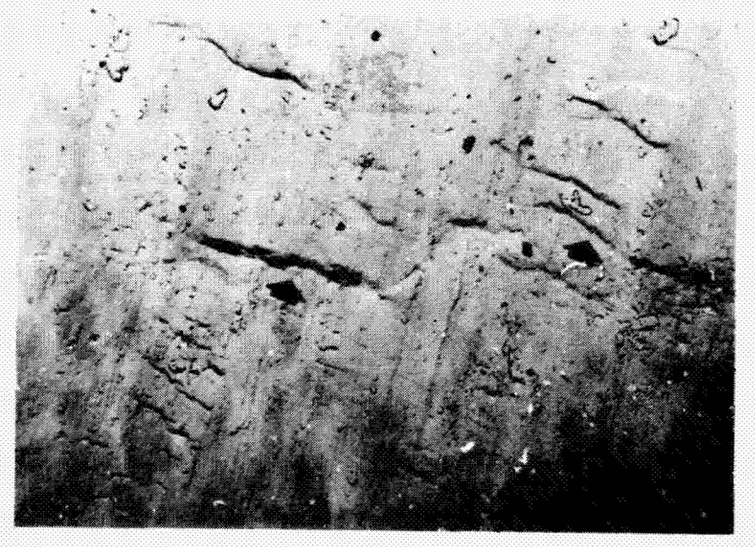

SAMPLE 3-2 Tested in H_2 gas at 50 psi pressure

Exposed to H_2 gas for 24 hours at a sustained load of 75% of the yield prior to testing.

FIGURE 7. ELECTRON MICROGRAPHS OF THE PLANE SURFACES OF THE Ti-6Al-4V TENSILE SAMPLES SHOWING LOCALIZED AREAS OF HIGH PLASTIC STRAIN. MAGN: 4000X

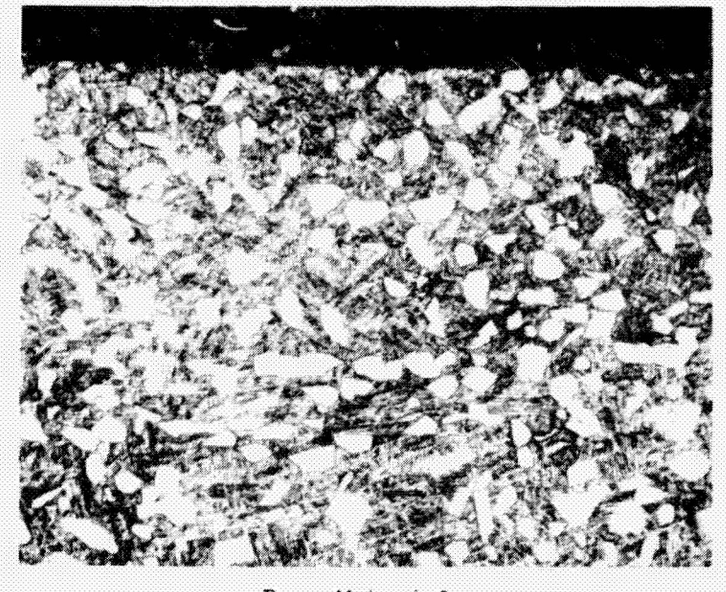

Base Material

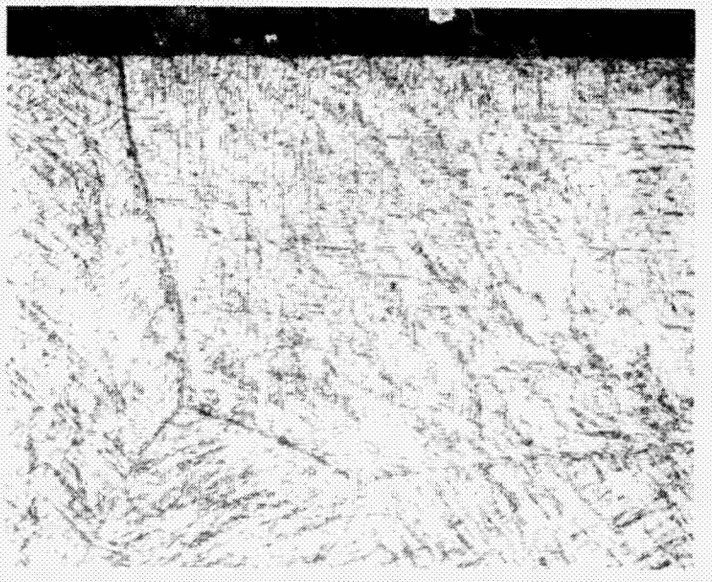

Weld Material

SAMPLE 3-2 Tested in H_2 gas at 50 psi pressure

Exposed to H_2 gas for 24 hours at a sustained load of 75% of the yield prior to testing.

FIGURE 8. MICROSTRUCTURE OF Ti-6Al-4V TENSILE SAMPLE SHOWING A CROSS-SECTION THROUGH THE SURFACE EXPOSED TO HYDROGEN GAS. MAGN: 300X

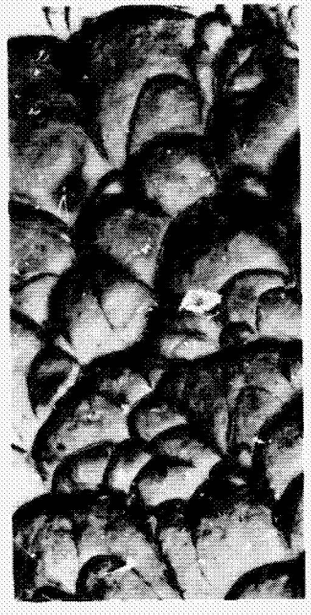

SAMPLE [illegible]

He gas at [illegible] psi

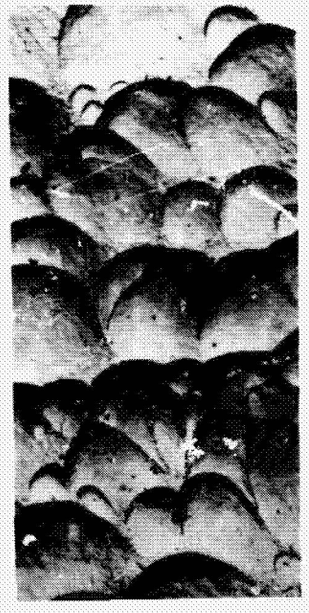

SAMPLE 5-6

H_2 gas at 14.7 psi

SAMPLE 5-4

H_2 gas at 50 psi

SAMPLE 5-13

H_2 gas at 14.7 psi

Exposed to H_2 gas for 24 hours at a sustained load of 75% of the yield prior to testing.

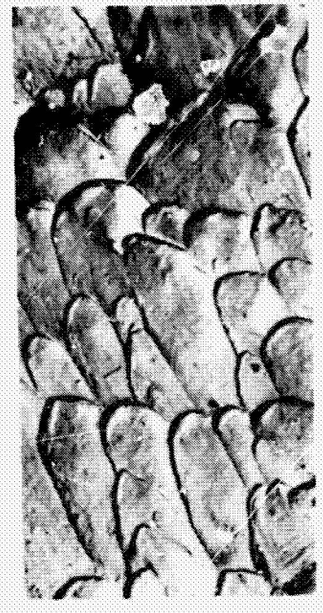

SAMPLE 5-10

H_2 gas at 50 psi

Exposed to H_2 gas for 24 hours at a sustained load of 75% of the yield prior to testing.

FIGURE 9. FRACTURE SURFACES SHOWING DIMPLE RUPTURE ON THE TENSILE SAMPLES PREPARED FROM WELDED Ti-6Al-4V ELI FORGED PLATE. THE SAMPLES WERE TESTED AT AMBIENT TEMPERATURE UNDER THE INDICATED TEST CONDITIONS. MAGN: 4000X

and analyzed for hydrogen. The results of the hydrogen analysis are given in Table 4. The data shows that the tensile samples did not absorb a substantial amount of hydrogen as a result of testing in a hydrogen atmosphere.

		Test Conditions		Hydrogen PPM	
Sample No.	Gas	Absolute Pressure PSI	Exposure Time Hours	Base Metal	Weld Area
5- 3	He	14.7	0	236	243
5- 6	H_2	14.7	0	211	221
5- 4	H_2	50	0	236	192
5-13	H_2	14.7	24*	222	230
5-10	H_2	50	24*	224	217
STD	215 ppm NBS standard			237	

*Sustained Load, 75% of the yield strength

Table 4

HYDROGEN ANALYSIS OF FRACTURED TENSILE SAMPLES.

The validity of using filings was determined by preparing a specimen from pure titanium containing 215 ppm of hydrogen as certified by the National Bureau of Standards. It was found that the filings contained 237 ppm of hydrogen. Additional specimens were tested and it was estimated that the accuracy in using filings was approximately $\pm$ 15%.

The average hydrogen content of the chemically milled forgings was previously shown to be 80 ppm, however, Table 4 indicates that the material contained a higher concentration of hydrogen. This difference may be associated with the locations in the forgings where the hydrogen analyses were made. The gas analysis samples taken after the chemical milling operation were removed from the edges of the forgings while the samples shown in Table 4 were removed from the center sections. During chemical milling, localized heating in the longitudinal center sections of the forgings resulted in a faster erosion

rate in these areas as compared to the longitudinal edges. This localized heating could have resulted in an increase in the hydrogen content in the center sections as compared to the edges of the forgings.

Conclusions

The data tabulated in Tables 2 and 3 show that there was no gross change in the tensile properties of forged and welded, oxide free Ti-6Al-4V ELI as a result of testing in hydrogen gas. The post test analysis, also, did not show conclusive evidence of a hydrogen-titanium reaction. There was, however, a slight decrease (approximately 1 to 3%) in the tensile properties for those samples tested in hydrogen gas regardless of the additional testing parameters.

TASK III -- FATIGUE TESTS

Experimental Procedure

Sample Preparation

The fatigue test samples were prepared by using the same material and sample configuration used in the tensile test program. Prior to testing in a controlled atmosphere, each sample was fatigue cracked in air. A 0.005 inch by 0.025 inch slot was machined through each sample in the area to be tested by using the electrical discharge machining method. To test the (STA) material, the slots were placed 0.300 inches above the center of the welds on the longitudinal center line of the samples. In the weld samples, the slots were positioned in the center of the welds. The samples were then fatigued in air using tension-tension loading until a 0.050 inch long crack formed through the slots. The primary purpose of the precrack was to produce a consistent starting point for the crack propagation tests.

The growth of the precracks through the machined slots was found to be inconsistent, particularly in the weld material. Crack length measurements made on opposite sides of each sample differed in some instances by approximately 0.015 inches. This condition was corrected by flexure fatiguing the discrepant samples in such a way as to promote crack growth only on the side of the sample that contained the short crack. This procedure resulted in uniform cracks through the thickness of the samples; however, the total crack length often exceeded the desired total length of 0.050 inches. Therefore, the precracks in all of the samples ranged in total length between 0.049 inches and 0.067 inches.

An accurate determination of the size and shape of the precrack can only be made by viewing the samples' fracture surfaces after failure. The precrack areas, however, could not be easily distinguished after the samples failed. To promote visual identification of the precrack areas, the precrack fracture surfaces were heat-tinted using the following procedure. Following precracking and prior to controlled atmosphere fatigue testing, the samples were heat treated at 600°F for 10 minutes in air.

Evaluation of Crack Length Measuring Technique

The determination of crack growth rates under fatigue loading requires measuring the crack lengths as a function of the applied cycles. Numerous methods have been used for measuring the change in crack length including microscopic examination, the use of crack propagation gages, surface staining, and electrical potential measurements. All of these methods have definite limitations in accuracy and ease of employment. The electrical potential method is the most versatile of those cited and it is the particular method which is most compatible with the present test conditions. The advantage of using this technique is that the change in crack length can be monitored while the sample is enclosed in a container having a controlled atmosphere at a constant temperature.

The electrical potential method for measuring crack growth has been used by several investigators.[46,47,48] This technique consists of passing a constant current through a precracked specimen and measuring the change in electrical potential across the crack interface as the crack extends, Figure 10. Under suitable conditions, an incremental change of 0.002 inches in crack length can be detected.[49] However, it has been found by most investigators that relatively large samples (approximately 3 inches wide) and high sample currents (approximately 20 amps) were necessary to obtain the desired accuracy. Since the existing samples machined from the Ti-6Al-4V forgings contained a relatively small reduced section (0.032 inches by 0.500 inches), an evaluation of the electrical potential method was necessary to determine if this technique could be used.

It was shown by Johnson[49] that for a razor-thin crack of length (2a), the potential difference (V) between two points at a distance (y) above and below the crack is a function of the half-crack length (a) and specimen width (w), Figure 10.

$$V \sim \text{Cosh}^{-1} \left(\frac{\cosh \pi y/w}{\cos \pi a/w}\right) \qquad (1)$$

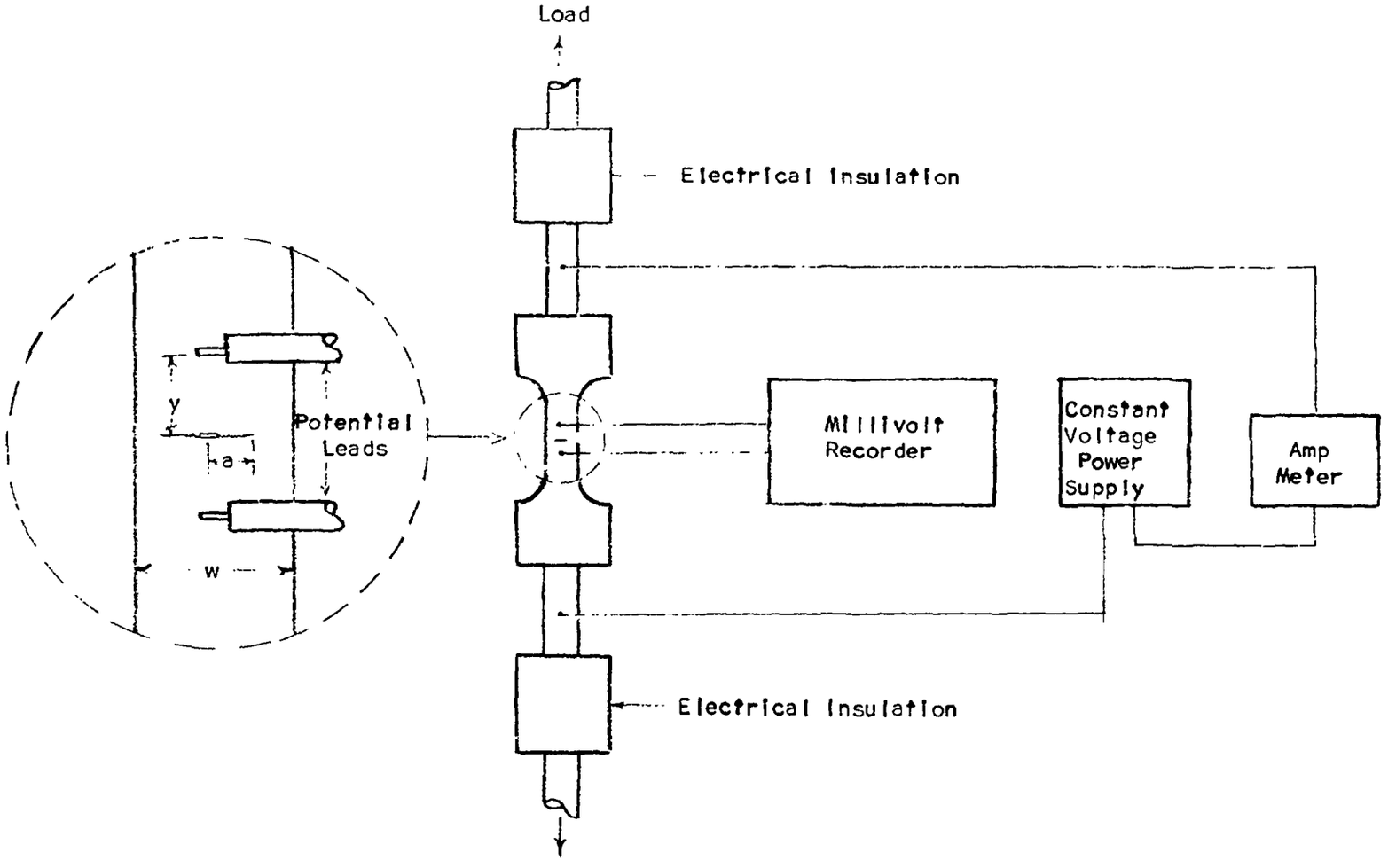

FIGURE 10. SCHEMATIC OF TEST SETUP FOR MEASURING CRACK GROWTH USING THE ELECTRICAL POTENTIAL TECHNIQUE.

To eliminate the proportionality constant, it is convenient to consider the potential ratio V/V_o where V_o is the potential across the initial crack.

$$\frac{V}{V_o} = \frac{\cosh^{-1}\left(\frac{\cosh \pi y/w}{\cos \pi a/w}\right)}{\cosh^{-1}\left(\frac{\cosh \pi y/w}{\cos \pi a_o/w}\right)} \qquad (2)$$

The above equation was programmed into a computer to obtain calibration curves. Using a sample width (w) of 0.500 inches and an initial crack size (2a) of 0.050 inches, the potential lead distance (y) was varied. The computer calculated curves presented in Figure 11 show the effect of changing the potential lead distance (y). An optimum balance between accuracy and sensitivity is achieved by using a (2a) value of 0.100 inches. Since a deviation of 0.010 inches in locating the potential leads on the sample will result in a significant shift in the calibration curve, the distance between the potential leads must be accurately measured.

Calibration samples were tested using the test setup shown in Figure 10. The potential leads were spot-welded on to the sample and the distances between the leads were accurately measured by using a microscope and micrometer stage. During the fatigue test, a constant D.C. current was passed through the sample. The change in electrical potential across the crack interface was monitored by using a millivolt recorder. The samples were fatigued at a rate of 500 cycles/min. under tension-tension loading using an upper stress of 30 KSI and a lower stress of 3 KSI. Cycling was stopped periodically and the actual crack lengths were measured by using a calibrated microscope.

The results of the calibration samples are shown in Figures 12 through 14. The experimental data points in Figures 12 and 13 were obtained by using Ti-6Al-4V (STA) sheet material, a sample current of one amp, and a distance between potential leads of 0.100 inches. The theoretical curves were established by using the computer program and the necessary measurements of the test samples. At ambient temperature, Figure 13, it was found that the theoretical curve predicted the actual crack length to an accuracy of

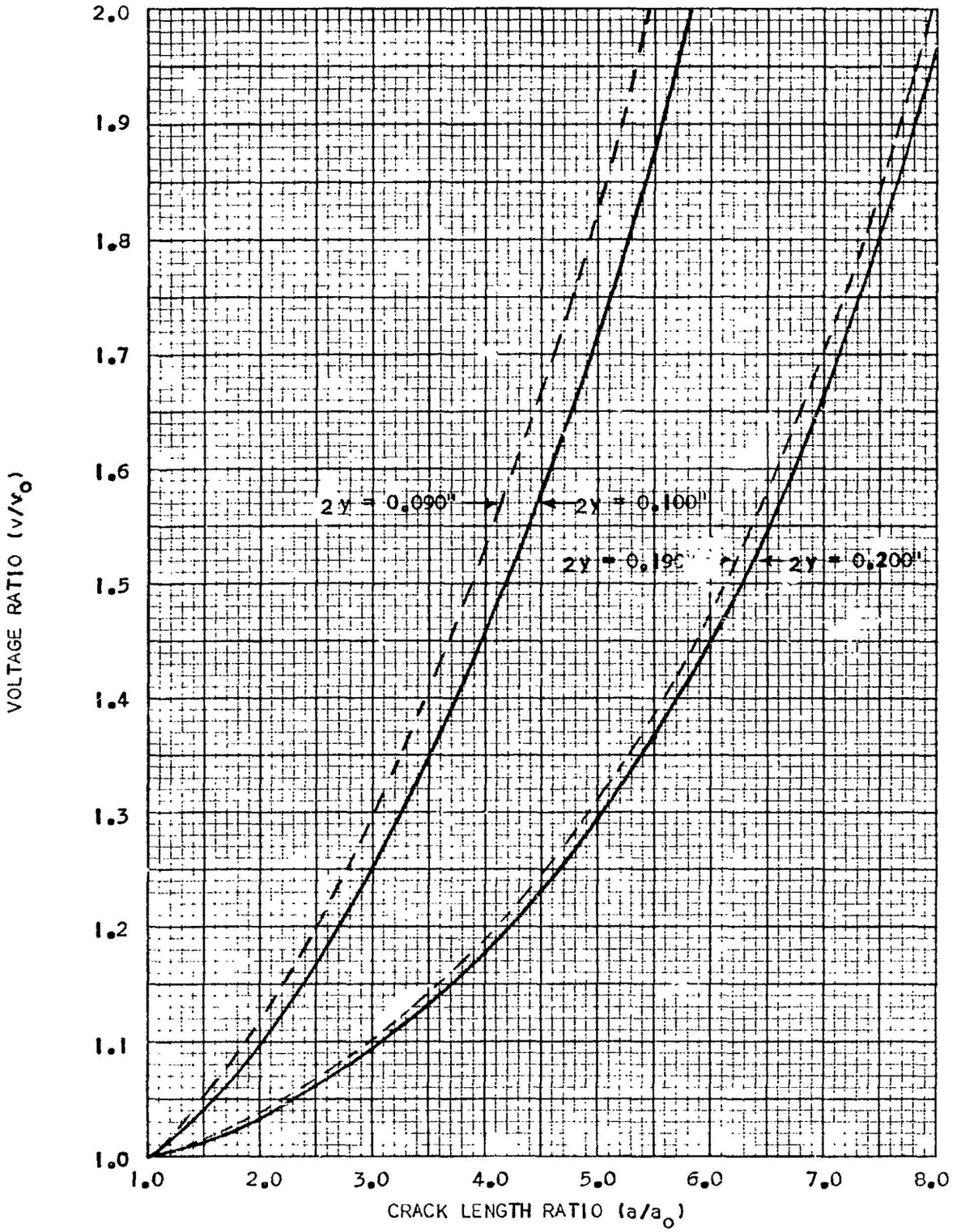

FIGURE 11. COMPUTER CALCULATED CURVES SHOWING THE EFFECT OF CHANGING THE DISTANCE (2Y) BETWEEN THE POTENTIAL LEADS ON THE SAMPLE.

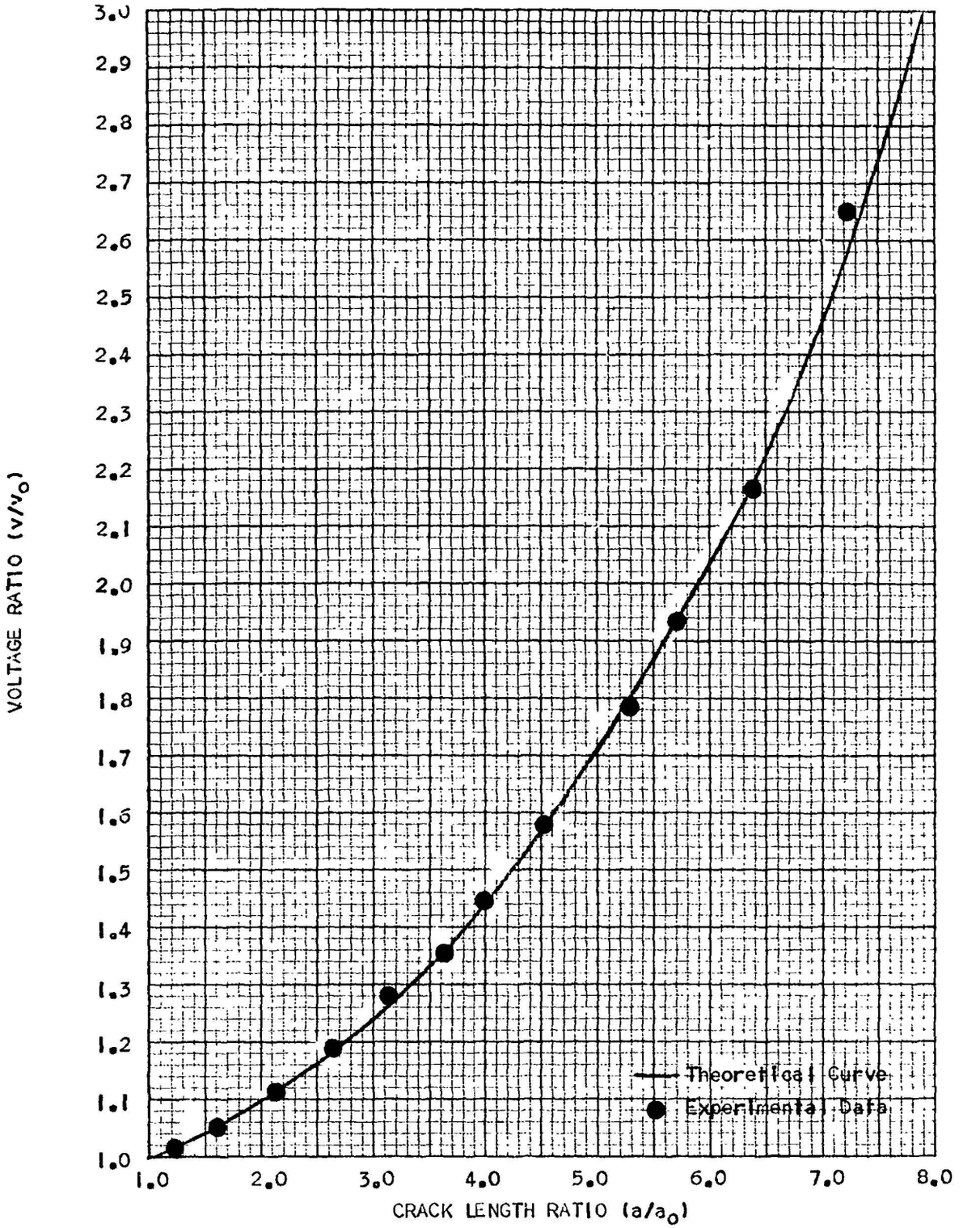

FIGURE 12. COMPARISON OF THE COMPUTER CALCULATED CURVE WITH THE EXPERIMENTAL DATA OBTAINED FOR Ti-6Al-4V IN THE (STA) CONDITION AT AMBIENT TEMPERATURE.

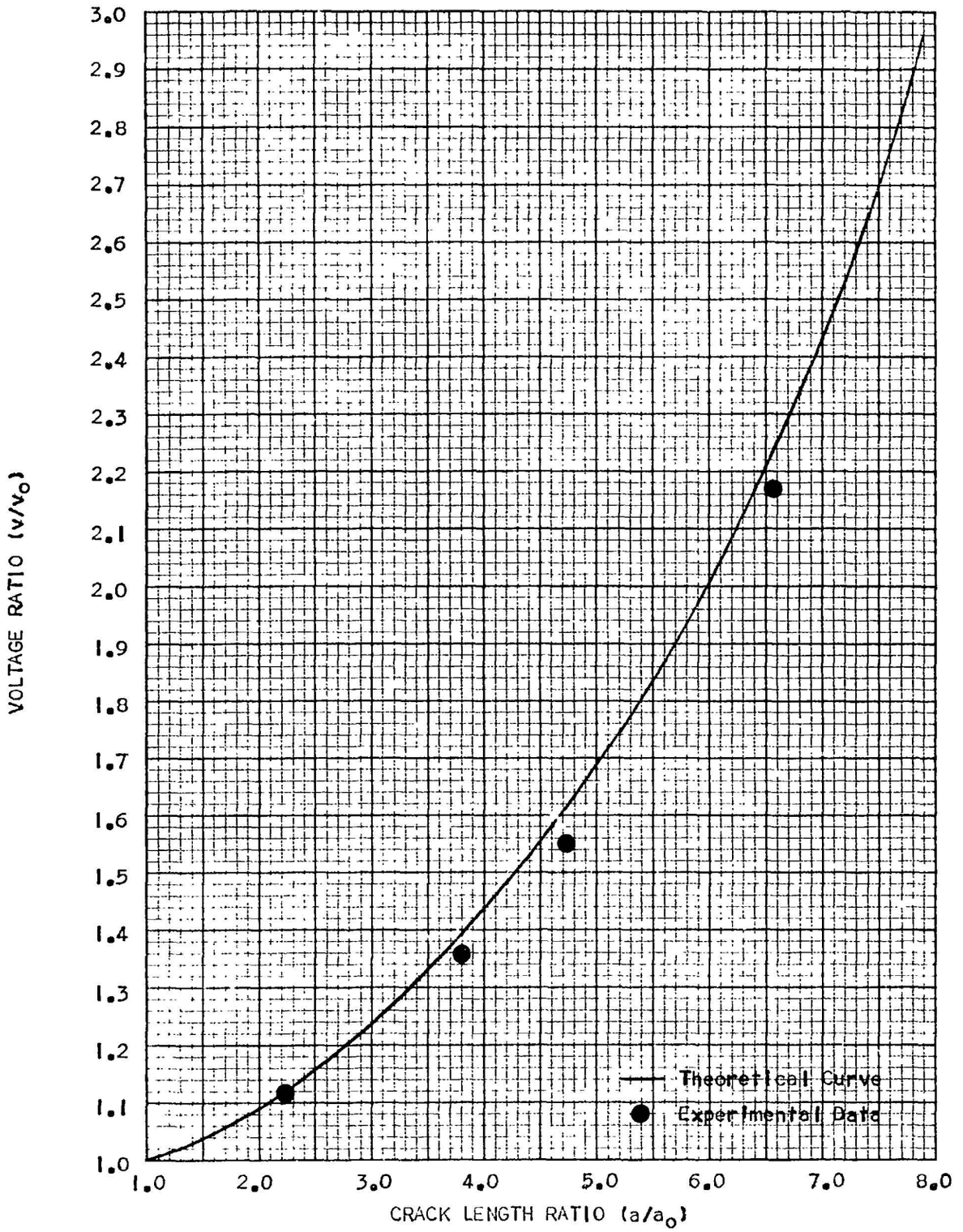

FIGURE 13. COMPARISON OF THE COMPUTER CALCULATED CURVE WITH THE EXPERIMENTAL DATA OBTAINED FOR Ti-6Al-4V IN THE (STA) CONDITION AT -200°F.

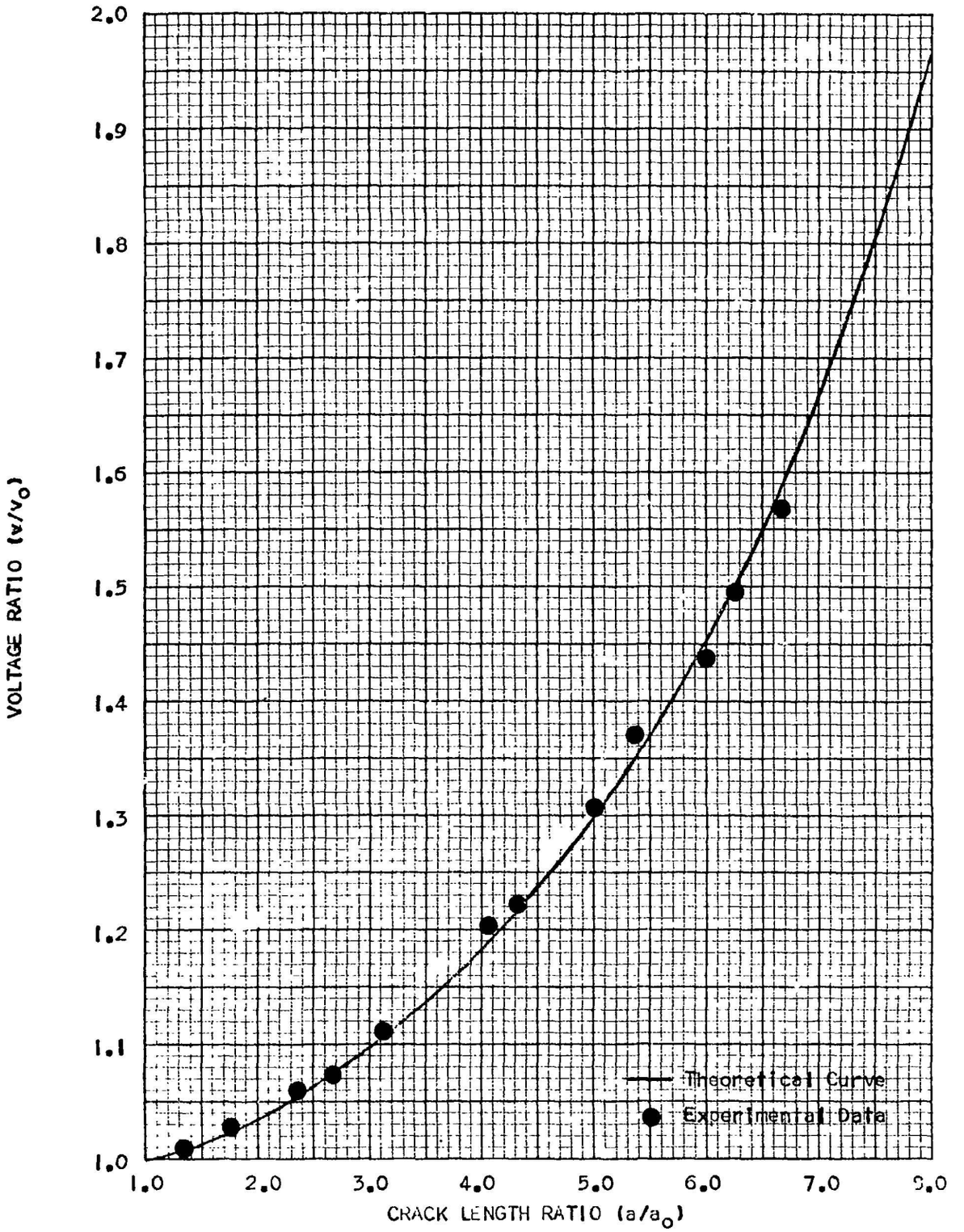

FIGURE 14. COMPARISON OF THE COMPUTER CALCULATED CURVE WITH THE EXPERIMENTAL DATA OBTAINED FOR Ti-6Al-4V WELD MATERIAL AT AMBIENT TEMPERATURE.

± 0.002 inches throughout the crack growth range. However, at -200°F the actual crack lengths were approximately 0.010 inches larger than that predicted by the theoretical curve, Figure 13.

The data in Figure 14 was obtained for a weld sample using a sample current of 0.5 amps and a distance between potential leads of 0.200 inches. Although these test conditions resulted in lower sensitivity and accuracy, good agreement was found between the theoretical curve and the experimental data.

It can be concluded from the above data that the analytical solution derived for a razor-thin crack agrees with the experimental crack growth curves for Ti-6Al-4V sheet samples throughout the crack growth range. In addition, the accuracy of this method of analysis is not significantly affected by differences in the samples' microstructure (weld and (STA) material) or temperature (70 to -200°F).

Equipment

The test chambers used in the tensile test program were modified for use with the fatigue test samples, Figure 15. Vacuum tight feed-throughs were welded into the side of the chambers for installation of the potential leads. It was also necessary to electrically insulate one end of the sample chambers. This was accomplished by using viton gaskets, vacuum flange hold-down rings made of plexiglass, and an insulating block in the external load train.

Evaluation of Test Conditions

Preliminary tests were conducted on Ti-6Al-4V sheet specimens in the (STA) condition to determine the effect of hydrogen pressure (14.7 psi and 50 psi absolute) on the crack growth rate. Since both hydrogen pressures were of interest and limited forging samples were available for testing, it was desired to use a hydrogen pressure that would yield the most useful information. It would be expected that the higher hydrogen pressure would have the greatest tendency to promote a hydrogen-titanium reaction. However, if the effect of the higher hydrogen pressure on the crack growth rate is negligible, testing of the samples would be simplified by using the lower hydrogen pressure of 14.7 psi.

FIGURE 15. FATIGUE SAMPLE TEST CHAMBER.

Three precracked samples of the Ti-6Al-4V sheet material were fatigue tested at ambient temperature using a maximum stress of 30 KSI, a minimum stress of 3 KSI and a cycle rate of 50 cycles/min. The samples were tested in atmospheres of 14.7 psi of helium, 14.7 psi of hydrogen and 50 psi of hydrogen gas. The results of these tests are given in Figure 1. The curves show that hydrogen gas at ambient pressure does increase the crack propagation rate in Ti-6Al-4V (STA); however, at a hydrogen pressure of 50 psi an even greater increase in the crack growth rate results. As a result of these tests, the Ti-6Al-4V forging samples were tested at hydrogen pressures of 50 psi (absolute).

Test Procedure

The following test procedure was established for testing the precracked Ti-6Al-4V ELI forging samples. Electrical potential leads were spot welded on the sample at a distance of 0.050 inches above and below the crack. The distance between the potential leads was measured using a microscope and micrometer stage. After sealing the sample in the test chamber, the chamber was installed in the fatigue machine. The sample chamber was purged by evacuating the system to 10^{-1} torr and back filling with the desired gas a minimum of 10 times. The test chamber was then filled with the desired gas at 50 psi absolute pressure and cooled to the test temperature. The sample was fatigue tested using an upper stress of 30 KSI, a lower stress of 3 KSI and a cycle rate of 500 cycles/min. During testing, a continuous record was made of the change in potential across the crack interface as a function of the applied cycles. Immediately after failure, the size of the precrack was measured and the sample placed in liquid nitrogen for storage. Using the precrack size, sample width, and potential lead distance, a V/V_o vs a/a_o calibration curve was computed for the sample. The actual crack length as a function of the applied cycles was determined using the calibration curve and the potential measurements obtained during testing.

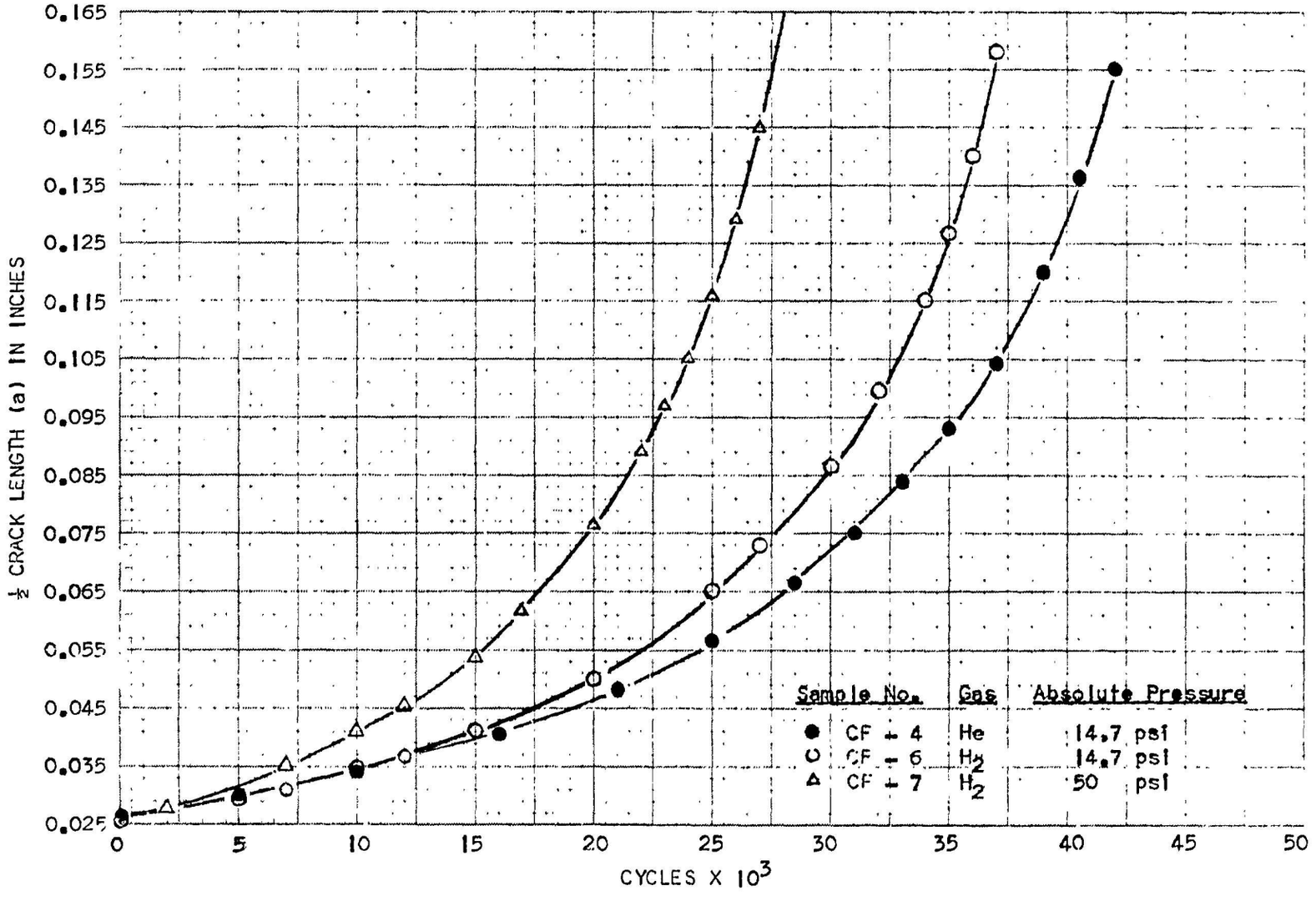

FIGURE 16. CRACK PROPAGATION DATA FOR Ti-6Al-4V (STA) SHEET MATERIAL TESTED AT AMBIENT TEMPERATURE SHOWING THE EFFECT OF H_2 PRESSURE.

Experimental Results

Fatigue Tests

The fatigue crack propagation tests were conducted on forged Ti-6Al-4V ELI (STA) and weld material under the environmental conditions shown in Table 5. A tabulation of the fatigue crack propagatior data for the samples shown in Table 5 is given in Appendix A. The data was adjusted to eliminate the initial fatigue cycles that did not contribute to crack growth by making (0) cycles coincide with the onset of crack growth. The number of cycles required to start the cracks growing ranged from 1,000 to 6,000 cycles.

The fatigue crack propagation data in Appendix A was analyzed using the following procedure. Accurate curves were made of the half crack lengths as a function of the applied cycles for each sample in Appendix A. The actual crack growth rates (da/dn) were determined by measuring the slopes of the curves at selected crack lengths. Using the half crack length and the following equation, the stress intensity range (ΔK) at the tip of the crack was calculated for each crack growth rate.[50]

$$\Delta K = \Delta\sigma \, (\pi c)^{1/2} \tag{3}$$

where

$\Delta\sigma$ = range of gross section stress

$c = \ell(w/\pi a \tan \pi a/w)$ = half crack length in an infinite sheet (4)

a = actual half crack length

w = sample width

The equivalent crack growth rates for an infinitely wide sheet (dc/dn) were determined by using the actual crack growth rates (da/dn) and the following relationship obtained by differentiating Equation (4).[51]

$$\frac{dc}{dn} = \frac{da}{dn} \sec^2 \frac{\pi a}{w} \tag{5}$$

In Appendix B, the actual and equivalent crack growth rates are tabulated for various crack tip stress intensity ranges.

SAMPLE NO.	TEMPERATURE °F	TEST CONDITIONS ATMOSPHERE	MATERIAL
1-9	Ambient	H_e	STA
1-4	Ambient	H_e	STA
1-5	Ambient	H_2e	STA
1-6	Ambient	H_2	STA
2-7	Ambient	H_e	Weld
2-2	Ambient	H_e	Weld
2-10	Ambient	H_2e	Weld
2-5	Ambient	H_2	Weld
4-6	0	H_e	STA
4-9	0	H_e	STA
4-7	0	H_2e	STA
1-11	0	H_2	STA
2-13	0	H_e	Weld
4-2	0	H_e	Weld
2-12	0	H_2e	Weld
3-13	0	H_2	Weld
4-8	-100	H_e	STA
1-7	-100	H_e	STA
1-1	-100	H_2e	STA
1-10	-100	H_2	STA
3-10	-100	H_e	Weld
2-8	-100	H_e	Weld
2-11	-100	H_2e	Weld
4-12	-100	H_2	Weld
1-2	-200	H_e	STA
4-4	-200	H_e	STA
1-12	-200	H_2e	STA
4-11	-200	H_2	STA
2-6	-200	H_e	Weld
3-12	-200	H_e	Weld
4-10	-200	H_2e	Weld
4-3	-200	H_2	Weld

Table 5

TABULATION OF TEST CONDITIONS FOR THE CRACK PROPAGATION TEST SAMPLES.

The equivalent crack growth rates are shown in Figures 17 through 24 as a function of the stress intensity range for the (STA) and weld material tested in both hydrogen and helium gas. It was found that the crack growth rate in helium gas could be expressed by the following empirical relationship.[52]

$$\frac{dc}{dn} = A(\Delta K)^N \qquad (6)$$

The value of the exponent (N) was approximately (4) for all of the helium gas samples. The samples tested in hydrogen gas, however, did not show a simple power function between $(dc/dn)_{H_2}$ and (ΔK).

The fatigue crack growth rate curves clearly show that hydrogen gas increases the crack growth rate in Ti-6Al-4V ELI (STA) and weld material in the temperature range of ambient to -100°F. In addition, the curves indicate that the magnitude of the increase in crack growth rate is dependent on the microstructure, stress intensity range, and temperature. These parameters and their effects on the crack growth rate in hydrogen gas are examined in the following discussion.

The degree of crack growth enhancement caused by hydrogen gas was determined at various crack tip stress intensity ranges by dividing the crack growth rate in hydrogen by that obtained in helium, Table 6. This data is shown graphically in Figures 25A and 25B. The curves show that the degree of embrittlement at each temperature for both materials changes significantly with (ΔK). At ambient temperature the crack growth rate ratios for both the (STA) and weld material increase with increasing (ΔK) to maximum values of 2.5 and 3.5 respectively. As (ΔK) continues to increase, the (STA) material remains at a constant crack growth rate ratio of 2.5 but the weld material ratio decreases rapidly to 1.2. These curves indicate that at ambient temperature and low crack tip stress intensity ranges, the weld material is more susceptible to hydrogen enhanced crack growth than the (STA) material. However, at high stress intensity ranges, the (STA) material is more susceptible to embrittlement. At decreasing test temperatures, both materials show a decreasing degree of embrittlement, particularly at the high crack tip stress intensity ranges.

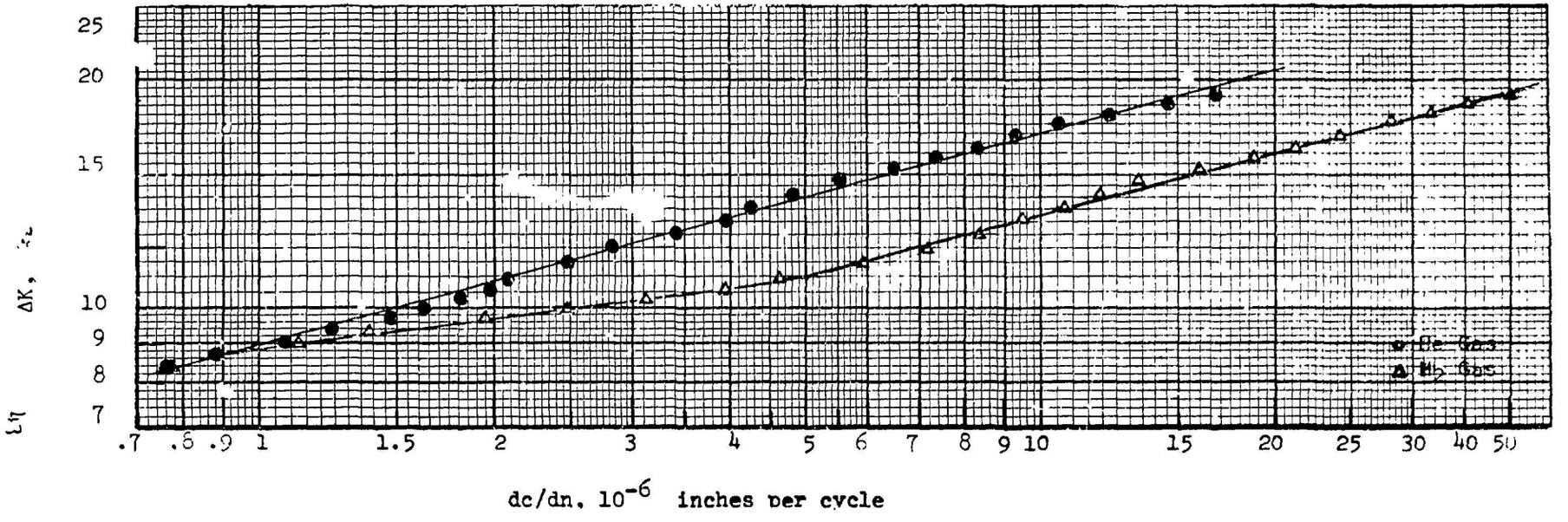

FIGURE 17. RATE OF FATIGUE CRACK PROPAGATION IN Ti-6Al-4V ELI FORGED MATERIAL TESTED IN THE (STA) CONDITION AT AMBIENT TEMPERATURE.

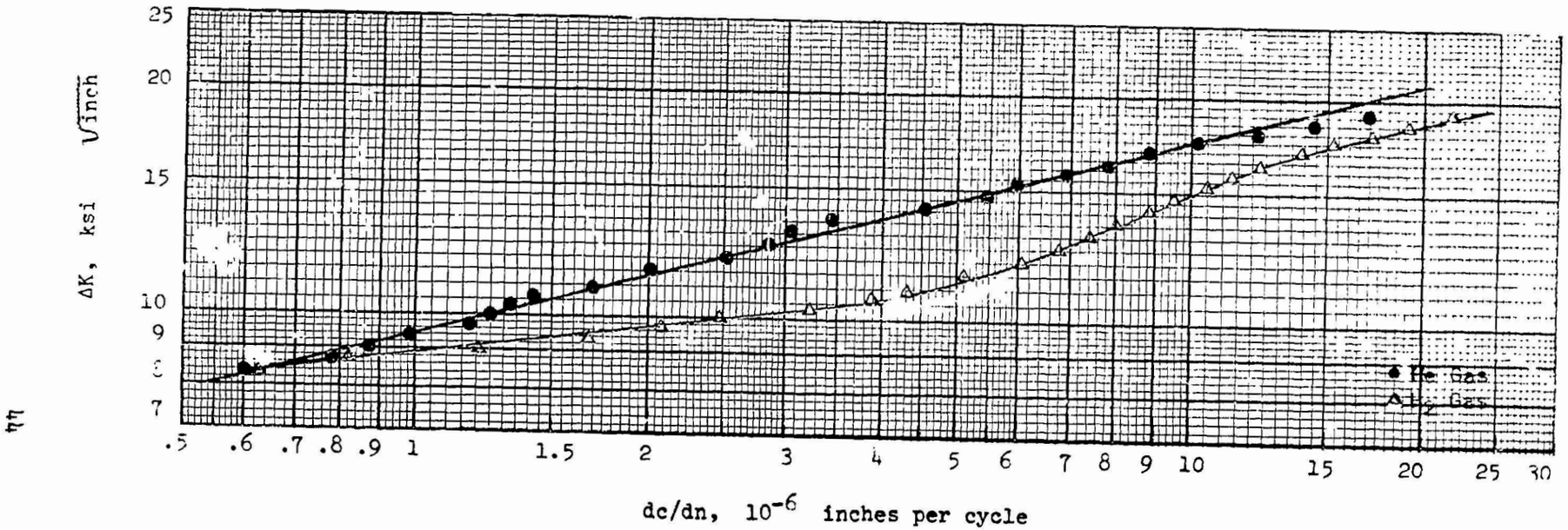

FIGURE 18. RATE OF FATIGUE CRACK PROPAGATION IN Ti-6Al-4V ELI FORGED MATERIAL TESTED IN THE (STA) CONDITION AT 0°F.

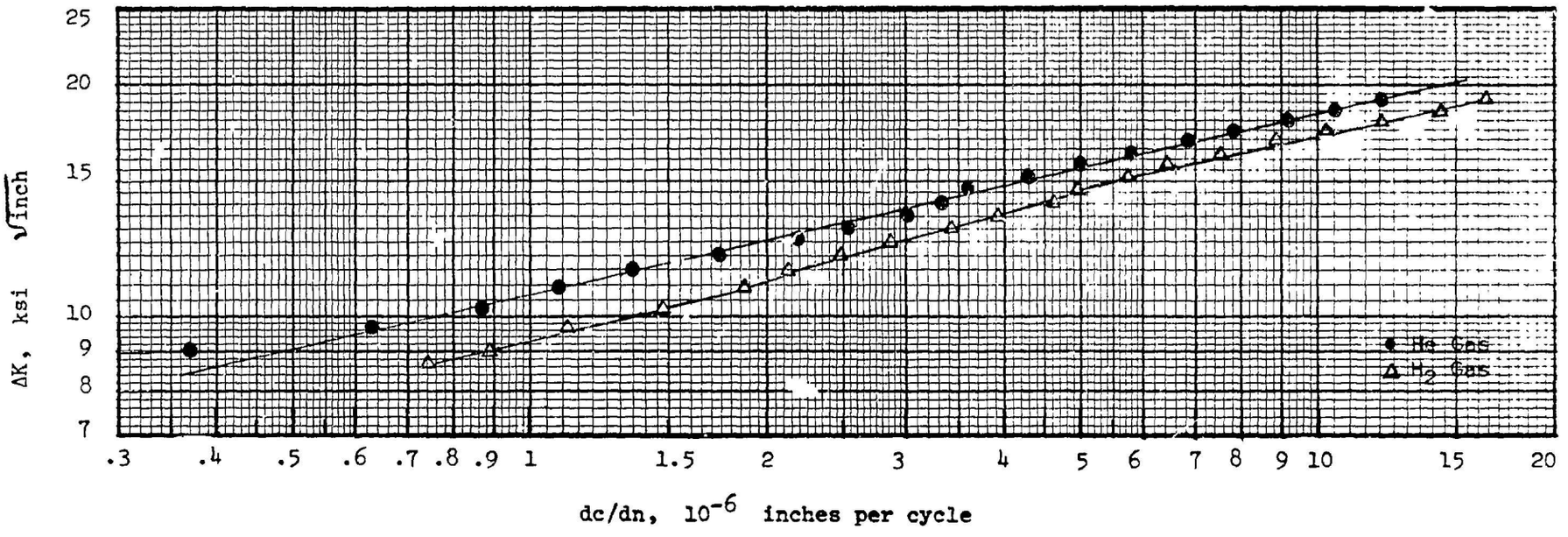

FIGURE 19. RATE OF FATIGUE CRACK PROPAGATION IN Ti-6Al-4V ELI FORGED MATERIAL TESTED IN THE (STA) CONDITION AT -100°F.

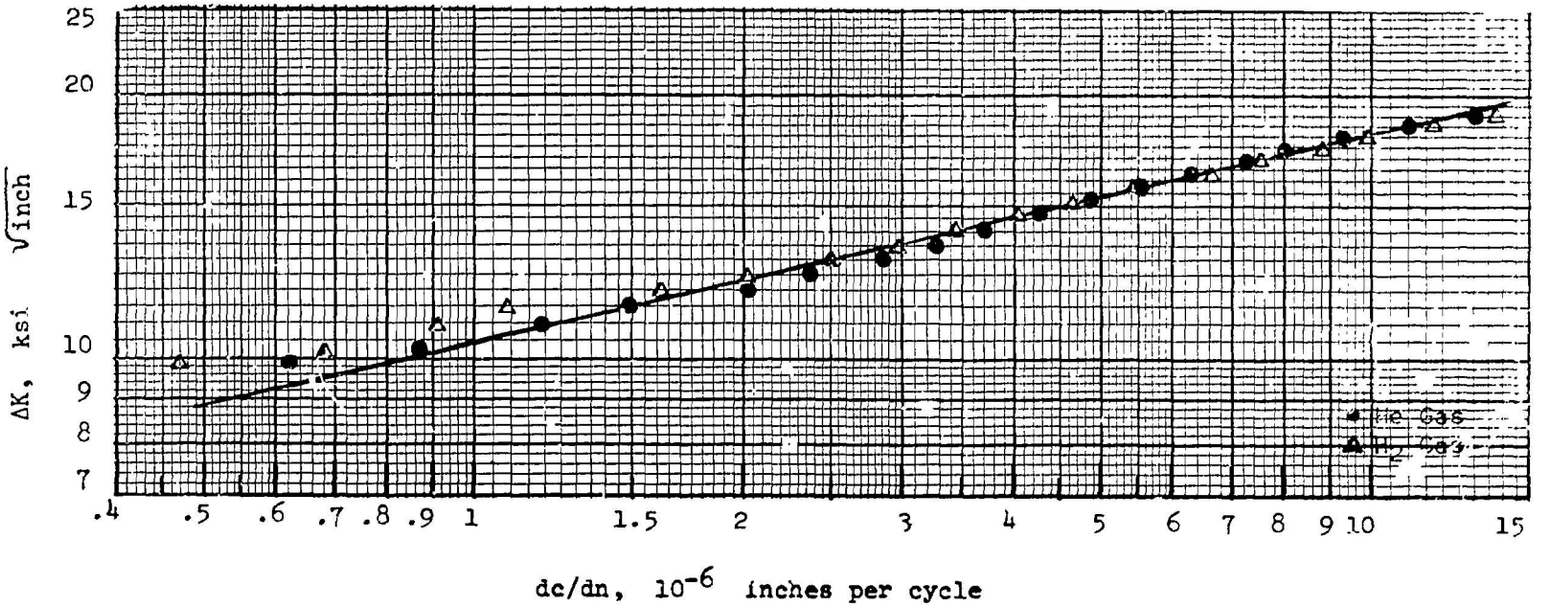

FIGURE 20. RATE OF FATIGUE CRACK PROPAGATION IN Ti-6Al-4V ELI FORGED MATERIAL TESTED IN THE (STA) CONDITION AT -200°F.

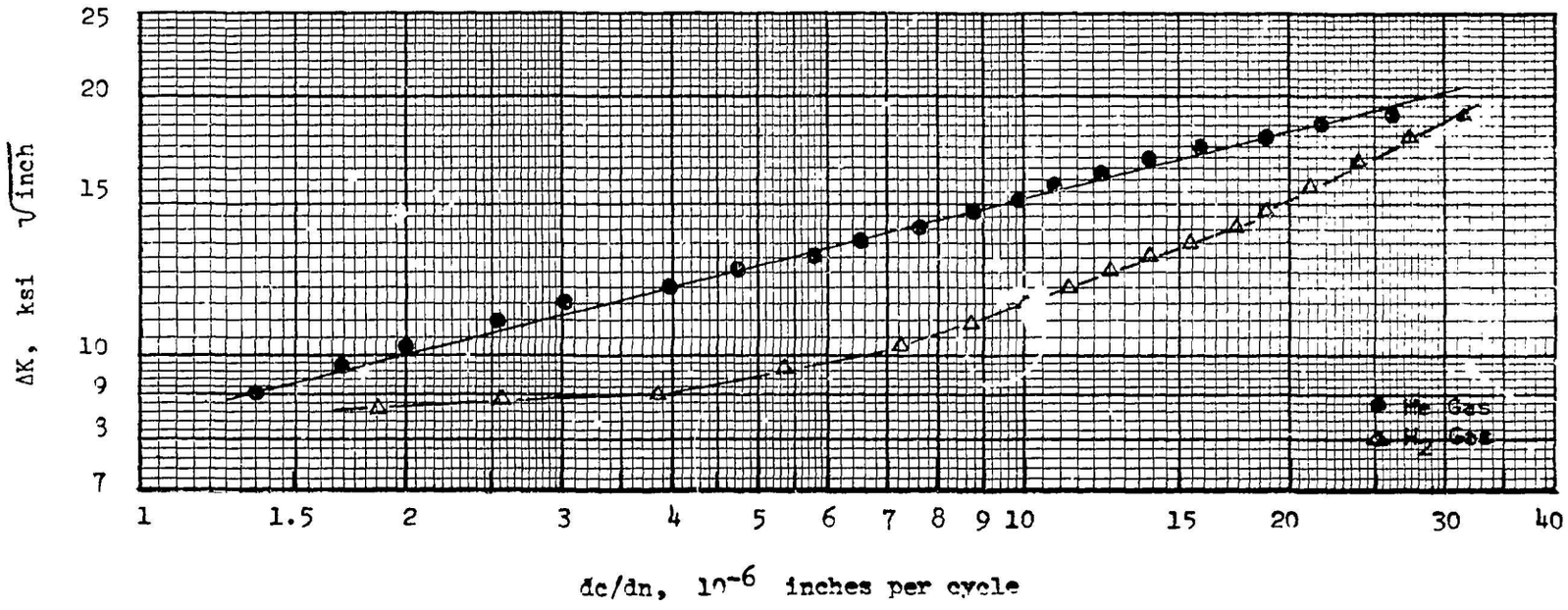

FIGURE 21. RATE OF FATIGUE CRACK PROPAGATION IN Ti-6Al-4V ELI FORGED MATERIAL TESTED IN THE WELD AREA AT AMBIENT TEMPERATURE.

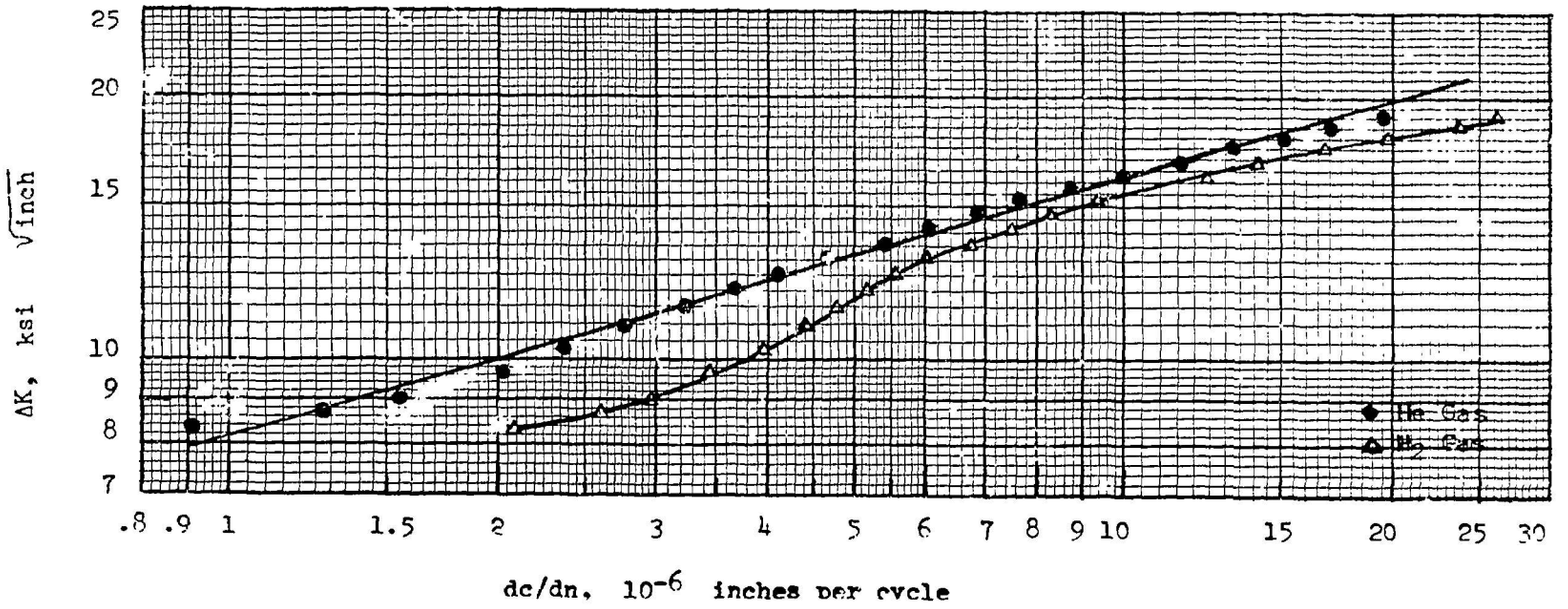

FIGURE 22. RATE OF FATIGUE CRACK PROPAGATION IN Ti-6Al-4V ELI FORGED MATERIAL TESTED IN THE WELD AREA AT 0°F.

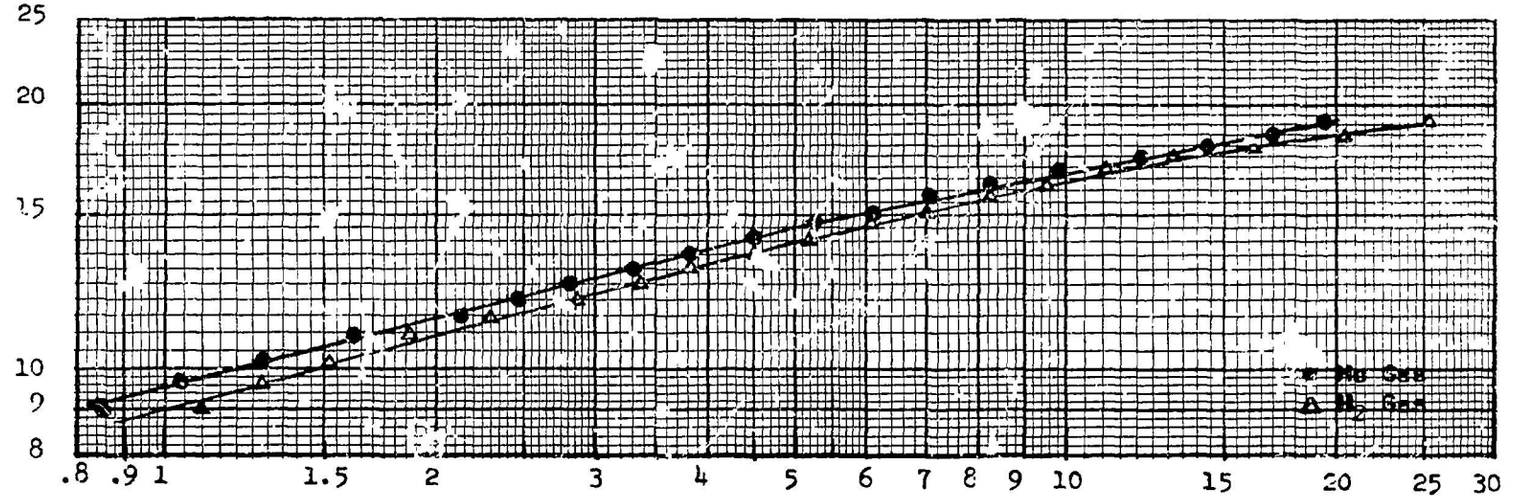

FIGURE 23. RATE OF FATIGUE CRACK PROPAGATION IN Ti-6Al-4V ELI FORGED MATERIAL TESTED IN THE WELD AREA AT -100°F.

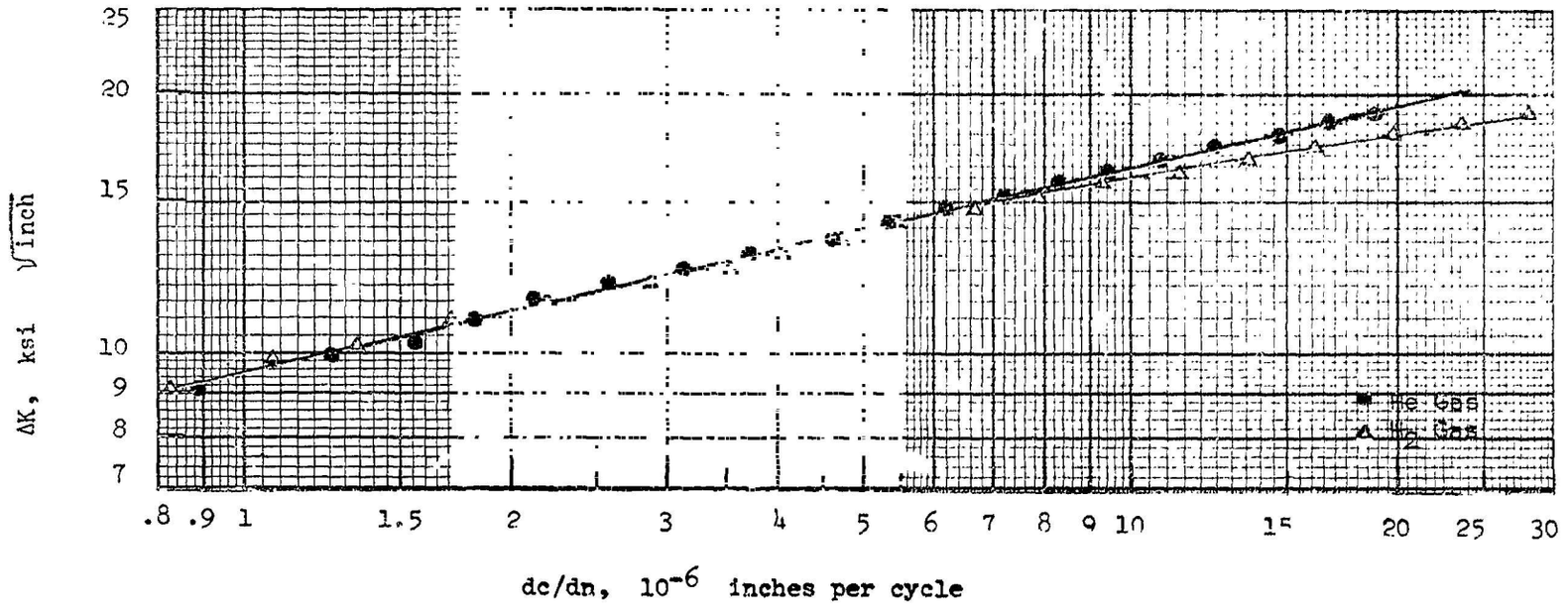

FIGURE 24. RATE OF FATIGUE CRACK PROPAGATION IN Ti-6Al-4V ELI FORGED MATERIAL TESTED IN THE WELD AREA AT -200°F.

ΔK KSI √in. \ Temp. °F	$(\frac{da}{dn})_{H_2}/(\frac{da}{dn})_{H_e}$ (STA) Material				$(\frac{da}{dn})_{H_2}/(\frac{da}{dn})_{H_e}$ Weld Material			
	75	0	-100	-200	75	0	-100	-200
8.34	1.03	1.05	-	-	-	2.28	-	-
8.69	1.01	1.14	-	-	-	2.04	-	-
9.03	1.05	1.39	2.40	-	2.84	1.91	1.29	.97
9.35	1.10	1.70	-	-	-	-	-	-
9.67	1.33	1.78	1.78	.76	3.18	1.72	1.22	.86
9.99	1.52	1.99	-	-	-	-	-	-
10.29	1.78	2.43	1.69	.78	3.62	1.69	1.18	.86
10.60	2.00	2.73	-	-	-	-	-	-
10.88	2.14	2.55	1.72	.76	3.45	1.59	1.15	.94
11.46	2.40	2.52	1.60	.82	3.19	1.48	1.07	1.04
12.01	2.53	2.40	1.42	.80	2.84	1.41	1.16	1.11
12.56	2.44	2.38	1.32	.85	2.62	1.36	1.19	1.12
13.10	2.44	2.19	1.35	.87	2.39	1.31	1.16	1.09
13.63	2.52	2.09	1.31	.91	2.36	1.25	1.18	1.03
14.16	2.48	1.95	1.39	.92	2.28	1.23	1.15	1.02
14.68	2.42	1.75	1.38	.94	2.14	1.21	1.16	1.07
15.21	2.45	1.76	1.35	.95	-	1.22	1.16	1.10
15.73	2.56	1.64	1.29	.98	1.95	1.22	1.17	1.12
16.27	2.55	1.56	1.30	1.04	-	1.23	1.16	1.21
16.81	2.60	1.58	1.30	1.04	1.73	1.22	1.13	1.26
17.36	2.68	1.50	1.31	1.09	-	1.26	1.10	1.29
17.93	2.58	1.40	1.33	1.06	1.45	1.31	1.12	1.34
18.50	2.43	1.33	1.36	1.06	-	1.39	1.21	1.34
19.09	2.40	1.28	1.35	1.05	1.21	1.34	1.34	1.49

Table 6

CRACK GROWTH RATE RATIOS FOR Ti-6Al-4V ELI (STA) AND WELD MATERIAL SHOWING THE EFFECT OF HYDROGEN ON THE CRACK GROWTH RATE.

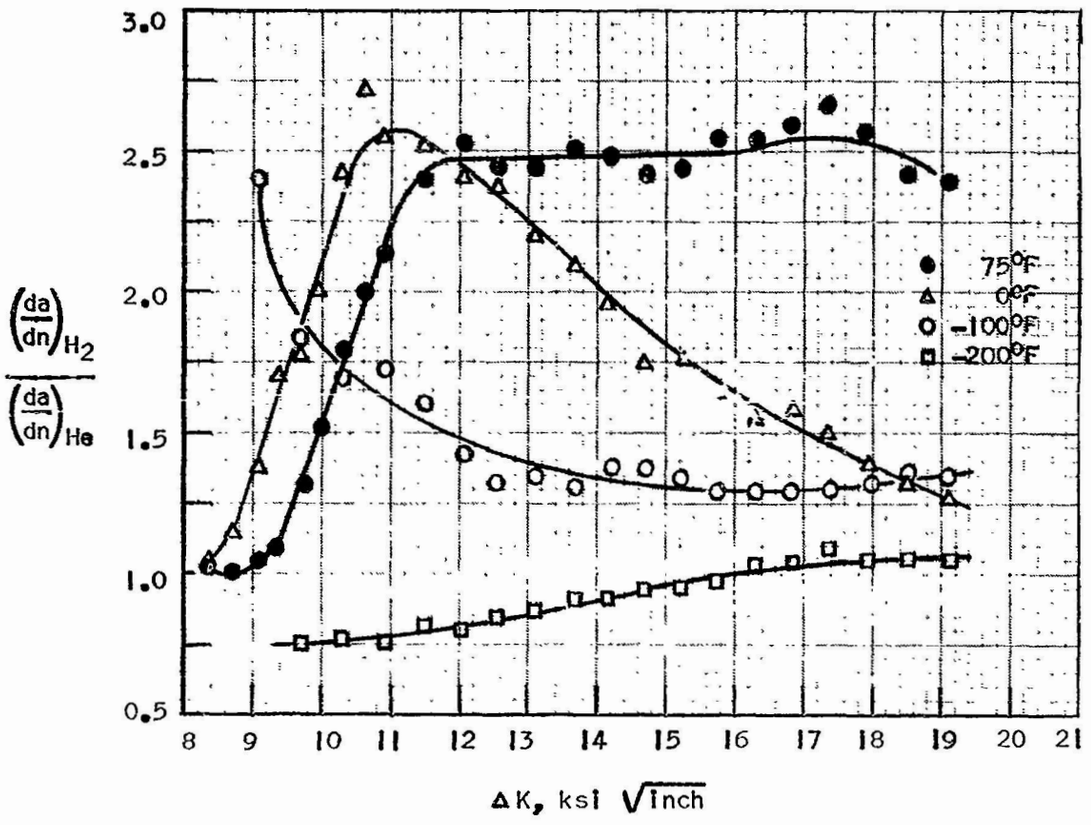

FIGURE 25A. FATIGUE CRACK GROWTH RATE RATIO CURVES FOR Ti-6Al-4V (STA) MATERIAL SHOWING THE DEGREE OF CRACK GROWTH ENHANCEMENT CAUSED BY HYDROGEN GAS.

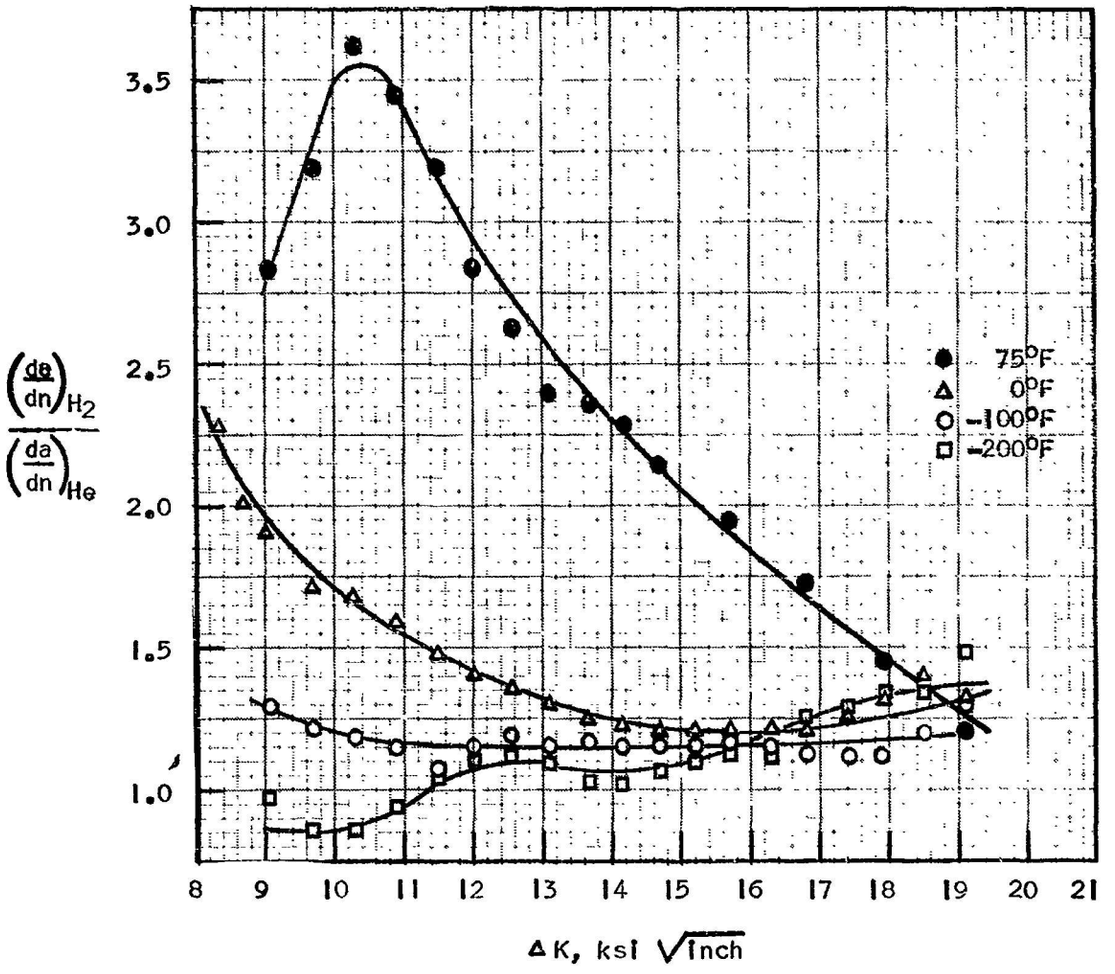

FIGURE 25B. FATIGUE CRACK GROWTH RATE RATIO CURVES FOR Ti-6Al-4V WELD MATERIAL SHOWING THE DEGREE OF CRACK GROWTH ENHANCEMENT CAUSED BY HYDROGEN GAS.

Metallography

Visual examination of the fractured (STA) samples showed that the fracture surfaces were relatively flat and contained numerous small, shiney facets, Figure 26. These facets were probably formed as a result of crack propagation occurring along alpha platelets within the material. The fracture surface shown in Figure 26 was typical of all the (STA) samples tested regardless of the test environment.

The macroscopic appearance of the fracture surfaces on the weld samples was distinctly different than that found for the (STA) samples. Crack propagation in the large grained weld material apparently occurred along specific crystallographic planes thus producing a rough, irregular fracture surface, Figure 27.

Metallographic specimens were prepared through the fracture surfaces of the samples fatigue tested at ambient temperature in hydrogen gas. The (STA) samples showed indications of hydrogen penetration initiating from the fracture surface, Figure 28. The weld samples, however, showed no evidence of hydrogen penetration in the area fatigued in hydrogen gas, Figure 29.

Fractography

(STA) Material

The fracture modes were identified for each test condition by using electron fractography. It was found that the fracture surfaces on the (STA) samples tested in helium gas were distinctly different from those obtained in hydrogen gas in the temperature range of ambient to -100°F. At ambient temperature, the sample tested in helium gas exhibited irregular fracture surfaces containing well defined fatigue striations and relatively flat plateaus, Figure 30. The sample tested in hydrogen gas, however, had fracture surfaces containing severe secondary cracking, Figure 31. This cracking appeared to be concentrated primarily along fatigue striations.

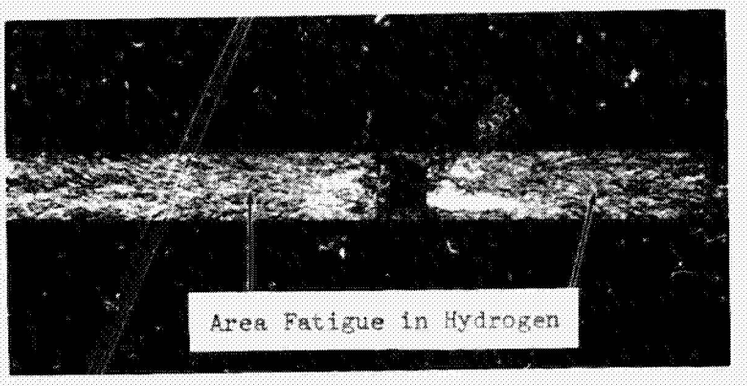

M5366 MAG: 10X

FIGURE 26. FRACTURE SURFACE OF (STA) SAMPLE 1-10 TESTED AT -100°F IN HYDROGEN GAS.

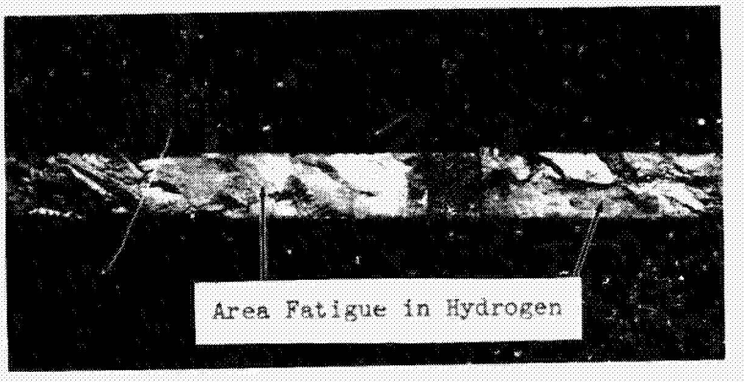

M5365 MAG: 10X

FIGURE 27. FRACTURE SURFACE OF WELD SAMPLE 2-11 TESTED AT -100°F IN HYDROGEN GAS.

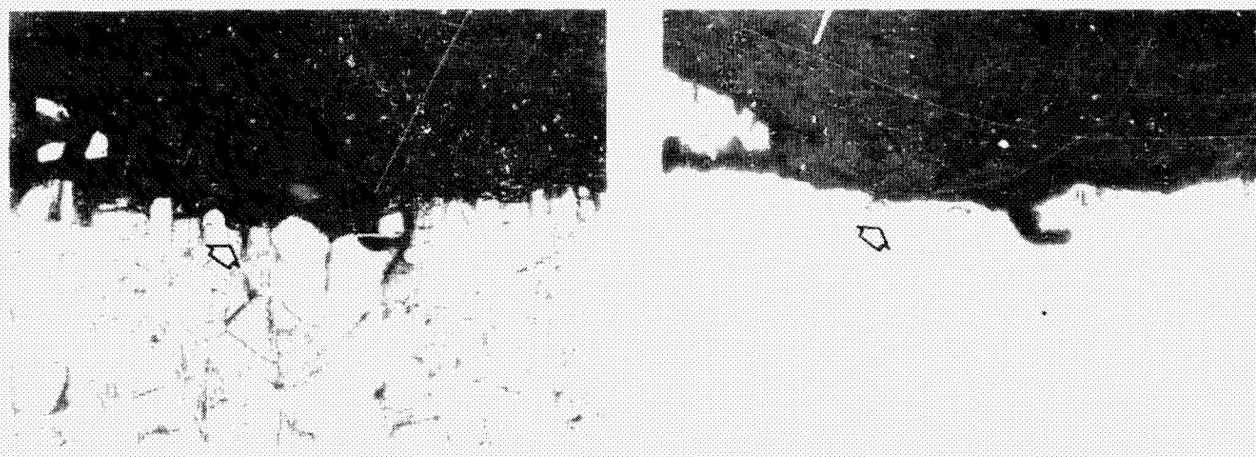

M5263 MAG: 500X M5270 MAG: 500X

Etched in Kroll's Etched Surface Partially Removed

FIGURE 28. CROSS-SECTION THROUGH FRACTURE SURFACE OF (STA) SAMPLE 1-5 FATIGUE TESTED AT AMBIENT TEMPERATURE IN HYDROGEN GAS SHOWING INDICATIONS OF HYDROGEN PENETRATION.

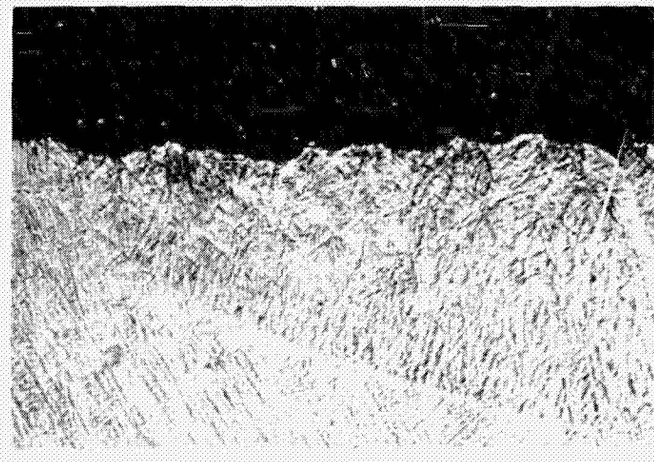

M5363 MAG: 300X

FIGURE 29. CROSS-SECTION THROUGH FRACTURE SURFACE OF WELD SAMPLE 2-10 FATIGUE TESTED AT AMBIENT TEMPERATURE IN HYDROGEN GAS SHOWING LACK OF HYDROGEN PENETRATION.

E22324

(A)

E22327

(B)

FIGURE 30. FRACTURE SURFACE OF (STA) SAMPLE 1-4 FATIGUE TESTED AT AMBIENT TEMPERATURE IN HELIUM GAS.

E22318

(A)

E22316

(B)

FIGURE 31. FRACTURE SURFACE OF (STA) SAMPLE 1-5 FATIGUE TESTED AT AMBIENT TEMPERATURE IN HYDROGEN GAS.

The fracture surfaces of the (STA) material tested at 0°F in helium gas showed primarily flat areas with faint fatigue striations, Figure 32. In some areas, shallow cracking was found presumably occurring within alpha grain boundaries, Figure 32B. The sample tested in hydrogen gas at 0°F had fracture surfaces similar to the ambient temperature sample. Numerous cracks within the fatigue striations dominated the fracture surfaces, Figure 33.

The (STA) material tested at -100°F showed the first indications of a decreasing hydrogen-titanium reaction. In helium gas, the fracture surfaces were irregular and in some areas seem to follow crystallographic features in the material, Figure 34. Faint discontinuous fatigue striations were also found in numerous areas. The fatigue surface of the sample tested in hydrogen gas is shown in Figure 35. In most areas, the fracture surfaces were rough with some cracking occurring along crystallographic features, Figure 35A. Only isolated areas were found that contained fatigue striation cracking, Figure 35B.

The crack growth rate curves for the (STA) material tested at -200°F showed no indications of a detrimental hydrogen-titanium reaction. Similar results were found on examining the fracture surfaces of these samples. Both test environments resulted in irregular fracture surfaces having flat areas and discontinuous fatigue striations, Figures 36 and 37.

Weld Material

The topography of the fracture surfaces in the weld material was strongly influenced by the microstructure and crystallographic orientation of the material. This condition is illustrated in Figure 38 by the sample tested in helium gas at ambient temperature. Flat areas containing fatigue striations are shown in Figure 38A. However, in an adjacent area on the fracture surface, failure of the material occurred along alpha platelets found in the weld microstructure. The sample tested in hydrogen gas at ambient temperature, Figure 39, exhibited extensive secondary cracking on the fracture surface. Although the cracks appeared to be associated with fatigue striations, areas containing random cracking were frequently found.

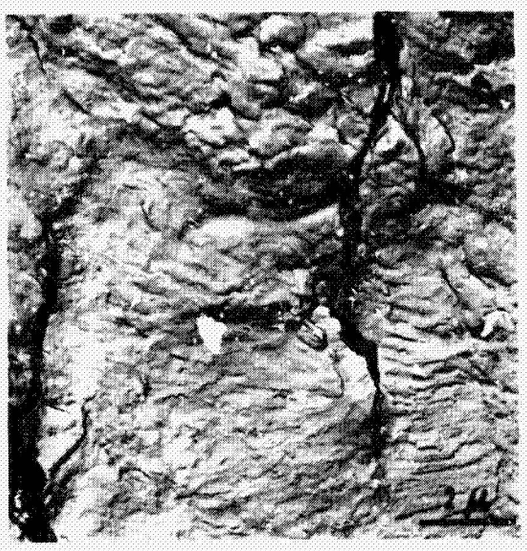

E22341

(A)

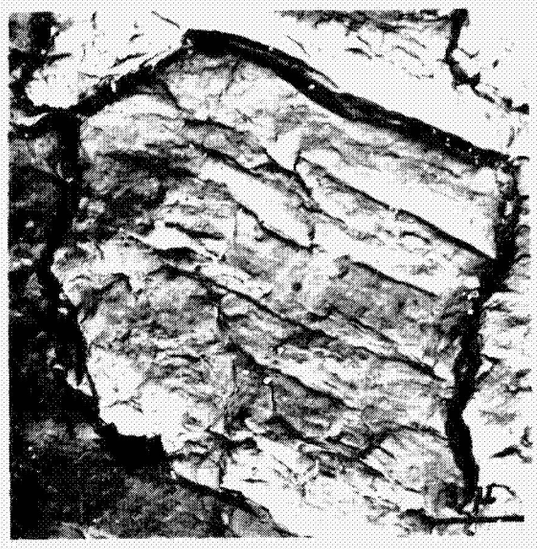

E22345

(B)

FIGURE 32. FRACTURE SURFACE OF (STA) SAMPLE 4-6 FATIGUE TESTED AT 0°F IN HELIUM GAS.

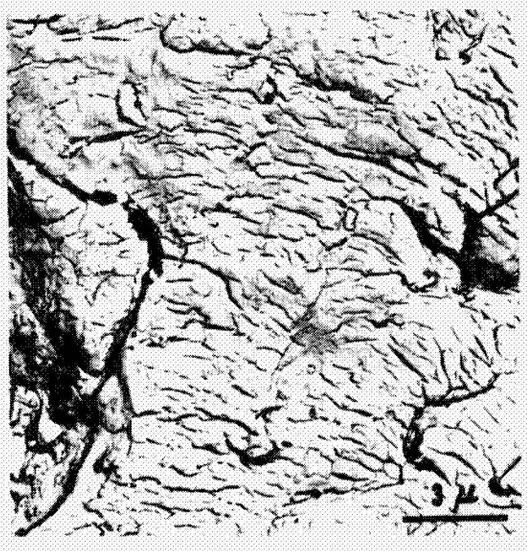

E22306

(A)

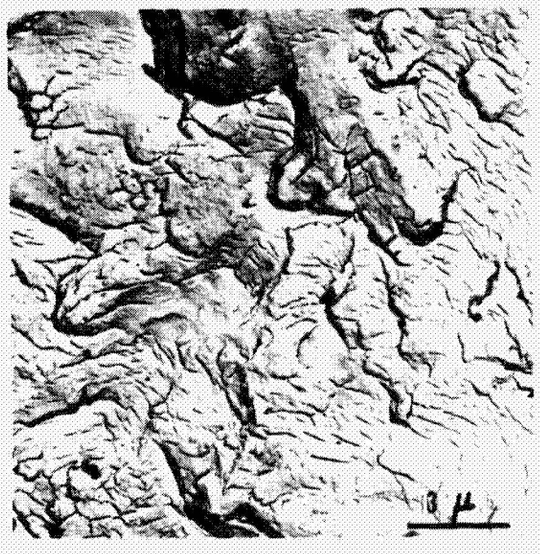

E22307

(B)

FIGURE 33. FRACTURE SURFACE OF (STA) SAMPLE 4-7 FATIGUE TESTED AT 0°F IN HYDROGEN GAS.

E22301

(A)

E22297

(B)

FIGURE 34. FRACTURE SURFACE OF (STA) SAMPLE 4-8 FATIGUE TESTED AT -100°F IN HELIUM GAS.

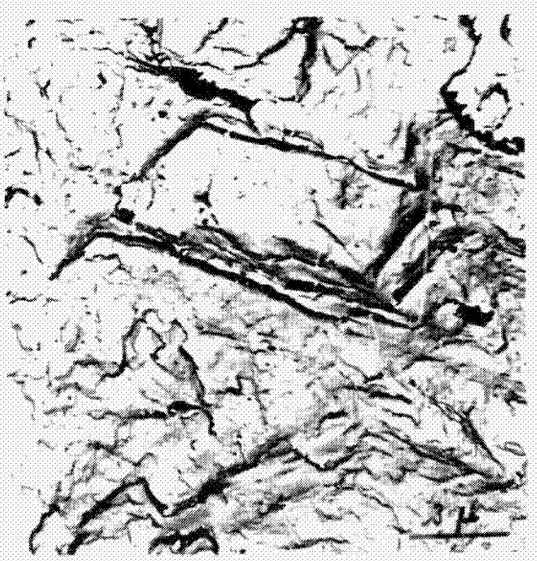

E22412

(A)

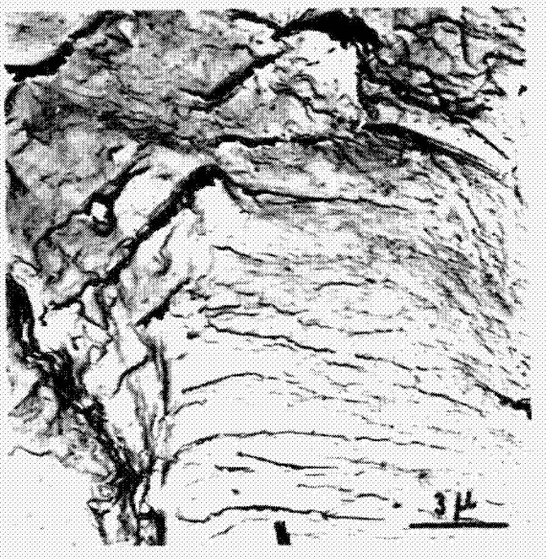

E22407

(B)

FIGURE 35. FRACTURE SURFACE OF (STA) SAMPLE 1-1 FATIGUE TESTED AT -100°F IN HYDROGEN GAS.

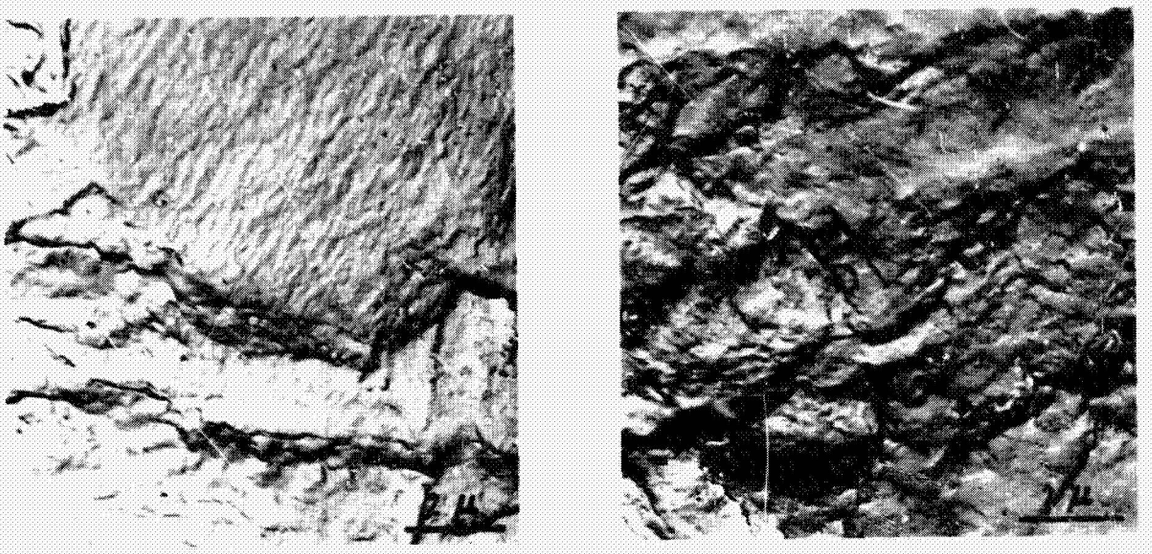

E22375 (A)

E22371 (B)

FIGURE 36. FRACTURE SURFACE OF (STA) SAMPLE 1-2 FATIGUE TESTED AT -200°F IN HELIUM GAS.

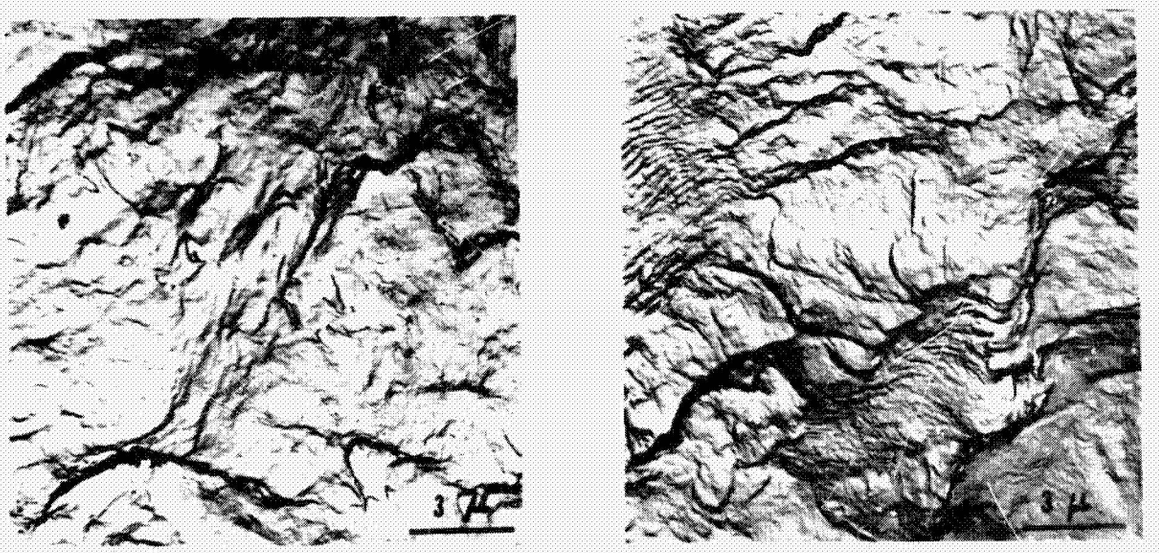

E22380 (A)

E22385 (B)

FIGURE 37. FRACTURE SURFACE OF (STA) SAMPLE 1-12 FATIGUE TESTED AT -200°F IN HYDROGEN GAS.

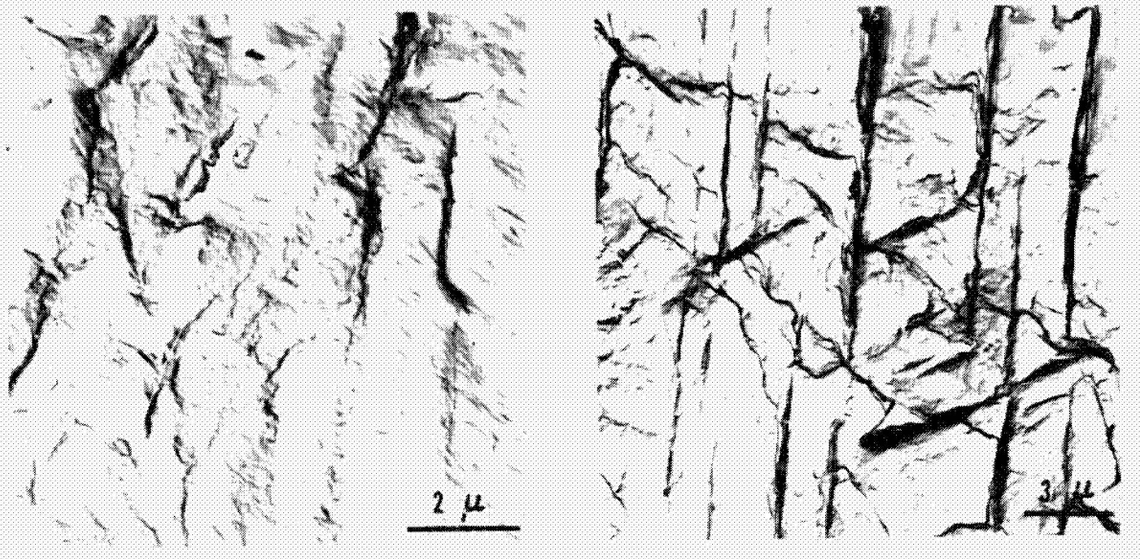

E22348 (A)

E22351 (B)

FIGURE 38. FRACTURE SURFACE OF WELD SAMPLE 2-7 FATIGUE TESTED AT AMBIENT TEMPERATURE IN HELIUM GAS.

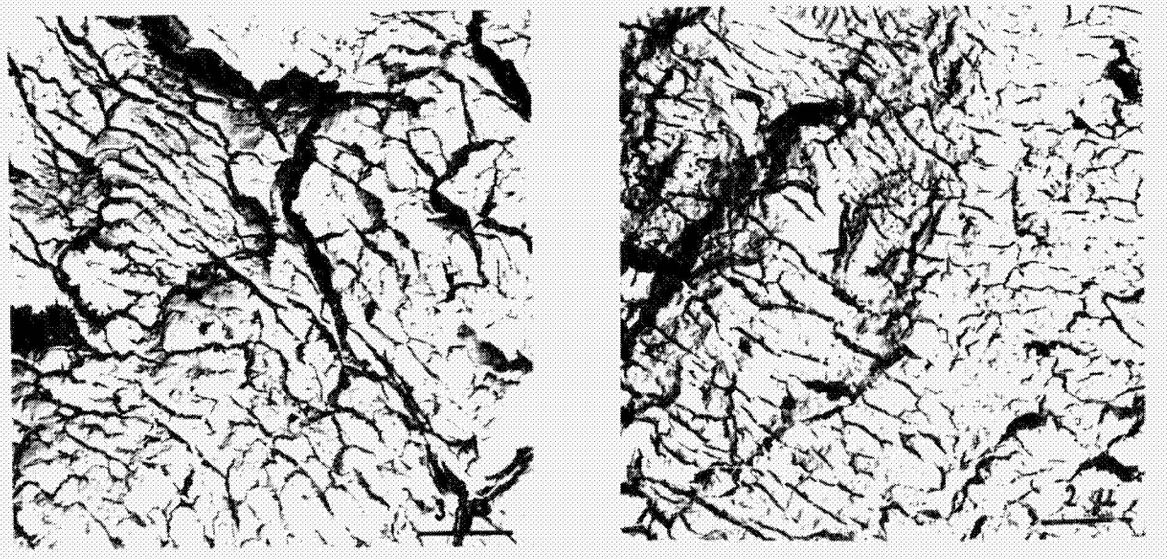

E22369 (A)

E22332 (B)

FIGURE 39. FRACTURE SURFACE OF WELD SAMPLE 2-10 FATIGUE TESTED AT AMBIENT TEMPERATURE IN HYDROGEN GAS.

The fracture surface of the sample tested at 0°F in helium, Figure 40, was similar in appearance to the surface found on the ambient temperature sample, Figure 38. The only obvious difference between the two samples was the lack of well defined fatigue striations on the fracture surface formed at 0°F. Examination of the fracture surface generated in hydrogen gas at 0°F revealed the presence of numerous surface cracks, Figure 41. This fracture mode was the same as that found in the ambient temperature sample tested in hydrogen, Figure 39, however, the degree of cracking seemed to be less at 0°F.

The curves in Figure 23 show that hydrogen gas does not significantly affect the crack growth rate in weld material at -100°F. Examination of the fracture surfaces showed that the fracture modes in both helium and hydrogen gas were the same, Figure 42 and 43. There were no indications of surface cracks on the fracture surface formed in hydrogen gas, Figure 43.

The fracture surfaces on the samples tested at -200°F in helium and hydrogen were extremely flat and featureless, Figure 44 and 45. No indications were found of a hydrogen-titanium reaction in the sample tested in hydrogen, Figure 45.

Discussion

The test results show that a hydrogen environment increases the fatigue crack growth rate in Ti-6Al-4V ELI (STA) and weld material in the temperature range of ambient to -100°F. The degree of hydrogen enhanced crack growth was found to be dependent on the stress intensity range, temperature, and microstructure of the material. The data, however, does not clearly define the mechanism of embrittlement. To understand the mechanisms involved in the embrittlement of this material, it is first necessary to examine the factors which control fatigue crack growth in nonreactive environments.

Several studies have been made examining the conditions occurring at the tip of a crack propagating a ductile material.[53-55] These studies indicated that the formation of a plastic zone ahead of the advancing crack is an important

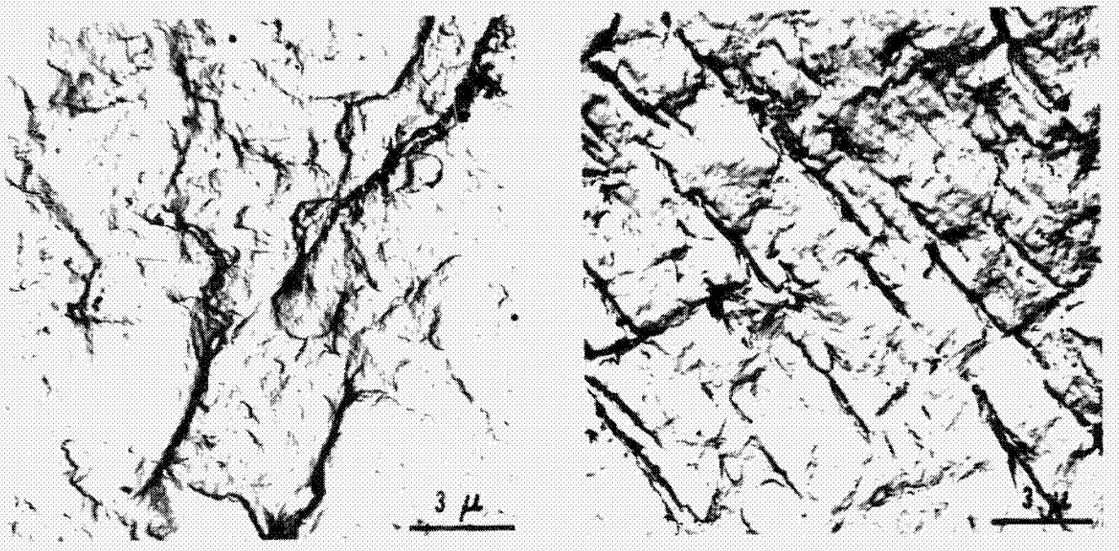

E22430 (A)

E22422 (B)

FIGURE 40. FRACTURE SURFACE OF WELD SAMPLE 4-2 FATIGUE TESTED AT 0°F IN HELIUM GAS.

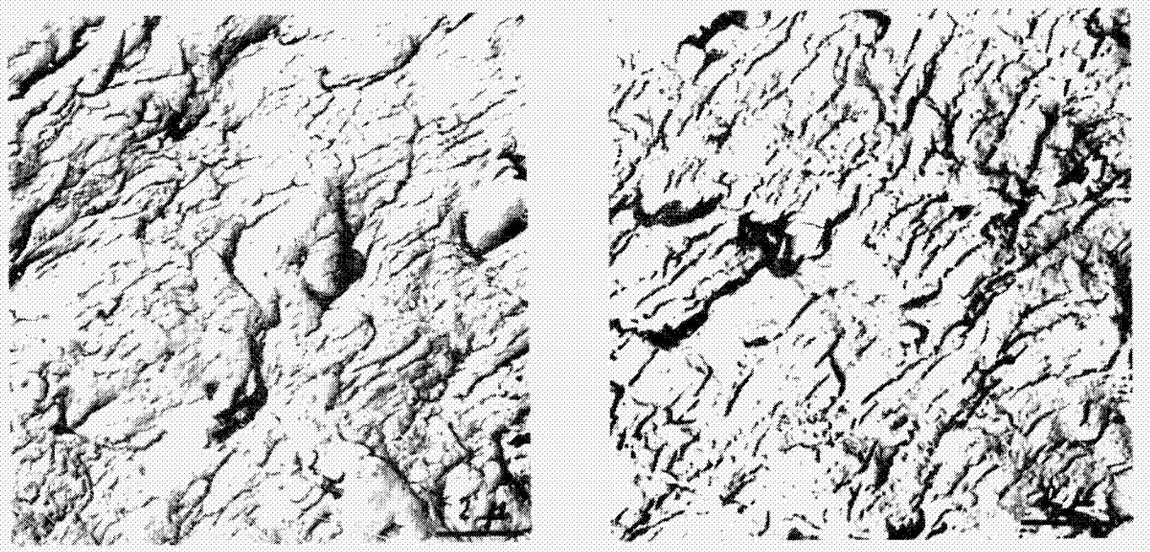

E22294 (A)

E22296 (B)

FIGURE 41. FRACTURE SURFACE OF WELD SAMPLE 2-12 FATIGUE TESTED AT 0°F IN HYDROGEN GAS.

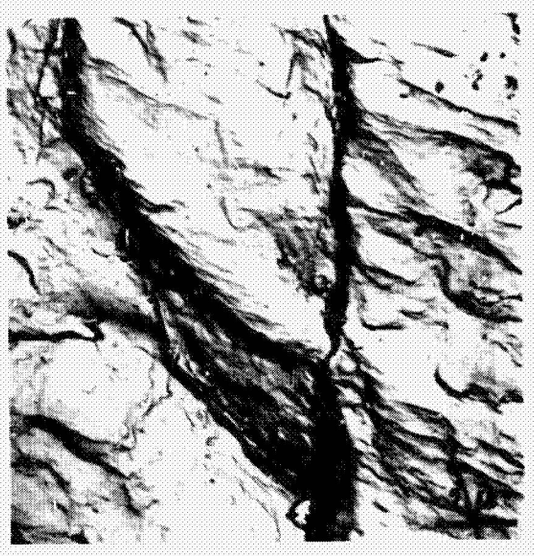

E22394 (A)

E22396 (B)

FIGURE 42. FRACTURE SURFACE OF WELD SAMPLE 3-10 FATIGUE TESTED AT -100°F IN HELIUM GAS.

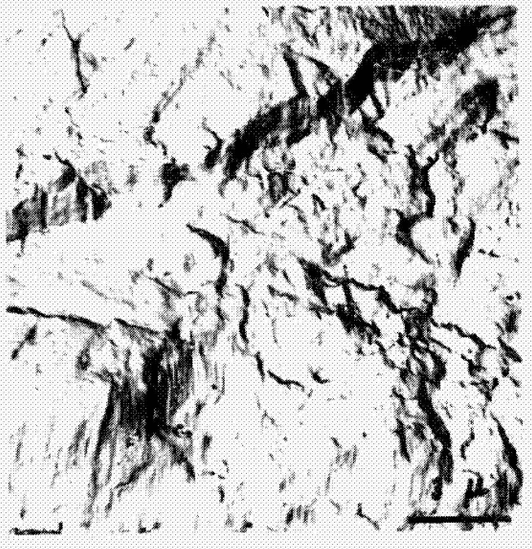

E22389 (A)

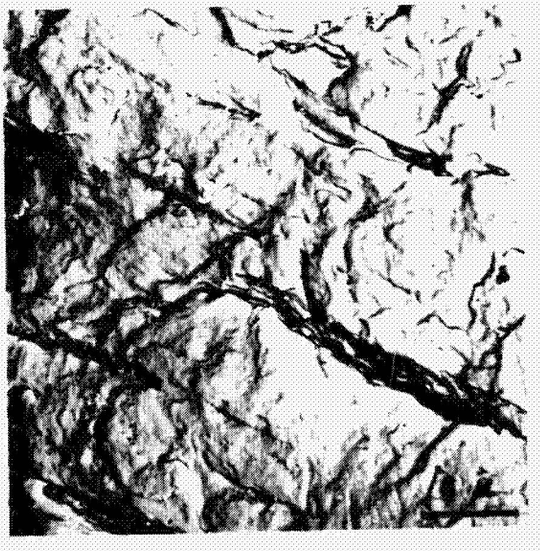

E22393 (B)

FIGURE 43. FRACTURE SURFACE OF WELD SAMPLE 2-11 FATIGUE TESTED AT -100°F IN HYDROGEN GAS.

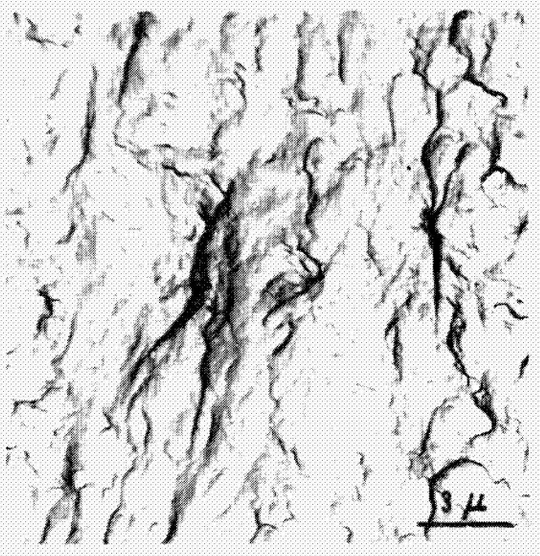

E22386

(A)

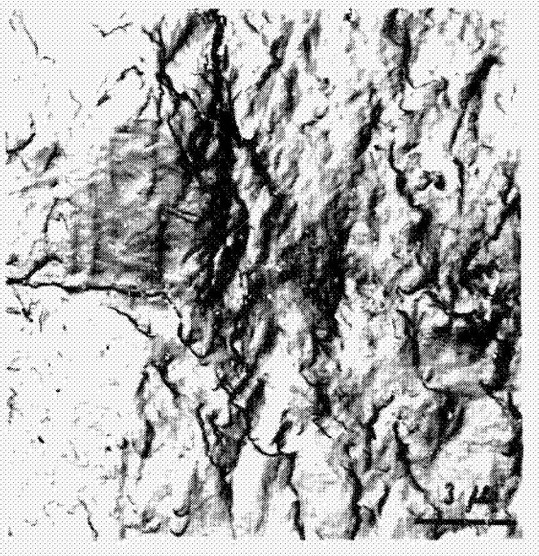

E22397

(B)

FIGURE 44. FRACTURE SURFACE OF WELD SAMPLE 2-6
FATIGUE TESTED AT -200°F IN HELIUM GAS.

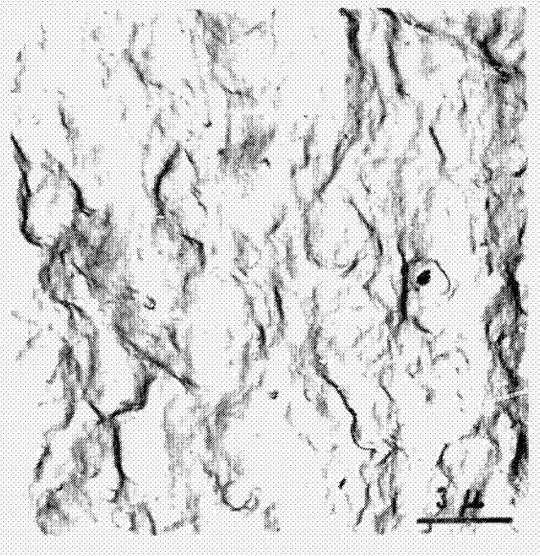

E22404

(A)

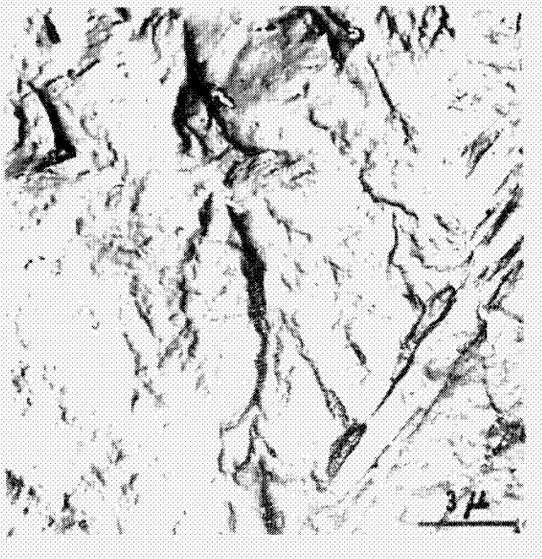

E22402

(B)

FIGURE 45. FRACTURE SURFACE OF WELD SAMPLE 4-10
FATIGUE TESTED AT -200°F IN HYDROGEN GAS.

factor in the crack propagation process. If the criteria for crack propagation in Ti-6Al-4V is considered to be directly related to the plastic zone ahead of the crack tip, the following process describing crack propagation in a ductile material can be applied to fatigue crack growth in Ti-6Al-4V.

Crack Growth In Nonreactive Environments

The application of a load to a ductile material results in a stress concentration at the tip of the crack.[50] This stress concentration produces a plastic zone having the shape shown in Figure 46.[55] As the load on the material increases, the degree of plastic deformation at the tip of the crack exceeds a critical value thus causing the crack to propagate. During crack propagation, the plastic zone ahead of the moving crack also increases in size. Crack propagation stops when the applied load falls below that needed to maintain the critical degree of plastic deformation at the crack tip. This condition occurs during the low load half of the fatigue cycle. Crack propagation through the material occurs by successive repetition of this process.

The propagation of a fatigue crack through Ti-6Al-4V results in the formation of fatigue striations on the fracture surfaces, Figures 30B and 38A. Laird and Smith proposed that the formation of fatigue striations in an isotropic, ductile material is a consequence of successive rounding and sharpening of the crack tip, Figure 47.[56] This model, however, does not explain the absence of fatigue striations in certain grains on the fracture surfaces of the Ti-6Al-4V fatigue samples. It would therefore seem that the formation of fatigue striations in this material must also depend on the crystallographic orientation of the slip planes in the vicinity of the crack tip.[57,58] In an anisotropic material such as Ti-6Al-4V, the "ear" formations at the crack tip, as proposed by Laird and Smith, may occur only when the slip planes are favorably oriented. By using the above fatigue striation model and considering the plastic zone analysis previously discussed, the propagation of a fatigue crack through Ti-6Al-4V in a nonreactive environment can be described by the process shown in Figure 48.

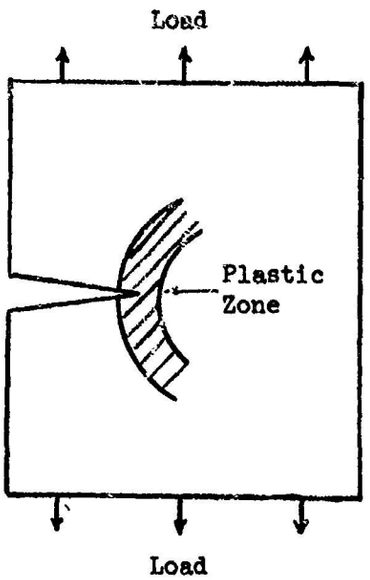

FIGURE 46. SCHEMATIC OF A CRACK SHOWING THE PLASTIC ZONE AT THE CRACK TIP AS DETERMINED BY HAHN AND ROSENFIELD.(53)

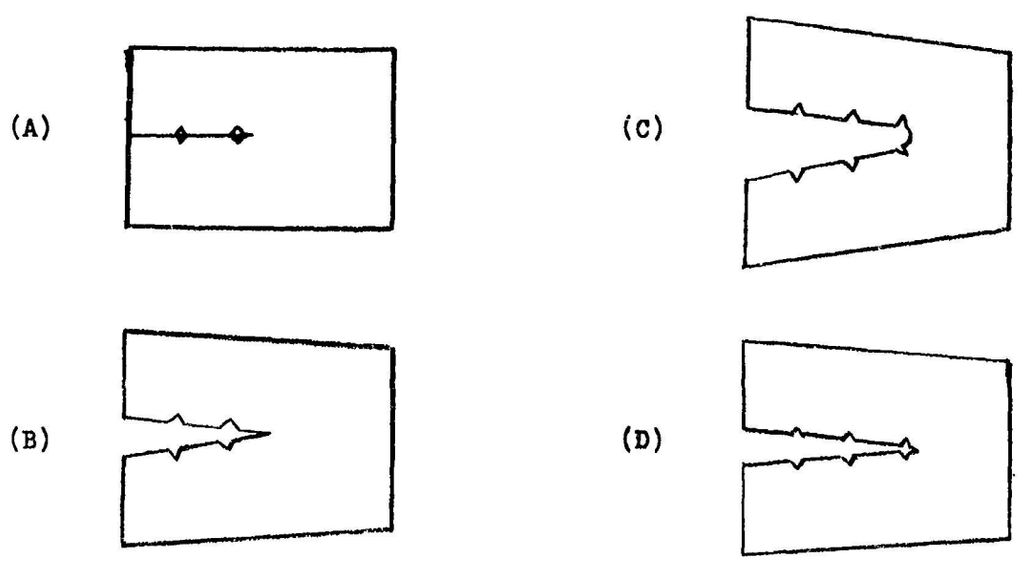

FIGURE 47. SCHEMATIC SHOWING A FATIGUE CRACK PROPAGATING DURING ONE CYCLE AS PROPOSED BY LAIRD AND SMITH.(56)

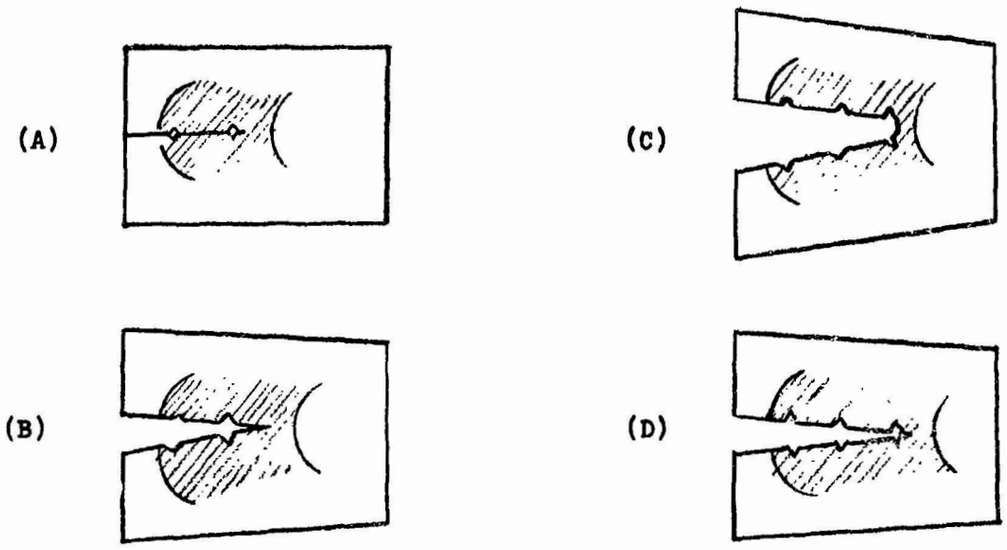

FIGURE 48. SCHEMATIC OF A CRACK PROPAGATING THROUGH A DUCTILE MATERIAL. SHADED AREAS INDICATE THE SHAPE OF THE PLASTIC ZONE.

Crack Growth In Reactive Environments

The first reaction that occurs when a crack propagates in a gaseous environment is the adsorption of the gas onto the fracture surfaces.[9] This adsorption can result in a lowering of the surface energy thereby decreasing the fracture stress of the material[14] and increasing the crack propagation rate. Since the adsorption characteristics of hydrogen on Ti-6Al-4V ELI are not known, a positive correlation between adsorption and the embrittlement found in this study can not be made.

The embrittlement found in this study can, however, be explained using a model based on hydrogen diffusing ahead of the advancing crack. The proposed mechanism of embrittlement is shown schematically in Figure 49. During the low stress half of the fatigue cycle, hydrogen diffuses into the plastic zone ahead of the striation notches and main crack front, Figure 49A. This embrittles the region in front of the main crack and the re-application of stress immediately causes the crack to propagate at a relatively low stress level, Figure 49B. After the applied stress reaches a maximum value, the main crack front has propagated beyond the embrittled area and is now propagating in a ductile matrix. Blunting of the crack tip occurs with the crack front assuming the shape proposed by Laird and Smith[56], Figure 49C. While the main crack front is propagating, secondary cracking is occurring at the striation notches produced by the previous fatigue cycle, Figure 49C. The conditions are favorable for crack formation in these areas since the small notches act as stress raisers and the areas in front of the notches are embrittled with hydrogen as previously noted. Cracking through the striation notches continues until the secondary cracks reach the ductile matrix beyond the embrittled areas. Decreasing the applied stress results in a sharpening of the crack tip, Figure 49D, accompanied by hydrogen again diffusing ahead of the crack front, Figure 49E. The main crack continues to propagate through the material by repetition of the above process.

The distance that hydrogen will diffuse ahead of the crack front depends on a number of variables. These variables include the temperature of the material, the fracture surface hydrogen concentration, the stress and strain

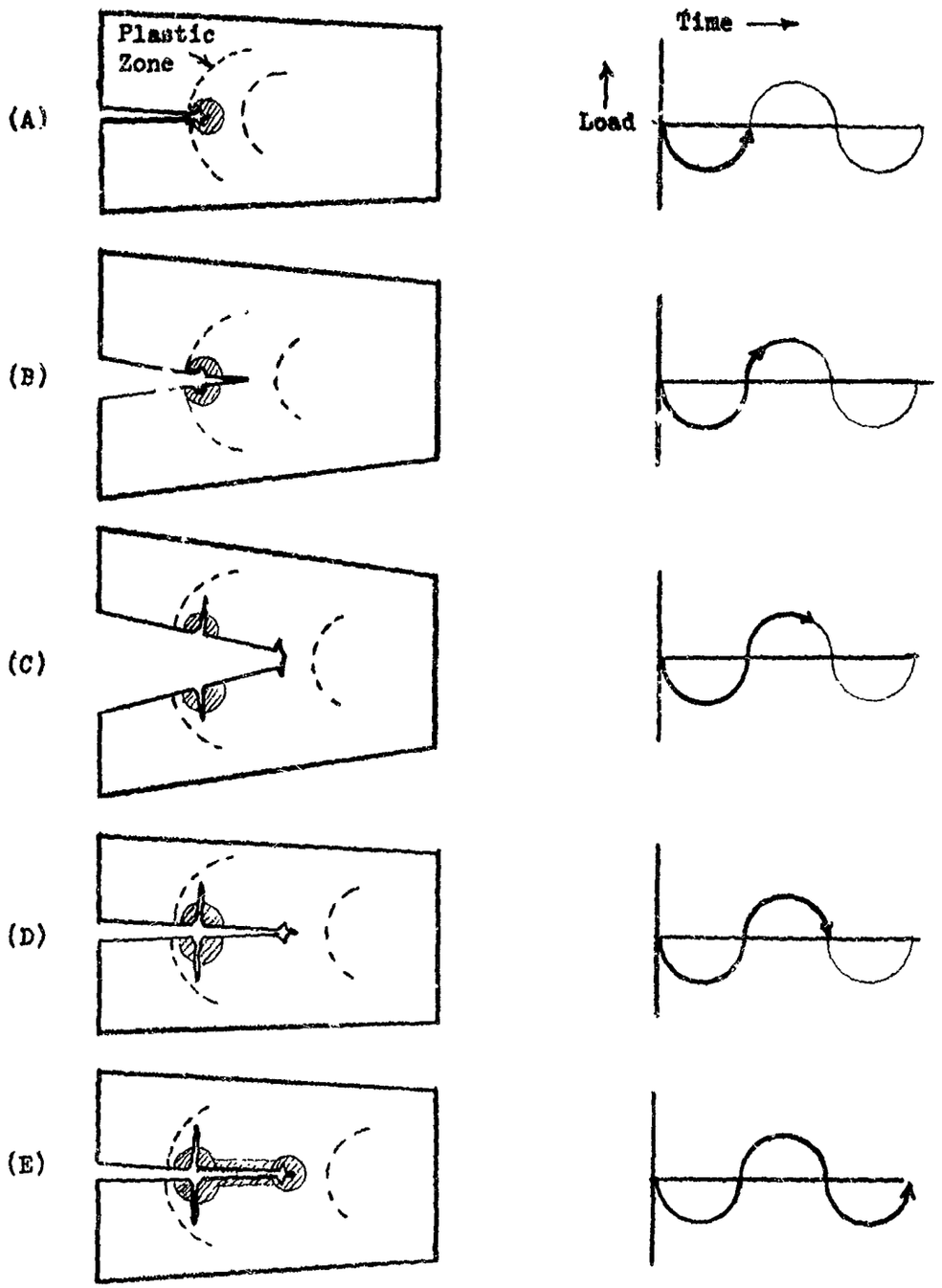

FIGURE 49. SCHEMATIC SHOWING THE PROPOSED MECHANISM OF EMBRITTLEMENT. THE SHADED AREAS INDICATE THE DEPTH OF HYDROGEN DIFFUSION.

distribution at the crack tip, and the quantity and distribution of the beta phase in the material. Since the conditions existing at the crack tip can not be defined at the present time, several assumptions must be made to estimate the mobility of hydrogen near the crack tip at ambient temperature.

The depth of hydrogen embrittlement resulting from diffusion occurring during a half cycle time period was estimated by using the diffusion equation derived for a semi-infinite medi having a constant solute surface concentration.[59] Since available diffusivity data of hydrogen in alpha titanium were determined at elevated temperatures,[4] it was necessary to extrapolate the data to obtain the diffusivity at ambient temperature. The surface concentration of hydrogen was assumed to remain at a constant value of 2,000 ppm, which is just under the concentration that promotes hydride precipitation in transformed Ti-6Al-4V.[60] Using an embrittlement hydrogen concentration of 800 ppm[61] and an initial material hydrogen content of 225 ppm, the depth of embrittlement at ambient temperature was calculated to be $.1 \times 10^{-6}$ inches. This value compares favorably with the crack growth rates of $.8$ to 3×10^{-6} inches/cycle found at low stress intensity levels. The calculated depth of embrittlement should, however, be considered only as an approximation because of the assumptions that were made.

The presence of the beta phase and plastic deformation at the crack tip were not considered in calculating the depth of hydrogen embrittlement. The plastic deformation ahead of the crack can increase the diffusion rate of hydrogen by providing high-diffusivity paths in the material.[62] This increase in the diffusion rate would result in a greater depth of embrittlement. The diffusion rate of hydrogen in the beta phase is greater than in the alpha phase;[4,24] therefore, the beta phase in Ti-6Al-4V would also increase the depth of hydrogen embrittlement.

The crack growth rate curves show that at constant temperature, the degree of crack growth enhancement resulting from the hydrogen environment generally decreases at high values of (ΔK) This effect can be explained by examining the distance that hydrogen diffuses ahead of the main crack. The distance

that hydrogen will penetrate in front of the crack during the low stress half of the fatigue cycle will remain nearly constant at all (ΔK) values. This limiting distance is a consequence of maintaining a constant temperature and diffusion time. The distance that the crack propagates in one cycle, however, increases with increasing (ΔK). Therefore, it can be reasoned that at a low (ΔK) value, the crack propagates only a short distance and the added distance of the embrittled area considerably changes the total distance that the crack propagates during that cycle. However, at high (ΔK) values, the incremental increase in the crack growth distance resulting from hydrogen diffusion is small compared to the total length that the crack propagates during one fatigue cycle. This condition results in a decrease in the degree of embrittlement with increasing (ΔK).

The decreasing degree of embrittlement at the lower temperatures gives further evidence of a diffusion dependent mechanism. It can be seen in Figure 25 that as the temperature decreases, the degree of hydrogen embrittlement also decreases particularly at the high (ΔK) values. This difference can be attributed to a decreasing hydrogen diffusion depth ahead of the crack front resulting from the lower diffusion rate of hydrogen in Ti-6Al-4V at the lower temperatures.

The electron fractographs taken of the surfaces of the reactive samples showed that a considerable degree of secondary cracking had occurred. These cracks appeared to be associated primarily with the fatigue striations, Figures 31 and 39. It can be seen in Figure 48 that cracking in the fatigue striations is consistent with the proposed mechanism of embrittlement.

Conclusions

The test results show that hydrogen gas reacts with the fracture surfaces of Ti-6Al-4V under fatigue loading in the temperature range of ambient to -100°F. This reaction results in an increase of the crack propagation rate and a change in the fracture mode for both (STA) and weld material. The degree of crack growth enhancement caused by the hydrogen environment was found to be dependent

on the stress intensity range, temperature and microstructure of the material. At -200°F, there was no significant difference between the crack growth rates obtained in helium and hydrogen gas. The data is consistent with an embrittlement mechanism involving hydrogen diffusion ahead of the crack front.

REFERENCES

1. C. J. Beevers, M. R. Warren and D. V. Edmonds, Fracture of Titanium - Hydrogen Alloys, J. Less - Common Metals, Vol. 14, 1968, p. 387.

2. D. N. Williams, F. R. Schwartzberg, and R. I. Jaffee, The Effects of Microstructure and Heat Treatment on the Hydrogen Embrittlement of Alpha-Beta Titanium Alloys, ASM Trans. Quart., Vol. 5, 1959, p. 802.

3. R. Haynes, Effect of Hydrogen on Room Temperature Properties of Titanium Low-Aluminum - Low Manganese Alloys, J. Inst. Metals, Vol. 89, 1960, p. 249.

4. T. P. Papazoglou and M. T. Hepworth, The Diffusion of Hydrogen in Titanium, Trans. AIME, Vol. 242, 1968, p. 682.

5. H. B. Bomberger and E. E. Knapek, Titanium Alloys Articles Resistant to Hydrogen Absorption for Dynamo-Electric Machines, United States Patent No. 3,113,227, December 3, 1963.

6. G. F. Pittinato, The Reactivity of Hydrogen with Ti-6Al-4V Under Fatigue Cycling at Ambient and Cryogenic Temperatures, Trans. ASM, Vol. 62, 1969, p. 410.

7. T. R. Gibb and N. W. Kruschmit, The Titanium - Hydrogen System and Titanium Hydride. I Low-Pressure Studies, J. Am. Chem. Soc., Vol. 72, 1950, p. 5365.

8. V. L. Stout and M. O. Gibbons, Gettering of Gas by Titanium, J. Appl. Phys., Vol. 26, 1955, p. 1488.

9. C. J. Smithells, Gases and Metals, Vol. 4, Pergamon Press, 1954.

10. I. Langmuir, Journal American Chemical Society, Vol. 40, 1918.

11. P. Cotteril, The Hydrogen Embrittlement of Metals, Progress in Metal Physics, Vol. 9, 1961.

.. A. F. Benton and T. A. White, Journal American Chemical Society, Vol. 52, 1930.

13. L. E. Berquist, Gauge Calibration at Extremely Low Pressures, Douglas Paper No. 4776, 1968.

14. N. J. Petch, The Lowering of Fracture Stress Due to Adsorption, Phil. Mag., Ser. 8, Vol, 1956.

15. E. A. Gulbransen and K. E. Andrew, Kinetics of the Reactions of Titanium with O_2, N_2, and H_2, Metals Transactions, Vol. 185, 1949.

16. B. G. Koehl, D. N. Williams, and E. S. Bartlett, Investigation of the Reaction of Titanium with Hydrogen, NASA Contract No. NASA 9-6565, Report No. NASA CR-92389, Mrach 18, 1969.

17. R. J. Fabor, O. E. Gideon, H. J. Grover, J. E. Hayes, and G. M. McClure, Investigation of Fatigue Behavior of Certain Alloys in the Temperature Range of Room Temperature to -423°F, Battelle Memorial Institute, Columbus, Ohio, Report WADD-TR-61-132, 1961.

18. J. D. Jackson and W. K. Boyd, Corrosion of Titanium, Defense Metals Information Center, Battelle Memorial Institute, Columbus, Ohio, DMIC Memorandum 218, September 1966.

19. G. F. Pittinato, An Examination of the Compatibility of Ti-6Al-4V with Hydrogen at Ambient and Cryogenic Temperatures, Douglas Report No. DAC 59584, October 1967.

20. C. R. McKinsey, M. Stern, and R. A. Perkins, Factors Affecting the Absorption and Distribution of Hydrogen in Titanium During Acid Pickling, ASM Preprint No. 38, 1958.

21. C. R. McKinsey and R. C. Martin, The Influence of Small Iron Additions on the Behavior of Titanium, Paper presented at AIME Regional Reactive Conference, Buffalo, New York, March 20, 1956.

22. G. A. Lenning, C. M. Craighead, and R. I. Jaffee, Hydrogen Contamination in Descaling and Acid Pickling of Titanium, Trans. ASM, Vol. 48, 1956.

23. R. J. Walter and W. T. Chandler, Effects of High Pressure on Metals, NASA Contract NAS 8-19, Task 7, Report Period Sept. 1967 to Feb. 1968.

24. R. J. Wasilewski and G. L. Kehl, Diffusion of Hydrogen in Titanium, Metallurgia, Vol. 50, 1954, p. 225.

25. E. K. Molchanova, Phase Diagrams of Titanium-Alloys, Israel Program for Scientific Translation, Jerusalem, 1965.

26. G. A. Lenning, J. W. Spretnak, and R. I. Jaffee, Effect of Hydrogen on Alpha Titanium Alloys, Journal of Metals, October 1956, p. 235.

27. M. Hansen, Constitution of Binary Alloys, McGraw-Hill Book Company, Inc., New York, 1958.

28. T. S. Lui and M. A. Steinberg, The Mode of Hydride Precipitation in Alpha Titanium and Alpha Titanium Alloys, Trans. ASM, Vol. 50, 1958, p. 455.

29. G. Sanderson and J. C. Scully, Hydride Formation in Thin Foils of Dilute Ti-Al alloys, Trans. AIME, Vol. 239, 1967, p. 1883.

30. T. L. Mackay and C. B. Gilpin, Stress Corrosion Cracking of Titanium Alloys at Ambient Temperature in Aqueous Solutions, Douglas Missile and Space Systems Div., Astropower Laboratory, Contract NAS 7-488, Yearly Summary Report, July, 1966 through June, 1967.

31. O. J. Huber, J. E. Gates, A. P. Young, M. Pobereskin, and P. D. Frost, Hydrogen Distribution in Heat-Treated Titanium as Established by Autoradiography, Journal of Metals, Vol. 5, 1957, p. 918.

32. D. N. Williams, Hydrogen in Titanium and Titanium Alloys, TML Report No. 100, May 16, 1958.

33. D. N. Williams, The Hydrogen Embrittlement of Titanium Alloys, J. Inst. Metals, Vol. 91, p. 147, 1962.

34. D. N. Williams, F. R. Schwartzberg, and R. I. Jaffee, Supersaturation as a Factor in the Hydrogen Embrittlement of Titanium Alloys, Trans. ASM, Vol. 52, p. 182, 1960.

35. V. A. Livanov, A. A. Buckhanova, B. A. Kolachev, and N. Ya. Gusel'Nikov, Hydrogen Embrittlement of Titanium Alloys, NASA-TT-F-362, 1966.

36. G. A. Lenning, C. M. Craighead, and R. I. Jaffee, Constitutional and Mechanical Properties of Titanium-Hydrogen Alloys, Trans. AIME, Vol. 200, p. 367, 1954.

37. C. M. Craighead, G. A. Lenning, and R. I. Jaffee, Hydrogen Embrittlement of Beta-Stabilized Titanium Alloys, Trans. AIME, Vol. 206, p. 923, 1956.

38. D. N. Williams and R. I. Jaffee, Relationship Between Impact and Low-Strain-Rate Hydrogen Embrittlement of Titanium Alloys, J. Less-Common Metals, Vol. 2, p. 42, 1960.

39. R. I. Jaffee and D. N. Williams, The Effect of Composition on the Hydrogen Embrittlement of Alpha-Beta Titanium Alloys, Trans. ASM, Vol. 51, p. 820, 1959.

40. R. J. Kotfila and H. M. Burte, Hydrogen Contamination in Titanium and Titanium Alloys, WADC Tech. Rept. 54-616, Part 1, 1955.

41. R. I. Jaffee, G. A. Lenning, and C. M. Craighead, Effect of Testing Variables on the Hydrogen Embrittlement of Titanium and A Ti-8 Pct Mn Alloy, Trans. AIME, Vol. 206, p. 907, 1956.

42. R. D. Daniels, R. J. Quigg, and A. R. Troiano, Hydrogen Embrittlement and Delayed Failure in Titanium Alloys, Trans. ASM, Vol. 51, p. 843, 1959.

43. R. Haynes, Effect of Hydrogen on Room-Temperature Mechanical Properties of Titanium - 4.5% Aluminum - 4.5% Manganese Alloy, J. Inst. Metals, Vol. 88, p. 509, 1960.

44. P. A. Blanchard, R. J. Quigg, F. W. Schaller, E. A. Steigerwald, and A. R. Troiano, Hydrogen Embrittlement in Steels, Titanium Alloys, and Several Face-Centered Cubic Alloys, WADC Tech. Rept. 59-172, 1959.

45. F. R. Schwartzberg, D. N. Williams, and R. I. Jaffee, Low Temperature Recovery of Ductility in a Hydrogen-Embrittled Alpha-Beta Titanium Alloy, J. Inst. Metals, Vol. 88, p. 352, 1960.

46. W. J. Bennett and A. R. Troiano, Crack Propagation in the Hydrogen-Induced Brittle Fracture of Steel, Trans. AIME, Vol. 209, p. 486, 1957.

47. E. A. Steigerwald and G. L. Hanna, Initiation of Flow Crack Propagation in High-Strength Materials, Proceedings ASTM, Vol. 62, p. 885, 1962.

48. A. A. Anctil, E. B. Kula, and E. D. Cesore, Electric-Potential Technique for Determining Slow Crack Growth, Proceedings ASTM, Vol. 63, p. 709, 1963.

49. H. H. Johnson, Calibrating the Electric Potential Method for Studying Slow Crack Growth, Materials Research and Standards, Vol. 5, p. 422, 1965.

50. ASTM Symposium, Fracture Toughness Testing and Its Applications, ASTM Special Technical Publication No. 381, June 21, 1964.

51. W. A. Spitzig, P. M. Talda, and R. P. Wei, Fatigue-Crack Propagation and Fractographic Analysis of 18 Ni (250) Maraging Steel Tested in Argon and Hydrogen Environments, Presented at the National Symposium on Fracture Mechanics, June 19-21, 1967, at Lehigh University, Bethlehem, Pennsylvania.

52. P. Paris and F. Erdogan, A Critical Analysis of Crack Propagation Laws, Trans. ASME, p. 528, 1963.

53. G. T. Hahn and A. R. Rosenfield, Experimental Determination of Plastic Constraint Ahead of a Sharp Crack Under Plane-Strain Conditions, BuShips Contract No. bs-92383, Battelle Memorial Institute, July 1, 1966.

54. G. T. Hahn and A. R. Rosenfield, Local Yielding and Extension of a Crack Under Plane Stress, Acta Metallurgica, Vol. 13, p. 293, March 1965.

55. A. S. Tetelman and W. D. Robertson, Direct Observation and Analysis of Crack Propagation in Iron - 3% Silicon Single Crystals, Thesis submitted by A. S. Tetelman to the School of Engineering, Yale University, 1961.

56. C. Laird and G. C. Smith, Crack Propagation in High Stress Fatigue, Phil. Mag., Vol. 7, p. 347, 1962.

57. P. J. Forsyth, Fatigue Damage and Crack Growth in Aluminum Alloys, Acta. Met., Vol. II, p. 703, 1963.

58. A. J. McEvily and R. C. Boettner, On Fatigue Crack Propagation in F.C.C. Metals, Acta. Met., Vol. II, p. 725, 1963.

59. J. Crank, The Mathematics of Diffusion, Oxford University Press, p. 30, 1956.

60. G. F. Pittinato, The Absorption of Hydrogen by Ti-6Al-4V, To be published.

61. D. M. Kokkos and S. R. Seagle, The Effect of Hydrogen on the Properties of Ti-6Al-4V, Reactive Metals Inc., Titanium Technical Bulletin, February 3, 1967.

62. P. G. Shewmon, Diffusion in Solids, McGraw-Hill Series in Materials Science and Engineering, 1963.

APPENDIX A

CRACK PROPAGATION DATA FOR FORGED AND WELDED Ti-6Al-4V ELI MATERIAL

CYCLES \ SAMPLE NO.	Crack Length (2a) in inches			
	1-9	1-4	1-5	1-6
0	.053	.052	.052	.053
1,000	.054	.054	.053	.054
2,000	.056	.055	.054	.055
3,000	.057	.056	.055	.056
4,000	.058	.057	.056	.057
5,000	.059	.058	.057	.058
6,000	.060	.061	.059	-
7,000	.061	.062	.060	.060
8,000	.062	.063	.062	.062
9,000	.063	.065	.063	.063
10,000	.066	.067	.065	.065
11,000	.068	.069	.067	.066
12,000	.070	.071	.069	.068
13,000	.072	.074	.071	.070
14,000	.074	.075	.073	.072
15,000	.076	.078	.075	.075
16,000	.078	.081	.078	.077
17,000	.081	.084	.082	.081
18,000	.083	.087	.086	.086
19,000	.085	.090	.093	.091
20,000	.088	-	.101	.097
21,000	.091	.099	.111	-
22,000	.094	.104	.122	.116
23,000	.097	.108	.137	.129
24,000	.100	.112	.156	.143
25,000	.104	.116	.176	.157
26,000	.108	.121	.205	.176
27,000	.112	.127	.239	.198
28,000	.117	.132	.282	.228
29,000	.122	.138	-	-
29,100	-	-	-	.271
29,500	-	-	-	.288
30,000	.129	.144	F	-

CYCLES \ SAMPLE NO.	Crack Length (2a) in inches			
	1-9	1-4	1-5	1-6
31,000	.134	.150		.314
32,000	.138	.155		-
33,000	.148	.162		F
34,000	.155	.169		
35,000	.163	.176		
36,000	.171	.186		
37,000	.181	.196		
38,000	-	.206		
38,200	.194	-		
39,000	.203	-		
39,300	-	.220		
40,000	.213	.229		
41,000	.227	.244		
42,000	.242	.264		
43,000	.260	.283		
44,000	.281	.303		
45,000	.310	.332		
46,000	-	F		
47,000	F			

CRACK PROPAGATION DATA FOR Ti-6Al-4V ELI
FORGED MATERIAL IN THE (STA) CONDITION
TESTED AT AMBIENT TEMPERATURE.

CYCLES \ SAMPLE NO.	Crack Length (2a) in inches			
	4-6	4-9	4-7	1-11
0	.054	-	.054	.053
1,000	.055	.055	.055	.055
2,000	.056	.056	.056	.056
3,000	.057	.057	.057	.057
4,000	.057	.057	.058	.058
5,000	.059	.058	.059	.059
6,000	.060	.060	.060	.060
7,000	.062	.061	.061	.062
8,000	.063	.063	.062	.063
9,000	.065	.064	.063	.064
10,000	.066	.065	.064	.066
11,000	.068	.067	.065	.068
12,000	.070	.068	.067	.071
13,000	.071	.069	.068	.075
14,000	.073	.070	.069	.080
15,000	.075	.072	.070	.085
16,000	.077	.073	.072	.091
17,000	.079	.075	.074	.099
18,000	.081	.076	.076	.108
19,000	.084	.078	.078	.120
20,000	.087	.080	.080	.133
21,000	.089	.082	.084	.147
22,000	.091	.084	.088	.162
23,000	.093	.086	.094	-
24,000	.096	.088	.101	.197
25,000	.099	.090	.108	.217
26,000	.102	.092	.116	.239
27,000	.105	.094	.124	.262
28,000	.109	.097	.133	.289
29,000	.112	.100	.142	.321
30,000	.116	.103	.153	-
31,000	.120	.107	.164	F

CYCLES \ SAMPLE NO.	Crack Length (2a) in inches			
	4-6	4-9	4-7	1-11
32,000	.126	.110	.176	
33,000	.131	.114	.190	
34,000	.136	.118	.202	
35,000	.140	.121	.215	
36,000	.148	.126	.232	
37,000	.154	.131	.249	
38,000	.161	.135	.269	
39,000	.168	.140	.294	
40,000	.176	.146	.325	
41,000	.185	.152	-	
42,000	.194	.158	F	
43,000	.203	.165		
44,000	.213	.174		
45,000	.224	.183		
46,000	.237	.192		
47,000	.253	.202		
48,000	.271	.212		
49,000	.292	.224		
50,000	.322	.239		
51,000	-	.256		
52,000	F	.276		
53,000		.297		
54,000		.312		
55,000		.372		
56,000		F		

CRACK PROPAGATION DATA FOR Ti-6Al-4V ELI FORGED MATERIAL IN THE (STA) CONDITION TESTED AT 0°F.

CYCLES \ SAMPLE NO.	Crack Length (2a) in inches 4-8	1-7	1-1	1-10
0	.062	.062	.062	.060
1,000	.062	.062	.063	.062
2,000	.062	.062	.064	.064
3,000	.063	.063	.066	.065
4,000	.063	.063	.067	.066
5,000	.064	.063	.068	.068
6,000	.064	.063	.070	.070
7,000	.064	.064	.072	.071
8.000	.065	.064	.074	.073
9,000	.065	.064	.075	.075
10,000	.066	.065	.077	.077
11,000	.066	.065	.078	.078
12,000	.067	.065	.081	.081
13,000	.067	.066	.082	.083
14,000	.068	.067	.085	.085
15,000	.068	.068	.088	.088
16,000	.069	.068	.091	.091
17,000	.071	.068	.093	.095
18,000	.071	.069	.096	.099
19,000	.072	.070	.099	.102
20,000	.072	.071	.103	.106
21,000	.072	.071	.106	.110
22,000	.073	.072	.110	.114
23,000	.074	.073	.115	.118
24,000	.074	.074	.119	.122
25,000	.075	.075	.125	.127
26,000	.076	.075	.129	.132
27,000	.077	.076	.133	.137
28,000	.078	.077	.140	.142
29,000	.079	.078	.146	.147
30,000	.080	.079	.151	.154
31,000	.081	.080	.158	.161
32,000	.082	.082	.165	.169
33,000	.083	.083	.172	.177
34,000	.084	.084	.179	.185
35,000	.086	.086	.188	.193
36,000	.087	.087	.198	.203
37,000	.088	.089	.208	.214
38,000	.089	.090	.219	.226
39,000	.090	.092	.232	.240
40,000	.091	.094	.249	.254
41,000	.093	.097	.269	.274
42,000	.095	.099	.290	.294
43,000	.096	.101	.322	.322
44,000	.098	.103	.372	F

CYCLES \ SAMPLE NO.	Crack Length (2a) in inches 4-8	1-7	1-1	1-10
45,000	.100	.105	F	
46,000	.101	.107		
47,000	.103	.110		
48,000	.105	.112		
49,000	.107	.115		
50,000	.109	.117		
51,000	.111	.120		
52,000	.112	.124		
53,000	.115	.128		
54,000	.118	.131		
55,000	.121	.135		
56,000	.123	.139		
57,000	.127	.143		
58,000	.130	.148		
59,000	.134	.152		
60,000	.138	.157		
61,000	.142	.161		
62,000	.146	.165		
63,000	.151	.171		
64,000	.156	.176		
65,000	.162	.182		
66,000	.167	.188		
67,000	.173	.195		
68,000	.178	.203		
69,000	.184	.211		
70,000	.186	.221		
71,000	.194	.231		
72,000	.200	.241		
73,000	.208	.254		
74,000	.216	.268		
75,000	.226	.284		
76,000	.237	.307		
77,000	.247	.333		
78,000	.259	.383		
79,000	-	F		
80,000	.288			
81,000	.303			
82,000	-			
83,000	.361			
84,000	F			

CRACK PROPAGATION DATA FOR Ti-6Al-4V ELI MATERIAL IN THE (STA) CONDITION TESTED AT -100°F.

CYCLES \ SAMPLE NO.	Crack Length (2a) in inches 1-2	4-4	1-12	4-11
0	.070	.070	.072	.070
1,000	.070	.070	.072	.070
2,000	.071	.071	.072	.071
3,000	.071	.071	.073	.071
4,000	.071	.071	.073	.072
5,000	.072	.071	.074	.072
6,000	.072	.072	.074	.073
7,000	.072	.072	.074	.074
8,000	--	.072	.075	.074
9,000	.072	.073	.076	.075
10,000	.073	.073	.076	.076
11,000	.074	.074	.077	.077
12,000	.074	.074	.077	.078
13,000	.075	.075	.078	.079
14,000	.076	.076	.079	.080
15,000	.076	.076	.080	.081
16,000	.077	.078	.080	.082
17,000	.078	.079	.081	.083
18,000	.079	.079	.082	.084
19,000	.080	.080	.083	.085
20,000	.081	.081	.084	.086
21,000	.082	.083	.084	.087
22,000	.083	.084	.086	.088
23,000	.085	--	.086	.089
24,000	.086	.086	.088	.090
25,000	.087	.088	.089	.091
26,000	.089	.090	.090	.092
27,000	.090	.092	.092	.094
28,000	.092	.093	.093	.096
29,000	.094	.095	.094	.097
30,000	.096	.097	.096	.098
31,000	.098	.099	.097	.100
32,000	.100	.101	.099	.101
33,000	.102	.103	.101	.103
34,000	.104	.106	.102	.105
35,000	.106	.108	.105	.106
36,000	.108	.111	.106	.108
37,000	.111	.114	.108	.111
38,000	.114	.117	.110	.113
39,000	.117	.121	.113	.115
40,000	.120	.125	.115	.117
41,000	.124	.130	.118	.119
42,000	.128	.134	.121	.122
43,000	.131	.138	.124	.124
44,000	.135	.143	.127	.128
45,000	.139	--	.131	.132
46,000	.144	.152	.134	.135
47,000	.149	.158	.138	.139
48,000	.155	.167	.142	.143
49,000	.160	.170	.147	.147
50,000	.166	.175	.152	.152
51,000	.172	.182	.156	.156
52,000	.180	.188	.161	.161
53,000	.186	.197	.166	.167
54,000	.194	.205	.172	.174
55,000	.202	.214	.178	.180
56,000	.212	.223	.185	.186
57,000	.220	.234	.192	.193
58,000	.231	.247	.201	.202
59,000	.243	.260	.209	.212
60,000	.256	--	.219	.222
61,000	.273	.301	.230	.232
62,000	.291	.331	.242	.243
63,000	.316	F	.258	.256
64,000	.361		.276	.272
65,000	F		.294	.290
66,000			.316	.310
67,000			.352	.341
68,000			F	F

CRACK PROPAGATION DATA FOR Ti-6Al-4V ELI
FORGED MATERIAL TESTED IN THE (STA) CONDITION
AT -200°F.

CYCLES \ SAMPLE NO.	Crack Length (2a) in inches			
	2-7	2-2	2-10	2-5
0	.062	-	.062	-
1,000	.064	-	.064	-
2,000	.066	.068	.068	-
3,000	.069	.070	.076	.071
4,000	.070	.073	.084	.083
5,000	.073	.076	.095	.100
6,000	.077	.079	.111	.116
7,000	.081	.082	.132	-
7,500	-	-	-	.146
8,000	.085	.085	.156	.158
9,000	.088	.088	.184	.188
10,000	.092	.090	.210	.219
11,000	.096	.094	.238	.250
12,000	.101	.099	.272	.283
13,000	.105	.103	.304	.315
14,000	.111	.107	F	F
15,000	.118	.112		
16,000	.125	.118		
17,000	.134	.125		
18,000	.144	.134		
19,000	.155	.140		
20,000	.168	.149		
21,000	.183	.159		
22,000	.204	.170		
23,000	.218	.183		
24,000	.234	.197		
25,000	.257	.213		
26,000	.288	.232		
27,000	F	-		
27,300		.266		
28,000		.294		
29,000		.325		
30,000		F		

CRACK PROPAGATION DATA FOR Ti-6Al-4V ELI FORGED MATERIAL TESTED IN THE WELD AREA AT AMBIENT TEMPERATURE.

CYCLES \ SAMPLE NO.	Crack Length (2a) in inches			
	2-13	4-2	2-12	3-13
0	.052	-	.051	.052
1,000	.052	-	.055	.055
2,000	.053	-	.060	.057
3,000	.054	-	.065	.060
4,000	.054	-	.072	.065
5,000	.055	.054	.079	.070
6,000	.056	.054	.087	.075
7,000	.056	.056	.094	.080
8,000	.057	.057	.101	.086
9,000	.058	.059	.110	.092
10,000	.059	.062	.120	.100
11,000	.060	.063	.131	.108
12,000	.062	.066	.140	.115
13,000	.064	.068	.151	.124
14,000	.066	.071	.162	.133
15,000	.069	.074	.173	.142
16,000	.072	.077	.185	.153
17,000	.076	.081	.201	.164
18,000	.080	.083	.214	.177
19,000	.084	.087	.236	.190
20,000	.089	.090	.260	.208
21,000	.094	.094	.290	.229
22,000	.099	.098	-	.256
23,000	.103	-	F	.290
24,000	.109	.111		F
25,000	.115	.117		
26,000	.121	.123		
27,000	.126	.130		
28,000	.132	.136		
29,000	.138	.145		
30,000	.147	.153		
31,000	.157	.161		
32,000	.168	.170		
33,000	.179	.180		
34,000	.191	.192		
35,000	.200	.206		
36,000	.218	.224		
37,000	.229	.243		
38,000	.243	.260		
39,000	.269	.284		
40,000	.299	.303		
41,000	F	F		

CRACK PROPAGATION DATA FOR Ti-6Al-4V FORGED MATERIAL TESTED IN THE WELD AREA AT 0°F.

CYCLES \ SAMPLE NO.	Crack Length (2a) in inches			
	3-10	2-8	2-11	4-12
0	.053	-	-	.053
1,000	.053	-	-	.053
2,000	.054	-	-	.054
3,000	.054	-	.055	.054
4,000	.055	-	.056	.056
5,000	.056	-	.057	.057
6,000	.057	-	.058	.058
7,000	.057	-	.059	.060
8,000	.058	-	.061	.062
9,000	.059	-	.062	.064
10,000	.060	-	.063	.066
11,000	.061	-	.064	.069
12,000	.063	-	.065	.071
13,000	.064	-	.066	.074
14,000	.065	.065	.067	.077
15,000	.067	.067	.069	.079
16,000	.068	.068	.071	.082
17,000	.070	.070	.073	.086
18,000	.071	.071	.074	.089
19,000	.073	.073	.076	.092
20,000	.075	.075	.078	.095
21,000	.076	.076	.079	.099
22,000	.079	.079	.081	.103
23,000	.081	.080	.083	.107
24,000	.083	.082	.085	.112
25,000	.085	.083	.087	.117
26,000	.088	.085	.090	.122
27,000	.090	.087	.092	.127
28,000	.093	.089	.093	.133
29,000	.095	.091	.096	.138
30,000	.098	.093	.098	.144
31,000	-	.095	.101	.151

CYCLES \ SAMPLE NO.	Crack Length (2a) in inches			
	3-10	2-8	2-11	4-12
32,000	.107	.097	.104	.159
33,000	.111	.100	.107	.169
34,000	.116	.103	.111	.180
35,000	.120	.106	.115	.191
36,000	.125	.109	.121	.202
37,000	.130	.112	.129	.215
38,000	.137	.115	.135	.234
39,000	.143	.119	.141	.264
40,000	.150	.123	.147	F
41,000	.157	.127	.154	
42,000	.164	.130	.160	
43,000	.172	.134	.166	
44,000	.182	.138	.174	
45,000	.192	.143	.182	
46,000	.203	.148	.192	
47,000	.218	.153	.204	
48,000	.232	.160	.216	
49,000	.251	.167	.233	
50,000	.266	.174	.255	
51,000	.296	.181	.284	
52,000	F	.186	.343	
53,000		.192	F	
54,000		.199		
55,000		.213		
56,000		.229		
57,000		.246		
58,000		.267		
59,000		.303		
60,000		F		

CRACK PROPAGATION DATA FOR Ti-6Al-4V ELI FORGED MATERIAL TESTED IN THE WELD AREA AT -100°F.

CYCLES \ SAMPLE NO.	Crack Length (2a) in inches 2-6	3-12	4-10	4-3
0	.055	-	.055	.054
1,000	.055	-	.055	.055
2,000	.056	-	.055	.056
3,000	.056	-	.056	.057
4,000	.057	-	.057	.057
5,000	.058	-	.058	.058
6,000	.058	-	.059	.059
7,000	.059	-	.060	.060
8,000	.060	-	.061	.061
9,000	.061	-	.063	.062
10,000	.062	-	.064	.063
11,000	.063	.065	.065	.064
12,000	.064	.066	.067	.066
13,000	.065	.067	.068	.067
14,000	.067	.068	.070	.069
15,000	.068	.069	.071	.070
16,000	.070	.070	.073	.071
17,000	.072	.072	.075	.073
18,000	.074	.073	.077	.075
19,000	.076	.075	.079	.077
20,000	.079	.078	.081	.079
21,000	.082	.080	.083	.081
22,000	.085	.082	.085	.083
23,000	.088	.084	.087	.085
24,000	.091	.087	.089	.088
25,000	.096	.089	.092	.091
26,000	.100	.091	.093	.094
27,000	.104	.093	.095	.097
28,000	.108	.095	.098	.100
29,000	.112	.097	.100	.103
30,000	.117	.100	.103	.107
31,000	.122	.102	.106	.112

CYCLES \ SAMPLE NO.	Crack Length (2a) in inches 2-6	3-12	4-10	4-3
32,000	.127	.105	.109	.116
33,000	.133	.108	.112	.120
34,000	.140	.110	.117	.126
35,000	.147	.113	.121	.131
36,000	.156	.117	.128	.137
37,000	.166	.120	.135	.143
38,000	.180	.124	.141	.152
39,000	.188	.128	.147	.160
40,000	.200	.132	.154	.169
41,000	.213	.137	.162	.179
42,000	.226	.141	.170	.192
43,000	.245	.146	.181	.208
44,000	.264	.151	.194	.229
45,000	.282	.158	.206	.270
46,000	.302	.164	.221	.310
47,000	F	.173	.245	F
48,000		.183	.287	
49,000		.195	.353	
50,000		.206	F	
51,000		.220		
52,000		.230		
53,000		.255		
54,000		.276		
55,000		.301		
56,000		.343		
57,000		F		

CRACK PROPAGATION DATA FOR T1-6A1-4V ELI FORGED MATERIAL TESTED IN THE WELD AREA AT -200°F.

APPENDIX B

FATIGUE CRACK GROWTH RATE DATA FOR FORGED AND WELDED Ti-6Al-4V ELI MATERIAL

	CRACK GROWTH RATE, 10^{-6} INCHES / CYCLE							
	$\frac{da}{dn}$	$\frac{da}{dn}$	$\frac{da}{dn}$	$\frac{dc}{dn}$	$\frac{da}{dn}$	$\frac{da}{dn}$	$\frac{da}{dn}$	$\frac{dc}{dn}$
SAMPLE NO. / ΔK KSI $\sqrt{IN.}$	1-9	1-4	Avg.	Avg.	1-5	1-6	Avg.	Avg.
8.34	.70	.75	.73	.76	.85	.65	.75	.78
8.69	.80	.88	.84	.88	.90	.80	.85	.89
9.03	.95	1.10	1.03	1.08	1.05	1.10	1.08	1.13
9.35	1.10	1.25	1.18	1.25	1.20	1.40	1.30	1.38
9.67	1.23	1.53	1.38	1.47	1.83	1.82	1.83	1.95
9.99	1.33	1.70	1.52	1.63	2.35	2.25	2.30	2.47
10.29	1.50	1.83	1.67	1.81	3.10	2.83	2.97	3.22
10.60	1.60	2.00	1.80	1.97	3.95	3.25	3.60	3.94
10.88	1.75	2.15	1.95	2.16	4.50	3.85	4.18	4.62
11.46	2.13	2.25	2.19	2.47	5.30	5.20	5.25	5.93
12.01	2.45	2.45	2.45	2.83	6.20	6.15	6.18	7.15
12.56	3.00	2.73	2.87	3.41	7.25	6.80	7.03	8.34
13.10	3.50	2.85	3.18	3.88	8.15	7.35	7.75	9.46
13.63	3.73	3.05	3.39	4.27	9.35	7.75	8.55	10.77
14.16	4.00	3.40	3.70	4.82	10.05	8.30	9.18	11.95
14.68	4.35	3.83	4.09	5.52	10.80	8.95	9.88	13.34
15.21	4.95	4.35	4.65	6.52	12.80	10.00	11.40	15.99
15.73	5.40	4.70	5.05	7.38	14.30	11.50	12.90	18.86
16.27	5.60	5.30	5.45	8.33	15.35	12.50	13.93	21.28
16.81	6.00	5.63	5.82	9.32	15.75	14.50	15.13	24.24
17.36	6.35	6.18	6.27	10.56	17.05	16.50	16.78	28.26
17.93	7.00	6.85	6.93	12.31	18.25	17.50	17.88	31.77
18.50	7.75	7.75	7.75	14.58	20.00	17.60	18.80	35.38
19.09	8.50	8.20	8.35	16.70	20.85	19.30	20.08	40.16

CRACK GROWTH RATE DATA FOR Ti-6Al-4V ELI MATERIAL IN THE (STA) CONDITION TESTED AT AMBIENT TEMPERATURE.

ΔK KSI $\sqrt{IN.}$	CRACK GROWTH RATE, 10^{-6} INCHES / CYCLE							
	$\frac{da}{dn}$	$\frac{da}{dn}$	$\frac{da}{dn}$	$\frac{dc}{dn}$	$\frac{da}{dn}$	$\frac{da}{dn}$	$\frac{da}{dn}$	$\frac{dc}{dn}$
SAMPLE NO.	4-6	4-9	Avg.	Avg.	4-7	1-11	Avg.	Avg.
8.34	0.60	0.55	0.58	0.60	0.51	0.70	0.61	0.63
8.69	0.80	0.70	0.75	0.78	0.68	0.90	0.79	0.82
9.03	0.85	0.80	0.83	0.87	0.80	1.50	1.15	1.21
9.35	0.95	0.90	0.93	0.98	0.90	2.25	1.58	1.67
9.67	1.20	1.00	1.10	1.17	1.40	2.50	1.95	2.08
9.99	1.25	1.05	1.15	1.24	1.80	2.80	2.30	2.47
10.29	1.30	1.15	1.23	1.33	2.75	3.20	2.98	3.23
10.60	1.33	1.28	1.30	1.42	3.10	3.98	3.54	3.88
10.88	1.50	1.55	1.53	1.69	3.40	4.40	3.90	4.31
11.46	1.80	1.80	1.80	2.03	4.00	5.03	4.52	5.11
12.01	2.35	2.03	2.19	2.53	4.35	6.15	5.25	6.07
12.56	2.60	2.20	2.40	2.85	4.65	6.75	5.70	6.77
13.10	2.88	2.65	2.77	3.38	4.90	7.20	6.05	7.39
13.63	3.08	3.00	3.04	3.83	5.20	7.50	6.35	8.00
14.16	3.43	3.53	3.48	4.53	5.60	7.95	6.78	8.83
14.68	4.00	4.05	4.03	5.44	5.83	8.30	7.05	9.52
15.21	4.08	4.40	4.24	5.95	6.20	8.75	7.48	10.49
15.73	4.48	4.93	4.71	6.89	6.50	9.00	7.75	11.33
16.27	4.90	5.35	5.13	7.84	6.80	9.25	8.03	12.27
16.81	5.20	5.75	5.48	8.78	7.38	9.90	8.64	13.84
17.36	5.90	6.20	6.05	10.19	7.75	10.40	9.08	15.29
17.93	6.55	7.25	6.90	12.26	8.00	11.30	9.65	17.15
18.50	7.45	7.85	7.65	14.40	8.60	11.80	10.20	19.20
19.09	8.30	8.60	8.45	16.90	9.15	12.50	10.83	21.66

CRACK GROWTH DATA FOR Ti-6Al-4V ELI FORGED MATERIAL IN THE (STA) CONDITION TESTED AT 0°F.

	CRACK GROWTH RATE, 10^{-6} INCHES / CYCLE							
	$\frac{da}{dn}$	$\frac{da}{dn}$	$\frac{da}{dn}$	$\frac{dc}{dn}$	$\frac{da}{dn}$	$\frac{da}{dn}$	$\frac{da}{dn}$	$\frac{dc}{dn}$
SAMPLE NO. / ΔK KSI $\sqrt{IN.}$	1-7	4-8	Avg.	Avg.	1-1	1-10	Avg.	Avg.
8.69	-	-	-		.65	.80	.71	.74
9.03	.35	.35	.35	.37	.85	.85	.85	.89
9.67	.63	.55	.59	.63	1.05	1.05	1.05	1.12
10.29	.90	.70	.80	.87	1.43	1.26	1.36	1.47
10.88	1.08	.90	.99	1.09	1.60	1.78	1.69	1.87
11.46	1.33	1.05	1.19	1.34	1.80	1.98	1.89	2.14
12.01	1.55	1.45	1.50	1.74	2.10	2.18	2.14	2.48
12.56	1.78	1.90	1.84	2.18	2.38	2.45	2.42	2.87
13.10	2.10	2.05	2.08	2.54	2.85	2.75	2.80	3.42
13.63	2.38	2.40	2.39	3.01	3.10	3.15	3.13	3.94
14.16	2.45	2.65	2.55	3.32	3.40	3.68	3.54	4.61
14.68	2.70	2.80	2.75	3.59	3.70	3.90	3.80	4.96
15.21	3.08	3.00	3.04	4.27	4.00	4.20	4.10	5.75
15.73	3.45	3.38	3.42	5.00	4.38	4.45	4.42	6.46
16.27	3.90	3.70	3.80	5.81	4.95	4.95	4.95	7.56
16.81	4.50	4.05	4.28	6.86	5.55	5.55	5.55	8.89
17.36	4.85	4.55	4.70	7.91	6.18	6.10	6.14	10.34
17.93	5.25	5.10	5.18	9.20	7.03	6.70	6.87	12.21
18.50	5.70	5.48	5.59	10.52	8.10	7.15	7.63	14.36
19.09	6.40	5.80	6.10	12.20	8.85	7.58	8.22	16.44

CRACK GROWTH RATE DATA FOR Ti-6Al-4V ELI
FORGED MATERIAL IN THE (STA) CONDITION
TESTED AT -100°F.

ΔK KSI √IN. \ SAMPLE NO.	CRACK GROWTH RATE, 10^{-6} INCHES / CYCLE							
	$\frac{da}{dn}$ 4-4	$\frac{da}{dn}$ 1-2	$\frac{da}{dn}$ Avg.	$\frac{dc}{dn}$ Avg.	$\frac{da}{dn}$ 1-12	$\frac{da}{dn}$ 4-11	$\frac{da}{dn}$ Avg.	$\frac{dc}{dn}$ Avg.
9.67	.60	.55	.58	.62	.40	.48	.44	.47
10.29	.80	.80	.80	.87	.65	.60	.63	.68
10.88	1.10	1.05	1.08	1.19	.83	.80	.82	.91
11.46	1.35	1.28	1.32	1.49	1.13	1.05	1.09	1.23
12.01	1.90	1.60	1.75	2.02	1.50	1.30	1.40	1.62
12.56	2.10	1.90	2.00	2.37	1.83	1.55	1.69	2.01
13.10	2.38	2.30	2.34	2.86	2.10	2.00	2.05	2.50
13.63	2.50	2.70	2.60	3.28	2.35	2.38	2.37	2.99
14.16	2.73	2.95	2.84	3.70	2.65	2.60	2.63	3.42
14.68	3.05	3.28	3.17	4.28	2.98	2.98	2.98	4.02
15.21	3.38	3.55	3.47	4.87	3.25	3.35	3.30	4.63
15.73	3.70	3.88	3.79	5.54	3.65	3.80	3.73	5.45
16.27	4.08	4.25	4.17	6.37	4.25	4.40	4.33	6.62
16.81	4.43	4.60	4.52	7.24	4.65	4.75	4.70	7.53
17.36	4.50	5.00	4.75	8.00	5.25	5.10	5.18	8.72
17.93	5.00	5.50	5.25	9.33	5.75	5.35	5.55	9.86
18.50	5.50	6.20	5.85	11.01	6.45	6.00	6.23	11.72
19.09	6.30	6.70	6.50	13.00	7.08	6.60	6.84	13.68

CRACK GROWTH RATE DATA FOR Ti-6Al-4V ELI
FORGED MATERIAL IN THE (STA) CONDITION
TESTED AT -200°F.

	CRACK GROWTH RATE, 10^{-6} INCHES / CYCLE							
	$\frac{da}{dn}$	$\frac{da}{dn}$	$\frac{da}{dn}$	$\frac{dc}{dn}$	$\frac{da}{dn}$	$\frac{da}{dn}$	$\frac{da}{dn}$	$\frac{dc}{dn}$
SAMPLE NO. / ΔK KSI $\sqrt{IN.}$	2-7	2-2	Avg.	Avg.	2-10	2-5	Avg.	Avg.
8.69	-	-	-	-	1.55	2.00	1.78	1.86
8.89	-	-	-	-	2.30	2.60	2.45	2.56
9.03	1.30	1.30	1.30	1.36	3.95	3.40	3.68	3.86
9.67	1.68	1.50	1.59	1.69	4.40	5.70	5.05	5.38
10.29	2.00	1.70	1.85	2.00	6.05	7.33	6.69	7.25
10.88	2.48	2.10	2.29	2.53	7.35	8.40	7.88	8.72
11.46	2.85	2.70	2.78	3.14	8.50	9.25	8.88	10.03
12.01	3.55	3.30	3.43	3.97	9.75	9.70	9.73	11.26
12.56	4.38	3.65	4.02	4.77	10.85	10.20	10.53	12.50
13.10	5.25	4.25	4.75	5.80	12.00	10.70	11.35	13.86
13.63	5.75	4.65	5.20	6.55	12.70	11.85	12.28	15.47
14.16	6.28	5.45	5.86	7.63	13.40	13.40	13.40	17.45
14.68	6.95	6.03	6.49	8.76	13.55	14.20	13.88	18.74
15.21	7.75	6.35	7.05	9.89	-	-	-	-
15.73	7.95	6.80	7.38	10.79	13.85	14.95	14.40	21.05
16.27	8.30	7.73	8.02	12.25	-	-	-	-
16.81	8.70	8.65	8.68	13.90	14.65	15.30	14.98	24.00
17.36	9.13	9.70	9.42	15.86	-	-	-	-
17.93	10.00	11.25	10.63	18.89	15.25	15.60	15.43	27.42
18.50	10.78	12.35	11.57	21.77	-	-	-	-
19.09	12.85	13.50	13.18	26.36	16.00	15.85	15.93	31.86

CRACK GROWTH RATE DATA FOR Ti-6Al-4V ELI FORGED MATERIAL TESTED IN THE WELD AREA AT AMBIENT TEMPERATURE.

	CRACK GROWTH RATE, 10^{-6} INCHES / CYCLE							
	$\frac{da}{dn}$	$\frac{da}{dn}$	$\frac{da}{dn}$	$\frac{dc}{dn}$	$\frac{da}{dn}$	$\frac{da}{dn}$	$\frac{da}{dn}$	$\frac{dc}{dn}$
SAMPLE NO. / ΔK KSI $\sqrt{IN.}$	2-13	4-2	Avg.	Avg.	2-12	3-13	Avg.	Avg.
8.34	.70	1.05	.88	.91	2.08	1.93	2.01	2.08
8.69	1.23	1.23	1.23	1.28	2.85	2.15	2.50	2.61
9.03	1.60	1.35	1.48	1.55	3.25	2.38	2.82	2.96
9.67	2.05	1.70	1.88	2.00	3.65	2.78	3.22	3.43
10.29	2.30	2.05	2.18	2.36	4.03	3.30	3.67	3.98
10.88	2.50	2.50	2.50	2.76	4.20	3.75	3.98	4.40
11.46	2.78	2.95	2.87	3.24	4.45	4.03	4.24	4.79
12.01	3.08	3.25	3.17	3.67	4.75	4.20	4.48	5.18
12.56	3.40	3.50	3.45	4.10	4.85	4.50	4.68	5.56
13.10	3.88	3.75	3.82	4.66	5.10	4.90	5.00	6.10
13.63	4.33	4.25	4.29	5.40	5.38	5.30	5.34	6.73
14.16	4.85	4.45	4.65	6.05	5.75	5.70	5.73	7.46
14.68	5.23	4.90	5.07	6.84	6.08	6.15	6.11	8.25
15.21	5.40	5.50	5.45	7.65	6.45	6.90	6.68	9.37
15.73	5.80	6.15	5.98	8.74	6.85	7.75	7.30	10.67
16.27	6.20	6.90	6.55	10.01	7.44	8.80	8.12	12.41
16.81	6.75	7.70	7.23	11.58	7.95	9.70	8.83	14.14
17.36	7.40	8.35	7.88	13.27	8.68	11.25	9.97	16.79
17.93	8.05	8.90	8.48	15.07	9.70	12.45	11.08	19.69
18.50	8.85	9.25	9.05	17.03	10.73	13.40	12.06	22.70
19.09	9.90	9.60	9.75	19.50	11.85	14.30	13.08	26.16

CRACK GROWTH RATE DATA FOR Ti-6Al-4V ELI FORGED MATERIAL TESTED IN THE WELD AREA AT 0°F.

ΔK KSI √IN. \ SAMPLE NO.	CRACK GROWTH RATE, 10^{-6} INCHES / CYCLE							
	$\frac{da}{dn}$ 3-10	$\frac{da}{dn}$ 2-8	$\frac{da}{dn}$ Avg.	$\frac{dc}{dn}$ Avg.	$\frac{da}{dn}$ 2-11	$\frac{da}{dn}$ 4-12	$\frac{da}{dn}$ Avg.	$\frac{dc}{dn}$ Avg.
9.03	.83	.78	.81	.85	.80	1.30	1.05	1.10
9.67	1.10	.85	.98	1.04	.93	1.45	1.19	1.27
10.29	1.38	.98	1.18	1.28	1.08	1.70	1.39	1.51
10.88	1.70	1.23	1.47	1.62	1.45	1.90	1.68	1.86
11.46	2.20	1.58	1.89	2.14	1.90	2.18	2.04	2.30
12.01	2.45	1.80	2.13	2.46	2.43	2.50	2.47	2.86
12.56	2.75	2.00	2.38	2.82	2.83	2.83	2.83	3.36
13.10	3.10	2.30	2.70	3.30	3.05	3.20	3.13	3.82
13.63	3.45	2.60	3.03	3.82	3.38	3.75	3.57	4.50
14.16	3.83	3.08	3.46	4.50	3.75	4.20	3.98	5.18
14.68	4.40	3.35	3.88	5.24	4.25	4.70	4.50	6.08
15.21	5.00	3.60	4.30	6.03	4.85	5.13	4.99	7.00
15.73	5.50	4.10	4.80	7.02	5.38	5.85	5.62	8.22
16.27	6.05	4.70	5.38	8.22	5.95	6.50	6.23	9.52
16.81	6.70	5.58	6.14	9.84	6.63	7.23	6.93	11.10
17.36	7.50	6.78	7.14	12.02	7.20	8.50	7.85	13.22
17.93	8.30	7.85	8.08	14.36	8.05	10.00	9.03	16.05
18.50	9.10	8.95	9.03	16.99	9.40	12.35	10.88	20.48
19.09	9.63	9.80	9.72	19.44	10.95	15.00	12.98	25.96

CRACK GROWTH RATE DATA FOR Ti-6Al-4V ELI
FORGED MATERIAL TESTED IN THE WELD AREA
AT -100°F.

ΔK KSI $\sqrt{IN.}$	CRACK GROWTH RATE, 10^{-6} INCHES / CYCLE							
	$\frac{da}{dn}$	$\frac{de}{dn}$	$\frac{da}{dn}$	$\frac{dc}{dn}$	$\frac{da}{dn}$	$\frac{da}{dn}$	$\frac{da}{dn}$	$\frac{dc}{dn}$
SAMPLE NO.	2-6	3-12	Avg.	Avg.	4-10	4-3	Avg.	Avg.
9.03	.95	.75	.85	.89	.85	.80	.83	.87
9.67	1.33	1.00	1.17	1.25	1.00	1.00	1.00	1.07
10.29	1.70	1.18	1.44	1.56	1.10	1.40	1.25	1.34
10.86	2.00	1.30	1.65	1.82	1.35	1.75	1.55	1.71
11.46	2.30	1.45	1.88	2.12	1.85	2.05	1.95	2.20
12.01	2.70	1.75	2.23	2.58	2.55	2.40	2.48	2.87
12.56	3.20	2.10	2.65	3.14	3.05	2.88	2.97	3.52
13.10	3.65	2.43	3.04	3.71	3.35	3.30	3.32	4.06
13.63	4.30	3.00	3.65	4.60	3.68	3.85	3.75	4.72
14.16	4.60	3.60	4.10	5.34	4.05	4.35	4.20	5.47
14.68	4.90	4.25	4.58	6.18	4.83	5.00	4.92	6.64
15.21	5.30	4.95	5.13	7.20	5.40	5.90	5.65	7.93
15.73	5.90	5.50	5.70	8.33	6.05	6.75	6.40	9.36
16.27	6.30	6.05	6.18	9.44	6.85	8.13	7.49	11.44
16.81	6.75	6.65	6.70	10.73	7.53	9.40	8.47	13.57
17.36	7.40	7.40	7.40	12.46	8.60	10.45	9.53	16.05
17.93	8.00	8.50	8.25	14.66	10.55	11.80	11.18	19.87
18.50	8.65	9.15	8.90	16.75	11.75	13.40	12.58	23.68
19.09	9.03	9.80	9.42	18.84	13.10	15.00	14.05	28.10

CRACK GROWTH RATE DATA FOR Ti-6Al-4V ELI FORGED MATERIAL TESTED IN THE WELD AREA AT -200°F.